Activation of lysosomal iron triggers ferroptosis in cancer

Tatiana Cañeque, Leeroy Baron, Sebastian Müller, Alanis Carmona, Ludovic Colombeau, Antoine Versini, Stéphanie Solier, Christine Gaillet, Fabien Sindikubwabo, Julio L Sampaio, et al.

Article

Activation of lysosomal iron triggers ferroptosis in cancer

https://doi.org/10.1038/s41586-025-08974-4

Received: 25 March 2024

Accepted: 3 April 2025

Published online: 7 May 2025

Open access

Check for updates

Tatiana Cañeque[1,21], Leeroy Baron[1,21], Sebastian Müller[1,21], Alanis Carmona[2], Ludovic Colombeau[1], Antoine Versini[1], Stéphanie Solier[1,3,4], Christine Gaillet[1], Fabien Sindikubwabo[1], Julio L. Sampaio[1], Marie Sabatier[2], Eikan Mishima[5], Armel Picard-Bernes[1], Laurène Syx[6], Nicolas Servant[6], Bérangère Lombard[7], Damarys Loew[7], Jiashuo Zheng[5], Bettina Proneth[5], Leishemba K. Thoidingjam[1], Laurence Grimaud[8], Cameron S. Fraser[2], Krystina J. Szylo[2], Emma Der Kazarian[9], Caroline Bonnet[9], Emmanuelle Charafe-Jauffret[9], Christophe Ginestier[9], Patricia Santofimia-Castaño[10], Matias Estaras[10], Nelson Dusetti[10], Juan Lucio Iovanna[10], Antonio Sa Cunha[11], Gabriella Pittau[11], Pascal Hammel[11], Dimitri Tzanis[12], Sylvie Bonvalot[12], Sarah Watson[13], Vincent Gandon[14], Aditya Upadhyay[15], Derek A. Pratt[15], Florêncio Porto Freitas[16], José Pedro Friedmann Angeli[16], Brent R. Stockwell[17,18,19], Marcus Conrad[5,20], Jessalyn M. Ubellacker[2] & Raphaël Rodriguez[1]✉

Iron catalyses the oxidation of lipids in biological membranes and promotes a form of cell death called ferroptosis[1]. Defining where this chemistry occurs in the cell can inform the design of drugs capable of inducing or inhibiting ferroptosis in various disease-relevant settings. Genetic approaches have revealed suppressors of ferroptosis[2–4]; by contrast, small molecules can provide spatiotemporal control of the chemistry at work[5]. Here we show that the ferroptosis inhibitor liproxstatin-1 exerts cytoprotective effects by inactivating iron in lysosomes. We also show that the ferroptosis inducer RSL3 initiates membrane lipid oxidation in lysosomes. We designed a small-molecule activator of lysosomal iron—fentomycin-1—to induce the oxidative degradation of phospholipids and ultimately ferroptosis. Fentomycin-1 is able to kill iron-rich CD44^{high} primary sarcoma and pancreatic ductal adenocarcinoma cells, which can promote metastasis and fuel drug tolerance. In such cells, iron regulates cell adaptation[6,7] while conferring vulnerability to ferroptosis[8,9]. Sarcoma cells exposed to sublethal doses of fentomycin-1 acquire a ferroptosis-resistant cell state characterized by the downregulation of mesenchymal markers and the activation of a membrane-damage response. This phospholipid degrader can eradicate drug-tolerant persister cancer cells in vitro and reduces intranodal tumour growth in a mouse model of breast cancer metastasis. Together, these results show that control of iron reactivity confers therapeutic benefits, establish lysosomal iron as a druggable target and highlight the value of targeting cell states[10].

Iron reacts with peroxides to produce oxygen-centred radicals. In the cell, such a process can initiate and propagate a radical chain reaction that leads to oxidized organic products, a chemistry broadly defined as the Fenton reaction[11]. Chemically reactive lipids in biological membranes are ideal substrates for such reactions and have been implicated in ferroptosis[12]. The accumulation of damaged phospholipids can eventually cause the loss of membrane integrity together with altered organelle functions and the release of various types of chemical entities in the cell, which can induce further cellular defects and cell death. Ferroptosis involves distinct organelles[13], including peroxisomes[14], mitochondria[15], the endoplasmic reticulum (ER)[16] and lysosomes[8,17]. However, it is currently unclear whether individual organelles contribute to ferroptosis through impaired cell signalling, metabolism and biosynthesis of specific biomolecules or whether membrane lipids

[1]Institut Curie, CNRS, INSERM, PSL Research University, Paris, France. [2]Department of Molecular Metabolism, Harvard T. H. Chan School of Public Health, Boston, MA, USA. [3]Department of Genetics, Institut Curie, Paris, France. [4]Paris Saclay University, UVSQ, Montigny-le-Bretonneux, France. [5]Institute of Metabolism and Cell Death, Helmholtz Zentrum München, Neuherberg, Germany. [6]Institut Curie, INSERM, Mines Paris Tech, PSL Research University, Paris, France. [7]Institut Curie, PSL Research University, Paris, France. [8]Ecole Normale Supérieure, CNRS, PSL Research University, Paris, France. [9]CRCM, CNRS, INSERM, Institut Paoli-Calmettes, Aix-Marseille University, Marseille, France. [10]CRCM, CNRS, INSERM, Institut Paoli-Calmettes, Aix-Marseille University, Parc Scientifique et Technologique de Luminy, Marseille, France. [11]Department of Digestive and Medical Oncology, Paris Saclay University and Paul-Brousse Hospital (APHP Sud), Villejuif, France. [12]Department of Surgical Oncology, Institut Curie, Paris, France. [13]Department of Medical Oncology, Institut Curie, INSERM, PSL Research University, Paris, France. [14]Institut de Chimie Moléculaire et des Matériaux d'Orsay, CNRS, Paris Saclay University, Orsay, France. [15]Department of Chemistry and Biomolecular Sciences, University of Ottawa, Ottawa, Ontario, Canada. [16]Rudolf-Virchow-Zentrum, Center for Integrative and Translational Bioimaging, Julius-Maximilians-Universität Würzburg, Würzburg, Germany. [17]Department of Chemistry, Columbia University, New York, NY, USA. [18]Department of Biological Sciences, Columbia University, New York, NY, USA. [19]Department of Pathology and Cell Biology, Vagelos College of Physicians & Surgeons, Columbia University, New York, NY, USA. [20]Translational Redox Biology, TUM Natural School of Sciences, Technical University of Munich, Garching, Germany. [21]These authors contributed equally: Tatiana Cañeque, Leeroy Baron, Sebastian Müller. ✉e-mail: raphael.rodriguez@curie.fr

of these compartments are also direct substrates for iron-mediated oxidation that leads to cell death. Cancer cells have been shown to require functional lysosomes to undergo ferroptosis[17]. This finding highlights the importance of cellular iron import and lends support for the idea that iron has a role in promoting cell death. Pharmacological inhibition of iron trafficking from lysosomes promotes the oxidation of lysosomal membrane lipids[8,18], which indicates that a redox-active pool of iron in this organelle can trigger ferroptosis. Synthetic endoperoxides, surrogates of peroxidized lipids with a propensity to accumulate in the ER, can induce ferroptosis, which suggests that lipid peroxidation can propagate through this organelle[19]. However, it is currently unclear where iron-mediated oxidation of membrane lipids is first initiated in the cell before propagating through other proximal membrane lipids.

Lysosomal iron initiates ferroptosis

We set out to identify the subcellular sites of action of liproxstatin-1 (Lip-1), a small molecule that protects cells against death induced through the inactivation of ferroptosis suppressors[20]. We labelled a clickable alkyne-containing analogue of Lip-1 (named cLip-1) using in-cell click chemistry and performed fluorescence microscopy[21] in various cell lines. The results revealed lysosomal accumulation in HT-1080 fibrosarcoma cells, in primary cells of human pancreatic ductal adenocarcinoma (PDAC), in lung and colon circulating tumour cells and in 4T1 mouse breast cancer cells (Fig. 1a and Extended Data Fig. 1a–f). Notably, labelled cLip-1 was detected only in the endolysosomal compartment, even at a concentration higher than the effective dose. This result supports the notion that Lip-1 exerts its anti-ferroptotic activity in this organelle. In vivo, cLip-1 increased the survival of mice in which acute renal failure was induced through genetic deletion of *Gpx4*, which encodes the ferroptosis suppressor glutathione peroxidase 4 (GPX4)[2] (Fig. 1b). Labelling cLip-1 in mouse tissues revealed its accumulation in the kidney, colocalizing with a lysosomal marker in renal proximal tubules (Fig. 1c and Extended Data Fig. 1g). In vitro, cLip-1 prevented the oxidation of membrane lipids and protected cells against the effects of genetic depletion of *Gpx4* or pharmacological inhibition of GPX4 with RSL3, thereby recapitulating the biological activity of Lip-1 (Extended Data Fig. 1h–j). These data validate cLip-1 as a suitable surrogate of Lip-1 to investigate ferroptosis.

The tight iron chelator deferoxamine (DFO) protects cells against erastin-induced ferroptosis[5]. By contrast, Lip-1 exhibits radical-trapping antioxidant (RTA) properties in vitro[22]. However, unlike most RTAs that inhibit ferroptosis, such as α-tocopherol, Lip-1 does not follow the general trend of many ferroptosis suppressors, whereby RTA activity is closely correlated with ferroptosis inhibition[23]. This result suggests that other properties of Lip-1 contribute to its anti-ferroptotic effects. In cancer cells, iron can be internalized by endocytosis[6,24] and regulates cell-state transitions and cell proliferation[6,25]. Because cLip-1 accumulates in lysosomes and contains nitrogen atoms susceptible to interactions with iron, we investigated the possibility that its ferroptosis inhibition properties can result from iron inactivation in this organelle. Nuclear magnetic resonance (NMR) spectroscopy indicated that Lip-1 interacts with iron(III) with stoichiometries of 1:1 and 2:1 (Fig. 1d). Titrating Lip-1 with iron(III) chloride induced signal broadening together with a shift downfield of signals of the protons adjacent to nitrogen atoms of Lip-1, which indicated the occurrence of coordination with the nitrogen lone pairs with the Lewis acid. By contrast, the proton signals of naphthalene, which was used as an internal control as it lacks heteroatoms, remained unaffected (Extended Data Fig. 1k). Moreover, adding a Brønsted acid to Lip-1 induced distinct shifts downfield of the proton signals, which indicated protonation of the nitrogen atoms (Fig. 1e). Notably, line broadening of the proton signals was observed only in the presence of the paramagnetic metal (Extended Data Fig. 1l–n). Furthermore, the addition of trifluoroacetic acid (TFA) to a solution of iron(III) and Lip-1 did not fully displace iron from Lip-1, as shown by chemical shifts that recapitulated the effects of Lewis and Brønsted acids. These data indicate that the binding of Lip-1 to iron can take place under acidic conditions, such as those found in lysosomes. The addition of sodium hydroxide restored the chemical shifts of unbound Lip-1, a result that demonstrates the reversible nature of Lip-1 interactions with iron (Extended Data Fig. 1o). Molecular modelling using discrete Fourier transform computation produced several possible binding modes between iron and Lip-1, including bimolecular tetrahedral iron complexes involving the piperidine, amidine and aniline functions of Lip-1 (Fig. 1f and Supplementary Information).

Cyclic voltammetry, which is used to quantify the redox potential of metals in solution[26], indicated that Lip-1 and DFO alter the redox properties of iron (Fig. 1g). As controls, we investigated two other synthetic analogues of Lip-1: metcLip-1 and alcLip-1. In metcLip-1, aromatic amines are methylated, which adversely affected RTA activity. By contrast, alcLip-1 is an aliphatic analogue with amines that have a higher negative logarithmic acid dissociation constant (pK_a) value compared with their aromatic counterparts. This analogue was expected to be fully protonated at neutral pH and therefore to exhibit a reduced propensity to enter cells and to accumulate in lysosomes (Extended Data Fig. 2a). Labelling of metcLip-1 in cells revealed a similar staining pattern to that of labelled cLip-1, showing colocalization with a lysosomal marker. By contrast, labelled alcLip-1 showed weak fluorescence (Extended Data Fig. 2b). Cyclic voltammetry results further indicated that metcLip-1 altered the redox potential of iron to a greater extent than alcLip-1 (Extended Data Fig. 2c). Consistently, metcLip-1 protected cells against RSL3-induced oxidation of membrane lipids more potently than alcLip-1 (Extended Data Fig. 2d), and neither metcLip-1 nor alcLip-1 exhibited RTA properties in vitro (Extended Data Fig. 2e). In-cell labelling of an alkyne-containing derivative of DFO (cDFO)[6] also revealed lysosomal signals, which provided support for the pro-ferroptotic activity of iron in this organelle (Extended Data Fig. 2f). Signals of cDFO were also found in the cell nucleus, which partially explains the toxicity of this iron chelator and its distinct associated phenotype compared with other iron-interacting small molecules, including Lip-1.

In a cell-free system, Lip-1 reduced the fluorescence of an iron(III)-specific fluorescent probe in the presence of iron(III)[27] (Extended Data Fig. 2g). Treatment of cells with hydroxychloroquine or bafilomycin-A1, which increase the lysosomal pH and prevent iron(III) unloading from its endocytic carriers, led to reduced pools of chelatable cellular iron(III) and reactive lysosomal iron(II), as measured using specific fluorescent probes[27,28]. These treatments also protected cells against RSL3-induced oxidation of membrane lipids in cancer cells (Fig. 1h–j and Extended Data Fig. 2h–j). Comparable results were obtained with Lip-1, which was consistent with the direct interactions of this compound with lysosomal iron (Fig. 1h–j and Extended Data Fig. 2h–j). After treatment with RSL3 for 1 h, oxidation of membrane lipids was predominantly detected in lysosomes, as assessed through Liperfluo and Bodipy 665/676 fluorescence levels (Fig. 1k and Extended Data Figs. 2k and 3a). By contrast, treatment with RSL3 for 4 h led to a staining pattern of oxidized membrane lipids that colocalized mainly with a fluorescently labelled biological marker of the ER (Extended Data Fig. 3b). Our data suggest that initiation of the radical chain reaction takes place early in the endolysosomal compartment, where redox-active iron can be found[8]. This radical chain reaction can then propagate to membrane lipids of other organelles in the vicinity, including the ER. In support of this hypothesis, treatment of cells with well-established ferroptosis inducers led to a depletion of glutathione and increased levels of oxygen-centred radicals in lysosomes (Extended Data Fig. 3c–e). Together, these data indicate that lysosomal iron has a central role in the induction of ferroptosis.

Iron activation promotes ferroptosis

Cancer cells that have acquired a drug-tolerant persister (DTP) cell state are vulnerable to ferroptosis[8,29,30]. DTP cancer cells are characterized

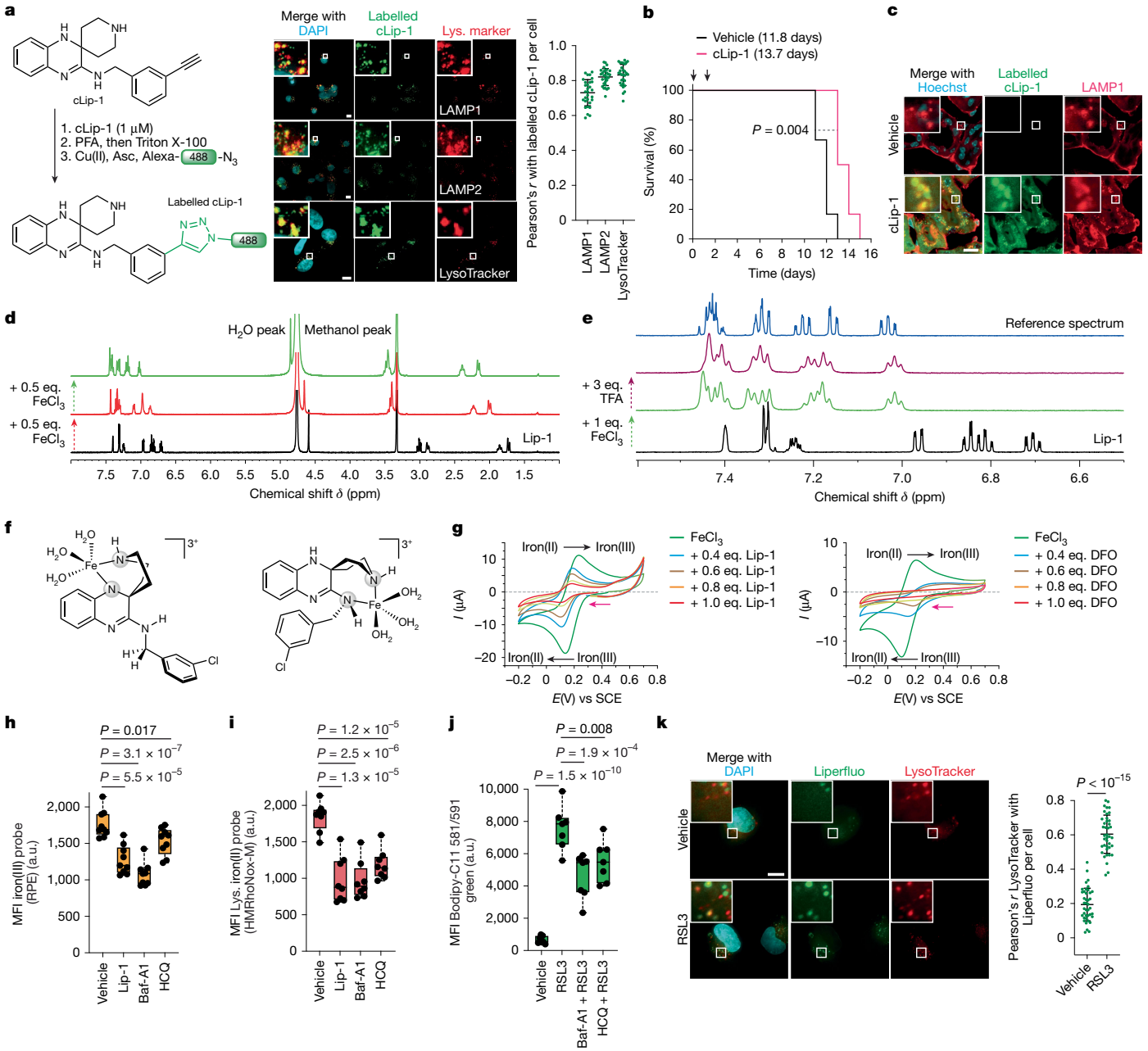

Fig. 1 | Lysosomal iron triggers the oxidation of membrane lipids. a, Schematic (left), images (middle) and quantification (right) of labelling cLip-1 (1 μM, 1 h) in cells. $n = 3$ independent experiments in HT-1080 cells. Data are the mean ± s.d. Asc, ascorbate; Lys., lysosome; PFA, paraformaldehyde. **b**, Kaplan–Meier survival curves of *Rosa26-CreERT2;Gpx4*$^{f/f}$ mice treated with cLip-1 (10 mg per kg per day by intraperitoneal injection; $n = 6$ mice per group). Mantel–Cox log-rank test. Arrows indicate the timing of the two tamoxifen injections. Average days of survival are indicated. **c**, Fluorescence images of labelled cLip-1 in renal proximal tubules of a *Rosa26-CreERT2;Gpx4*$^{f/f}$ mouse 7 days after tamoxifen treatment. Images representative of $n = 2$ mice. **d**, ^{1}H NMR spectra of Lip-1 titrated with $FeCl_3$ (red, 2:1 Lip-1 to iron; green, 1:1 Lip-1 to iron). **e**, ^{1}H NMR spectra of Lip-1 titrated with $FeCl_3$ and then TFA. The blue reference spectrum is Lip-1 + 3 eq. TFA. **f**, Putative binding modes of Lip-1 and iron obtained from molecular modelling. **g**, Cyclic voltammetry of a $FeCl_3$ solution with Lip-1 (left) or DFO (right) (reduction potentials indicated by pink arrows). SCE, saturated calomel electrode. **h**–**k**, Data are for HT-1080 cells. **h**, Flow cytometry of cells treated with the indicated compounds for 15 min and then with the iron(III) probe RPE for 15 min. $n = 9$ independent experiments. a.u., arbitrary unit; MFI, mean fluorescence intensity. **i**, Flow cytometry of cells treated with the indicated compounds for 15 min and then with the iron(II) probe HMRhoNox-M for 15 min. $n = 8$ independent experiments. **j**, Bodipy-C11 581/591 flow cytometry of cells treated with RSL3 (1 h) and with bafilomycin-A1 (Baf-A1) or hydroxychloroquine (HCQ) 2 h before. $n = 7$ independent experiments. One-way analysis of variance (ANOVA). **k**, Fluorescence imaging of Liperfluo in cells treated with RSL3 (1 h). $n = 3$ independent experiments. Two-sided unpaired *t*-test. Data are the mean ± s.d. **d**,**e**, NMR spectra recorded at 310 K in methanol-d_4. For **h** and **i**, *P* values are from two-sided unpaired *t*-test compared with vehicle. The following concentrations were used: **h**,**i**, Lip-1 (10 μM), HCQ (100 μM); **h**–**j**, Baf-A1 (75 nM); **j**, HCQ (10 μM), RSL3 (200 nM); **k**, RSL3 (1 μM). Box plots show the interquartile range, with centre lines indicating the medians and whiskers indicating the minimum and maximum values. Scale bar, 10 μm (**a**,**c**,**k**).

by high expression of the iron-uptake protein CD44, a cell membrane glycoprotein that is internalized by endocytosis and is used as a marker of cancer cell stemness and metastasis[6,31]. Thus, these cells exhibit upregulated iron uptake, which leads to increased cellular iron levels that in turn promote the activity of iron-dependent demethylases[6]. This process activates specific epigenetic and transcriptional programs

that underlie cell-state transitions and the acquisition of a DTP phenotype[6]. Thus, lysosomal iron has emerged as a druggable target to promote ferroptosis in a cell-state-dependent manner[9]. With this in mind and the knowledge that lysosomal iron can trigger the oxidation of membrane lipids[8], we designed a small molecule to target lipids at the plasma membrane and to activate iron(II) in lysosomes upon endocytosis. Such a compound would exploit nearby reactive membrane lipids as substrates for oxidation. To this end, we synthesized a bifunctional compound composed of the fluorescent lipophilic natural product marmycin and the synthetic Chen–White ligand, which we named fentomycin-1 (Fento-1) (Fig. 2a and Extended Data Fig. 4a–e). Marmycin accumulates at the plasma membrane and is internalized by endocytosis[32], whereas the Chen–White ligand is commonly used in chemical synthesis to oxidize organic substrates by activating iron(II)[33]. In the presence of hydrogen peroxide and under mild acidic aqueous conditions, such as those found in lysosomes, the Chen–White iron catalyst is thought to form a reactive iron-oxo species[33]. Like hydroxyl and hydroperoxyl radicals, this intermediate can abstract a hydrogen atom from organic substrates, including saturated ones, to produce reactive carbon-centred radicals and subsequently oxidation products. Fento-1 is therefore reminiscent of a bifunctional small molecule that is able to induce proximity de novo between a catalyst and nucleic acids or proteins to promote degradation[34,35]. We proposed that by exploiting the abundant amount of reactive iron(II) in DTP cancer cells[6–8], such a bifunctional molecule would form an active catalyst in the cell to promote the oxidative degradation of lysosomal membrane lipids and ultimately trigger ferroptosis.

In a cell-free system, Fento-1 enhanced the iron-induced oxidation of a liposome-forming unsaturated phospholipid under experimental conditions comparable to that found in lysosomes. That is, acidic pH, the presence of hydrogen peroxide and a water-soluble iron(II) salt (Fig. 2b and Supplementary Table 1). Notably, iron promoted oxidation of the phospholipid bilayer in the presence of hydrogen peroxide without enzymes, which therefore supports the idea that such a process occurs in the cell. The intrinsic fluorescence of Fento-1 revealed its localization at the plasma membrane when experiments were conducted at a low temperature to reduce endocytic flux (Extended Data Fig. 5a), thereby recapitulating the photophysical properties of the parental natural product. By contrast, at a physiological temperature, which enables endocytosis to take place, Fento-1 and marmycin were detected in the endolysosomal compartment (Fig. 2c). Chemical labelling of a clickable alkyne-containing Chen–White ligand (cCW) revealed weak pan-cellular staining (Fig. 2c and Extended Data Fig. 4f), which suggested that the untethered ligand does not specifically accumulate in the endolysosomal compartment. Moreover, Fento-1 did not predominantly target other organelles (Extended Data Fig. 5b). This small molecule induced the oxidation of membrane phospholipids and reduced cell viability in several human and mouse cancer cell lines and primary cells, whereas the effects of cCW and marmycin were marginal (Extended Data Fig. 5c–e). Mass-spectrometry (MS)-based lipidomics revealed that Fento-1 induced the oxidation of phospholipids in several cell lines to a greater extent than well-established ferroptosis inducers under these conditions (Extended Data Fig. 5f,g, Supplementary Information and Supplementary Tables 2 and 3). Analyses of lysosomes isolated from HT-1080 cells treated with Fento-1 for 1 h confirmed the oxidation of associated phospholipids at this early time point (Extended Data Fig. 5h, Supplementary Information and Supplementary Table 4). Consistent with the oxidation of membrane phospholipids, sublethal doses of Fento-1 increased levels of ferroptosis suppressors in HT-1080 cells, including GPX4, ferroptosis suppressor protein 1 (FSP1) and the cystine–glutamate antiporter (composed of SLC7A11 and SLC3A2) (Fig. 2d and Extended Data Fig. 5i). Quantitative proteomics revealed that cells treated with sublethal doses of Fento-1 for 48 h promoted the upregulation of ferroptosis[1,36] and lysosome-associated proteins, including ferroptosis suppressors and lysosome-associated membrane proteins (LAMPs), respectively, a result that provides support for the role of lysosomes in ferroptosis induction (Fig. 2d,e and Supplementary Tables 5 and 6). Cells were also characterized by the downregulation of iron homeostasis-associated proteins, including the iron-uptake protein CD44 and the iron-storage protein ferritin. These cells also exhibited increased levels of transferrin receptor 1 (TFR1) and iron-responsive element-binding protein 2 (IRP2), which are characteristic of cellular iron depletion[37]. Sublethal doses of Fento-1 promoted the downregulation of mesenchymal markers, which have been linked to the acquisition of cancer cell states refractory to standard-of-care treatments[38]. Last, these cells exhibited upregulation of other transcription factors involved in the regulation of cell states, such as SOX4 and SOX13, as well as epithelial markers. These data indicate that the effects of Fento-1 treatment on HT-1080 cells, which are of mesenchymal origin, are due to the acquisition of a distinct cell state that resembles that of epithelial cells typically sensitive to standard antiproliferative treatments. This result also suggests that cancer cells can adapt to Fento-1 exposure and develop a ferroptosis-tolerant cell state. That is, cells treated with a low dose of Fento-1 exhibit sustained viability and a distinct phenotype due to cellular adaptation rather than clonal selection[38]. Western blot analyses further corroborated the proteomic data (Extended Data Fig. 5j). Furthermore, increased levels of GPX4 were detected in lysosome-enriched fractions isolated from HT-1080 cells treated with Fento-1 (Fig. 2f).

Oxidation of membrane phospholipids induced by Fento-1 was reduced by the lipophilic RTA α-tocopherol, the iron chelator deferiprone and Lip-1 (Fig. 2g, Extended Data Fig. 5k, Supplementary Information and Supplementary Table 7). Furthermore, treatment with Fento-1 induced the production of 4-hydroxynonenal (4-HNE) (Extended Data Fig. 5l), a result indicative of peroxidation and the breakdown of phospholipids that contain polyunsaturated fatty acids[39]. Notably, 4-HNE can cause cellular damage, and its production is a hallmark of ferroptosis[40]. Treatment with Fento-1 also led to increased levels of lysophospholipids and glycerol, further indicating the degradation of oxidized phospholipids (Fig. 2h, Extended Data Fig. 5m, Supplementary Information and Supplementary Table 8). This result, together with the upregulation of lipid metabolism after treatment with Fento-1 (Fig. 2e), suggests that oxidized membrane lipids trigger a membrane-damage response[41]. Cell death induced by Fento-1 was antagonized by well-established ferroptosis inhibitors, which included iron chelators and RTAs, but not by apoptosis or necroptosis inhibitors (Fig. 2i and Extended Data Fig. 6a–f). Notably, Fento-1 exhibited a residual toxicity that ferroptosis inhibitors could not fully overcome, which reflects the potency of Fento-1. α-Tocopherol did not prevent lysosome targeting with Fento-1, which indicated that this ferroptosis inhibitor exerts its protective activity by acting as a RTA in membrane lipids and not by competing for interaction at the plasma membrane (Extended Data Fig. 6g). Fento-1 was synthetically lethal after cotreatment with GPX4 inhibitors, and cell viability was rescued by Lip-1 (Extended Data Fig. 6h), a result that further confirmed the pro-ferroptotic activity of Fento-1. Finally, knocking down ferroptosis suppressors sensitized cells to Fento-1, whereas knocking down *Cd44* conferred a protective effect (Extended Data Fig. 6i). Consistently, knocking down *Cd44* partially protected cells against oxidation of membrane lipids, whereas genetic suppression of the canonical iron endocytosis pathway involving TFR1 was less effective (Extended Data Fig. 6j). This result confirms the role of CD44 as the main effector of iron uptake in the mesenchymal state of cancer cells[6].

We next explored the activity of structural variants of Fento-1 (Extended Data Fig. 7a). Fento-2, which contains a longer linker between marmycin and the Chen–White ligand, exhibited a lower potency against PDAC and sarcoma cells than Fento-1. This result supports the notion that Fento-1 exerts its activity by promoting proximity between a reactive iron catalyst and membrane lipids (Extended Data Fig. 7b,c).

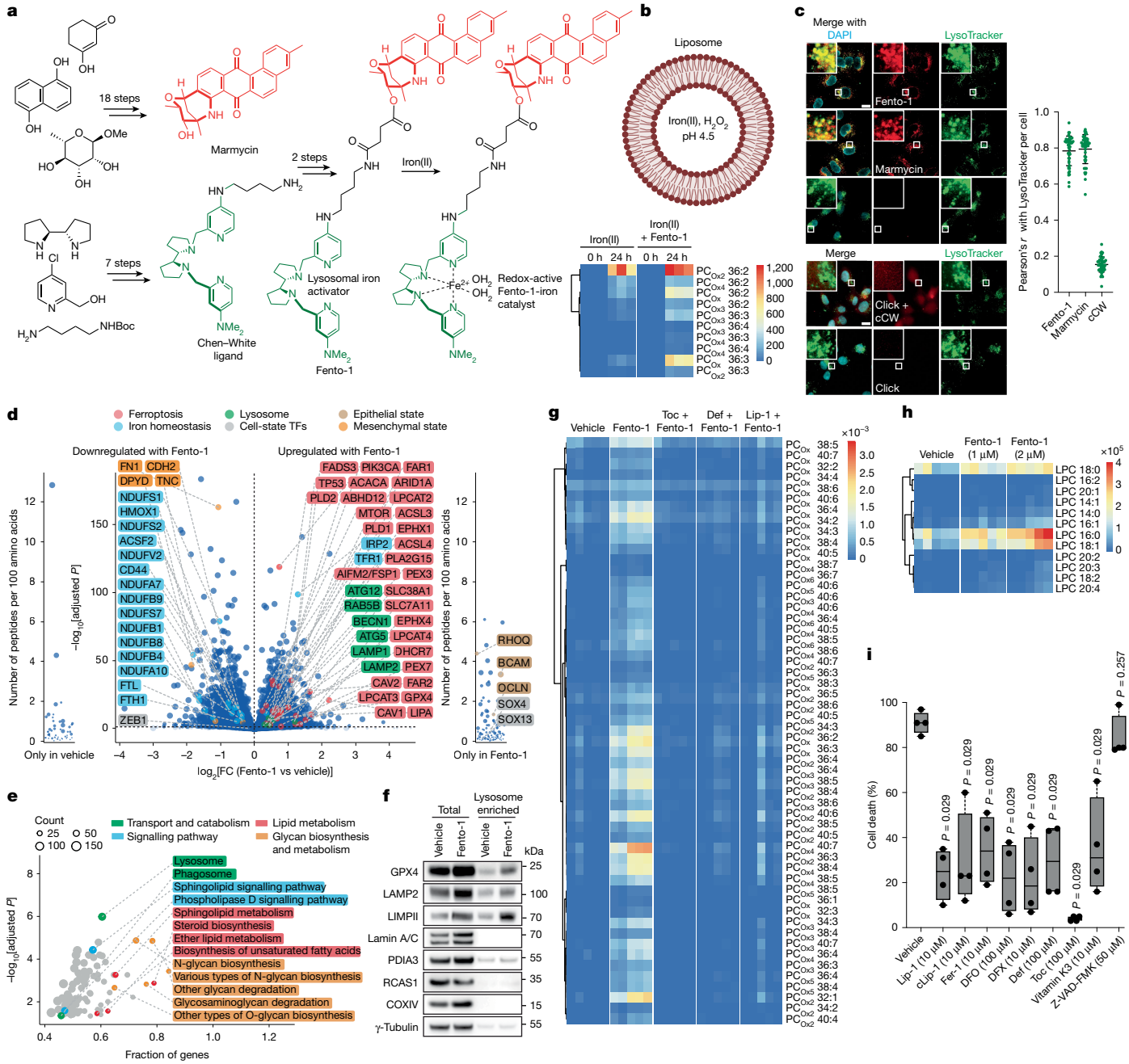

Fig. 2 | Induction of ferroptosis by a lysosome-selective iron-dependent phospholipid degrader. a, Chemical synthesis of Fento-1 and redox-active iron catalyst formation. **b**, Top, illustration of a liposome loaded with iron(II) and H_2O_2. Bottom, lipidomics of oxidized DOPC-forming liposomes with iron(II) and Fento-1. $n = 3$ independent experiments. **c**–**i**, Data are for HT-1080 cells. **c**, Fluorescence imaging of Fento-1, marmycin and labelled cCW (1 μM) in cells treated at 37 °C for 1 h. Scale bar, 10 μm. $n = 3$ independent experiments. Data are the mean ± s.d. **d**, Quantitative proteomics of cells treated with Fento-1 (48 h). The dashed vertical line indicates adjusted $P = 0.05$. $n = 5$ independent experiments. FC, fold change; TFs, transcription factors. **e**, KEGG enrichment analysis of upregulated proteins in cells treated with Fento-1 (48 h). $n = 5$ independent experiments. **f**, Western blot of proteins from total and lysosome-enriched extracts from cells treated with Fento-1 (48 h). Representative of $n = 3$ independent experiments. γ-Tubulin is a sample-processing control. **g**, Lipidomics of oxidized phospholipids in cells treated with Fento-1 (24 h) and inhibitors (added 2 h before Fento-1). $n = 5$ independent experiments. Full heat map is in Supplementary Information. **h**, Lipidomics of lysophospholipids in cells treated with Fento-1 (24 h). $n = 5$ independent experiments. **i**, Lactate dehydrogenase (LDH) release from cells treated with Fento-1 (10 μM for 6 h) and with inhibitors added 2 h before. $n = 4$ independent experiments. Two-sided Mann–Whitney test compared to vehicle. The box plots show the interquartile range, with the centre lines indicating the medians and the whiskers the minimum and maximum values. Def, deferiprone; DFX, deferasirox; Fer-1, ferrostatin-1; Toc, α-tocopherol. The following concentrations were used unless stated otherwise: Fento-1 (1 μM), Toc (100 μM), Def (100 μM) and Lip-1 (1 μM). Phosphatidylcholine (PC) lipids are displayed in the main figure. Subscript Ox*n* denotes the addition of *n* oxygens. Phosphatidylethanolamine (PE), phosphatidylinositol (PI) and phosphatidylserine (PS) are shown in the Supplementary Information. Lysophosphatidylcholine (LPC) lipids are displayed in the main figure. LPE, LPI and LPS are shown in the Supplementary Information. For **d** and **e**, linear model, two-sided *t*-test on fold change. *P* adjusted with Benjamini–Hochberg false-discovery rate. Illustration in **b** was created using BioRender (https://biorender.com).

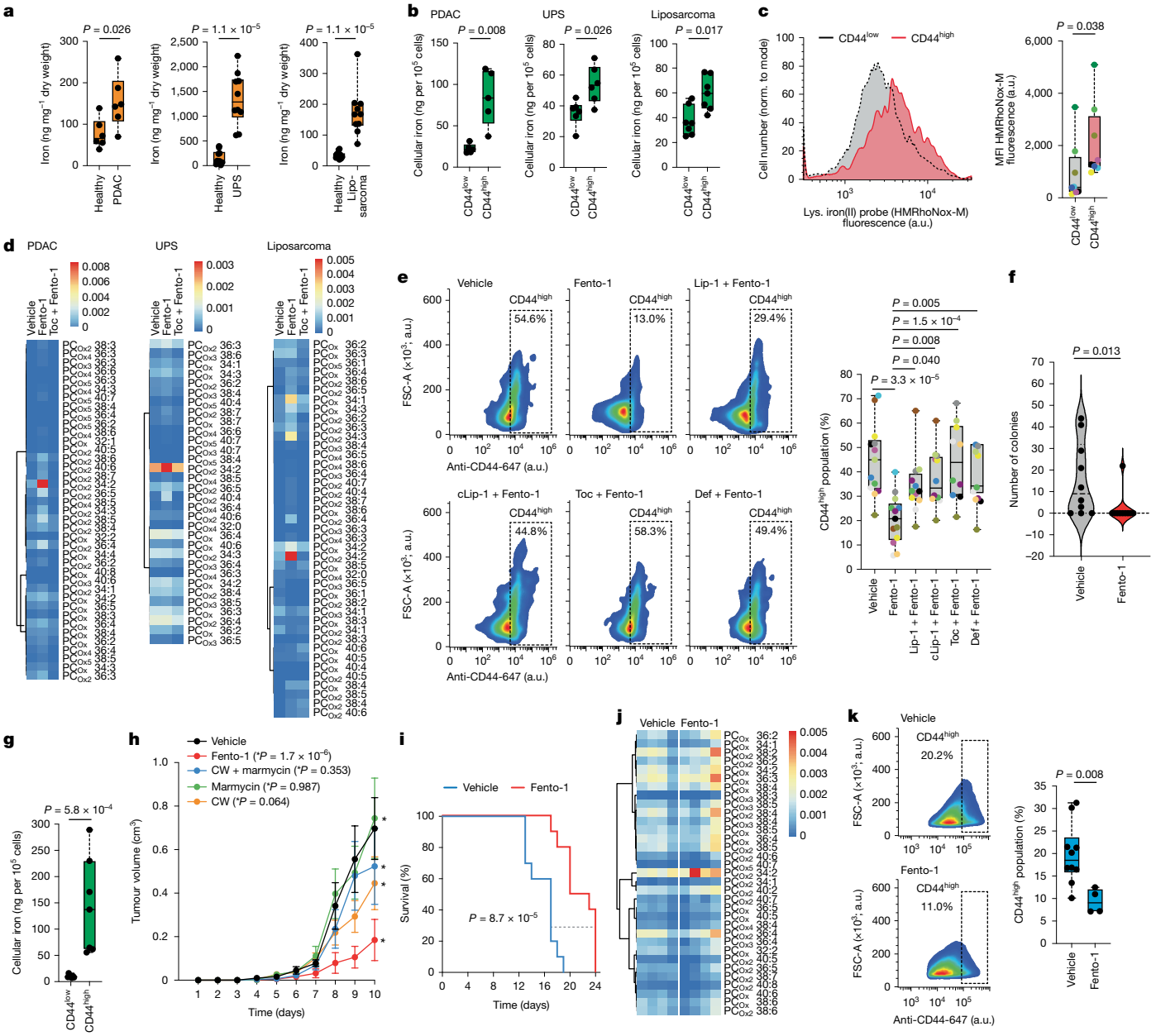

Fig. 3 | Activation of lysosomal iron targets CD44^{high} cancer cells and reduces tumour growth. a, ICP-MS of human healthy and cancer tissues. PDAC, $n = 6$ pieces per tissue; UPS and liposarcoma, $n = 10$ pieces per tissue. **b**, ICP-MS of dissociated human tumour cancer cells (CD45$^-$CD31$^-$FAP$^-$). PDAC, $n = 5$; UPS, $n = 6$; liposarcoma, $n = 7$ replicates per tumour. **c**, HMRhoNox-M flow cytometry of dissociated human PDAC cancer cells (CD45$^-$CD31$^-$FAP$^-$). $n = 8$ patients. **d**, Lipidomics of oxidized phospholipids of dissociated human tumour cells treated with Fento-1 (1 µM, 24 h) and Toc (2 h before). **e**, CD44 flow cytometry of dissociated human PDAC cancer cells (CD45$^-$CD31$^-$FAP$^-$) treated with Fento-1 (1 µM, 24 h) and inhibitors (2 h before). $n = 13$ patients. One-way ANOVA. **f**, Colony-formation assay of DTP SUM159 cancer cells after doxorubicin treatment (150 nM, 72 h), then Fento-1 (5 µM) or DMSO (0.2%) treatment for 72 h. Data are the mean ± s.d. **g**, ICP-MS of sorted 4T1 tumour cells (CD45$^-$CD31$^-$MCHII$^+$). $n = 7$ replicates. **h**, Tumour volume in 4T1 tumour-bearing mice. $n = 5$ mice per condition. Two-way ANOVA. P values (day 10) compared to vehicle. Data are the mean ± s.e.m. CW, Chen–White ligand. **i**, Maximum tumour diameter as the survival end point of tumour-bearing mice. Mantel–Cox log-rank test. **j**, Lipidomics of oxidized phospholipids in mouse 4T1 tumours (treatment for 15 days). $n = 4$ mice per condition. **k**, CD44 flow cytometry of dissociated tumour cancer cells (CD45$^-$CD31$^-$MCHII$^+$) from 4T1 tumour-bearing mice treated with Fento-1 (0.003 mg per animal every other day). Vehicle, $n = 10$ mice, Fento-1, $n = 4$ mice. The following concentrations were used unless stated otherwise: Toc (100 µM), Def (100 µM), Lip-1 (1 µM) and cLip-1 (1 µM). For **a**–**c**, **f**, **g** and **k**, P values are from two-sided Mann–Whitney tests. For **c** and **e**, each coloured dot represents a tumour of a distinct patient per given panel. Full heat maps for **d** and **j** are provided in the Supplementary Information. Box plots show the interquartile range, with centre lines indicating the medians and whiskers the minimum and maximum values.

We also replaced marmycin with cholesterol, an apolar natural product that can intercalate between phospholipids at the plasma membrane[42] and has a role in the mesenchymal state of cancer cells[43], potentially at the plasma membrane. This modification led to the non-fluorescent analogue Fento-3, which exhibited a potency comparable to that of Fento-1. Together, these analogues illustrate the versatile nature of this strategy (Extended Data Fig. 7a–c). As a control, replacing the apolar scaffold with a more polar moiety, such as morpholine, produced Fento-4, which was biologically inactive (Extended Data Fig. 7a–c). Finally, replacing the Chen–White ligand with the structurally more hindered

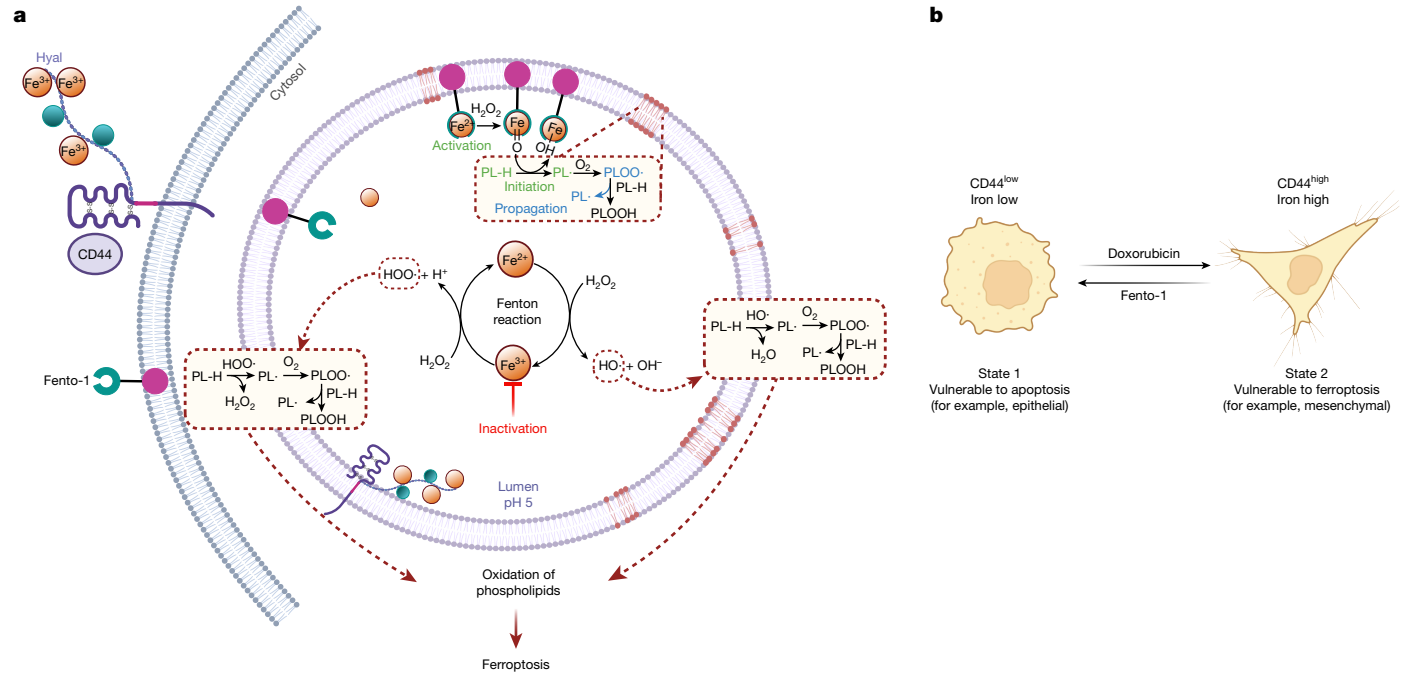

Fig. 4 | Iron in ferroptosis and cell-state transitioning. a, Iron is internalized by endocytosis. Lysosomal iron catalyses the production of oxygen-centred radicals from hydroperoxides under acidic conditions. These radicals can abstract a hydrogen from reactive phospholipids to produce carbon-centred radicals, which leads to oxidation products and ferroptosis. Inactivation of lysosomal iron protects cells against iron-redox chemistry. Activation of lysosomal iron triggers the oxidation of membrane lipids and ferroptosis. Hyal, hyaluronate **b**, Cell-state transitions induced by standard-of-care and pro-ferroptotic drugs. Illustrations in **a** and **b** were created using BioRender (https://biorender.com).

Nordlander–Costas[44] iron-activating ligand produced Fento-5, which exhibited similar cytotoxic and membrane-lipid-oxidation properties to those of Fento-1, albeit with a delayed cell-death response. This result reflects the distinct reactivity of the iron catalyst towards organic substrates[45] (Extended Data Fig. 7a–c). Together, these data indicate that pharmacological activation of lysosomal iron can trigger ferroptosis.

Iron activation reduces tumour growth

Next, we investigated the effect of lysosomal iron activation in disease-relevant models. To this end, we quantified the iron content of primary tumour tissues of distinct cancer types, including human PDAC, various human sarcoma subtypes and a mouse model of spontaneous breast cancer metastasis. These cancer tissues were chosen for their refractory nature to standard-of-care treatments and their capacity to form metastases, which contribute to poor clinical outcomes. Furthermore, these indications have been shown to be vulnerable to ferroptosis[8,29,30,46].

Total iron content was higher in cancer tissues of PDAC, undifferentiated pleomorphic sarcoma (UPS), angiosarcoma, liposarcoma and an epithelioid sarcoma compared with adjacent non-cancerous tissues, as measured by inductively coupled plasma mass spectrometry (ICP-MS) (Fig. 3a and Extended Data Fig. 8a). Moreover, the cellular iron load was higher in subpopulations of cancer cells with high CD44 expression (Fig. 3b and Extended Data Fig. 8b). Cells from freshly dissociated human primary PDAC and sarcoma tissues showed higher levels of redox-active lysosomal iron(II) in the CD44^{high} subpopulations of cancer cells than their CD44^{low} counterparts (Fig. 3c and Extended Data Fig. 8c). This result is consistent with previous findings showing that CD44 mediates iron endocytosis in cancer cells that have acquired a DTP phenotype[6]. In cells obtained from freshly dissociated human primary tumours, Fento-1 induced oxidation and lipolysis of membrane phospholipids, an effect that was antagonized by ferroptosis inhibitors (Fig. 3d Extended Data Fig. 8d–g, Supplementary Information and Supplementary Tables 9 and 10). Fento-1 also reduced the number of CD44^{high} cells in dissociated human PDAC and UPS, and this effect was antagonized by ferroptosis inhibitors (Fig. 3e and Extended Data Fig. 8h,i).

In primary PDAC cells and human PDAC-derived organoids, Fento-1 decreased cell viability more potently than standard-of-care drugs (Extended Data Fig. 9a,b) and synergized with these drugs in several primary cancer cells of human PDAC (Extended Data Fig. 9c,d). In a colony-formation assay, Fento-1 eradicated DTP of triple-negative breast cancer SUM159 cells overexpressing CD44 that survived treatment with doxorubicin (Fig. 3f). In line with this, Fento-1 was more potent against HT-1080 cells that were treated with low doses of doxorubicin for a prolonged period of time (Extended Data Fig. 9e). Under these conditions, HT-1080 cells adopted a distinct morphology and were characterized by increased levels of CD44 and ferritin together with upregulated mesenchymal markers (Extended Data Fig. 9f–h). These data suggest that cells exposed to doxorubicin increase CD44 to promote iron uptake and adopt a more mesenchymal phenotype to escape the doxorubicin-sensitive state. This adaptation leads to higher vulnerability to ferroptosis and sensitivity to Fento-1. Conversely, HT-1080 cells exposed to low doses of Fento-1 exhibited reduced CD44 and ferritin levels together with downregulated mesenchymal markers, which indicated that these cells adapt to lysosomal iron targeting (Fig. 2d and Extended Data Fig. 9g, i).

Regional lymph-node cancer lesions are predictors of distant metastases and mortality, and metastasizing cells are protected against ferroptosis in the lymph[47]. Measurements in mice showed that total iron levels in lymph fluid were lower than in blood and serum (Extended Data Fig. 10a). Thus, we evaluated the effect of Fento-1 on the viability of cancer cells directly in the lymphatics. To this end, we used the 4T1 immunocompetent mouse model of spontaneous triple-negative breast cancer metastases in Balb/c mice. Quantification of iron in cells isolated from intranodal 4T1 tumours showed a higher iron load in CD44^{high} cancer cells than in CD44^{low} subpopulations (Fig. 3g). These

CD44^{high} cells also exhibited a higher iron(II) redox activity in lysosomes (Extended Data Fig. 10b). When mice with intranodal 4T1 tumours were treated with Fento-1 (intralymphatic administration every other day), the mice showed reduced tumour growth, increased tumour-size-based survival end points and no adverse effects on body weight (Fig. 3h,i and Extended Data Fig. 10c–e). Further analyses of residual tumours indicated that Fento-1 induced oxidation of membrane lipids and the production of lysophospholipids, which affected preferentially CD44^{high} over CD44^{low} cancer-cell subpopulations (Fig. 3j,k, Extended Data Fig. 10f, Supplementary Information and Supplementary Tables 11 and 12). Together, these data show that Fento-1 induces ferroptosis in vivo by exploiting the higher abundance of lysosomal iron(II) in CD44^{high} cancer-cell subpopulations.

Discussion

Ferroptosis is a form of cell death resulting from the uncontrolled oxidation of membrane lipids. Where and how it is initiated in the cell remained unclear. Iron can react with hydroperoxides to initiate or propagate a radical chain reaction independently of enzymes. The lysosomal compartment is a crucial regulator of cellular iron homeostasis[6,24,48], and its acidic nature, together with the presence of reactive iron and hydrogen peroxide, provide an ideal chemical environment to catalyse the oxidation of membrane phospholipids (Fig. 4a). Specific cancer-cell subpopulations upregulate the iron-uptake protein CD44 to promote oxidative demethylation of repressive chromatin marks and to unlock the expression of genes that regulate cell-state transitions involved in cancer progression[6]. Thus, although higher iron levels enable these cells to acquire a DTP profile, this characteristic also inexorably confers vulnerability to ferroptosis[6,9] (Fig. 4b). The fact that CD44 also marks development, self-renewal, wound healing and immune-cell activation suggests that lysosomal iron also contributes to the induction of ferroptosis in these biological settings. Enhancing the redox activity of lysosomal iron through genetic interventions to eradicate cancer cells is challenging. Here we developed a phospholipid degrader that takes advantage of the higher iron load of specific cancer-cell subpopulations to induce ferroptosis by activating lysosomal iron(II) (Fig. 4a). Sublethal doses of this degrader triggered the acquisition of a ferroptosis-resistant cell state, which partially recapitulated features of epithelial cells (Fig. 4b). This result highlights the value of combining cell-state-specific drugs to treat cancer. The anticancer drug doxorubicin can induce damage to genomic DNA in proliferating cells, which, if unrepaired, triggers apoptosis[49]. Conversely, the ferroptosis-resistant cell state, which is characterized by the upregulation of ferroptosis suppressors, epoxide hydrolases, phospholipases and by increased lipid metabolism (Fig. 2d), can arise as a result of cells being able to efficiently repair damaged membranes.

This study shows that fine-tuning the redox activity of lysosomal iron provides control over membrane lipid oxidation, thereby supporting the idea that lysosomal iron is a trigger of ferroptosis. This knowledge can now inform the design of ferroptosis modulators. Fento-1 exhibits a distinct chemotype to investigate ferroptosis and provides a conceptual framework to target DTP cancer cells[38].

Online content

Any methods, additional references, Nature Portfolio reporting summaries, source data, extended data, supplementary information, acknowledgements, peer review information; details of author contributions and competing interests; and statements of data and code availability are available at https://doi.org/10.1038/s41586-025-08974-4.

1. Dixon, S. J. & Olzmann, J. A. The cell biology of ferroptosis. *Nat. Rev. Mol. Cell Biol.* **25**, 424–442 (2024).
2. Friedmann Angeli, J. P. et al. Inactivation of the ferroptosis regulator Gpx4 triggers acute renal failure in mice. *Nat. Cell Biol.* **16**, 1180–1191 (2014).
3. Bersuker, K. et al. The CoQ oxidoreductase FSP1 acts parallel to GPX4 to inhibit ferroptosis. *Nature* **575**, 688–692 (2019).
4. Doll, S. et al. FSP1 is a glutathione-independent ferroptosis suppressor. *Nature* **575**, 693–698 (2019).
5. Yang, W. S. & Stockwell, B. R. Synthetic lethal screening identifies compounds activating iron-dependent, nonapoptotic cell death in oncogenic-RAS-harboring cancer cells. *Chem. Biol.* **15**, 234–245 (2008).
6. Müller, S. et al. CD44 regulates epigenetic plasticity by mediating iron endocytosis. *Nat. Chem.* **12**, 929–938 (2020).
7. Solier, S. et al. A druggable copper-signalling pathway that drives inflammation. *Nature* **617**, 386–394 (2023).
8. Mai, T. T. et al. Salinomycin kills cancer stem cells by sequestering iron in lysosomes. *Nat. Chem.* **9**, 1025–1033 (2017).
9. Rodriguez, R., Schreiber, S. L. & Conrad, M. Persister cancer cells: iron addiction and vulnerability to ferroptosis. *Mol. Cell* **82**, 728–740 (2022).
10. Franca, G. S. et al. Cellular adaptation to cancer therapy along a resistance continuum. *Nature* **631**, 876–883 (2024).
11. Fenton, H. J. H. Oxidation of tartaric acid in presence of iron. *J. Chem. Soc.* **65**, 899–910 (1894).
12. Seiler, A. et al. Glutathione peroxidase 4 senses and translates oxidative stress into 12/15-lipoxygenase dependent- and AIF-mediated cell death. *Cell Metab.* **8**, 237–248 (2008).
13. Chen, X., Kang, R., Kroemer, G. & Tang, D. Organelle-specific regulation of ferroptosis. *Cell Death Differ.* **28**, 2843–2856 (2021).
14. Zou, Y. et al. Plasticity of ether lipids promotes ferroptosis susceptibility and evasion. *Nature* **585**, 603–608 (2020).
15. Gao, M. et al. Role of mitochondria in ferroptosis. *Mol. Cell* **73**, 354–363 (2019).
16. Dixon, S. J. et al. Pharmacological inhibition of cystine–glutamate exchange induces endoplasmic reticulum stress and ferroptosis. *eLife* **3**, e02523 (2014).
17. Torii, S. et al. An essential role for functional lysosomes in ferroptosis of cancer cells. *Biochem. J.* **473**, 769–777 (2016).
18. Antoszczak, M. et al. Iron-sensitive prodrugs that trigger active ferroptosis in drug-tolerant pancreatic cancer cells. *J. Am. Chem. Soc.* **144**, 11536–11545 (2022).
19. von Krusenstiern, A. N. et al. Identification of essential sites of lipid peroxidation in ferroptosis. *Nat. Chem. Biol.* **19**, 719–730 (2023).
20. Jiang, X., Stockwell, B. R. & Conrad, M. Ferroptosis: mechanisms, biology and role in disease. *Nat. Rev. Mol. Cell Biol.* **22**, 266–282 (2021).
21. Cañeque, T., Müller, S. & Rodriguez, R. Visualizing biologically active small molecules in cells using click chemistry. *Nat. Rev. Chem.* **2**, 202–215 (2018).
22. Zilka, O. et al. On the mechanism of cytoprotection by ferrostatin-1 and liproxstatin-1 and the role of lipid peroxidation in ferroptotic cell death. *ACS Cent. Sci.* **3**, 232–243 (2017).
23. Shah, R., Farmer, L. A., Zilka, O., Van Kessel, A. T. M. & Pratt, D. A. Beyond DPPH: use of fluorescence-enabled inhibited autoxidation to predict oxidative cell death rescue. *Cell Chem. Biol.* **26**, 1594–1607 (2019).
24. Schonberg, D. L. et al. Preferential iron trafficking characterizes glioblastoma stem-like cells. *Cancer Cell* **28**, 441–455 (2015).
25. Basuli, D. et al. Iron addiction: a novel therapeutic target in ovarian cancer. *Oncogene* **36**, 4089–4099 (2017).
26. Elgrishi, N. et al. A practical beginner's guide to cyclic voltammetry. *J. Chem. Ed.* **95**, 197–206 (2018).
27. Wei, Y., Aydin, Z., Zhang, Y., Liu, Z. & Guo, M. A turn-on fluorescent sensor for imaging labile Fe^{3+} in live neuronal cells at subcellular resolution. *ChemBioChem* **13**, 1569–1573 (2012).
28. Niwa, M., Hirayama, T., Okuda, K. & Nagasawa, H. A new class of high-contrast Fe(II) selective fluorescent probes based on spirocyclized scaffolds for visualization of intracellular labile iron delivered by transferrin. *Org. Biomol. Chem.* **12**, 6590–6597 (2014).
29. Viswanathan, V. S. et al. Dependency of a therapy-resistant state of cancer cells on a lipid peroxidase pathway. *Nature* **547**, 453–457 (2017).
30. Hangauer, M. J. et al. Drug-tolerant persister cancer cells are vulnerable to GPX4 inhibition. *Nature* **551**, 247–250 (2017).
31. Günthert, U. et al. A new variant of glycoprotein CD44 confers metastatic potential to rat carcinoma cells. *Cell* **65**, 13–24 (1991).
32. Cañeque, T. et al. Synthesis of marmycin A and investigation into its cellular activity. *Nat. Chem.* **7**, 744–751 (2015).
33. Chen, M. S. & White, M. C. A predictably selective aliphatic C-H oxidation reaction for complex molecule synthesis. *Science* **318**, 783–787 (2007).
34. Hertzberg, R. P. & Dervan, P. B. Cleavage of double helical DNA by methidium-propyl-EDTA-iron(II). *J. Am. Chem. Soc.* **104**, 313–315 (1982).
35. Schreiber, S. L. The rise of molecular glues. *Cell* **184**, 3–9 (2021).
36. Qiu, B. et al. Phospholipids with two polyunsaturated fatty acyl tails promote ferroptosis. *Cell* **187**, 1177–1190 (2024).
37. Rodriguez, R. et al. Metal ion signaling in biomedicine. *Chem. Rev.* **125**, 660–744 (2025).
38. Marine, J. C., Dawson, S. J. & Dawson, M. A. Non-genetic mechanisms of therapeutic resistance in cancer. *Nat. Rev. Cancer* **20**, 743–756 (2020).
39. Yin, H., Xu, L. & Porter, N. A. Free radical lipid peroxidation: mechanisms and analysis. *Chem. Rev.* **111**, 5944–5972 (2011).
40. Dai, E. et al. A guideline on the molecular ecosystem regulating ferroptosis. *Nat. Cell Biol.* **26**, 1447–1457 (2024).
41. Pamplona, R. Membrane phospholipids, lipoxidative damage and molecular integrity: a causal role in aging and longevity. *Biochim. Biophys. Acta* **1777**, 1249–1262 (2008).
42. Sezgin, E., Levental, I., Mayor, S. & Eggeling, C. The mystery of membrane organization: composition, regulation and roles of lipid rafts. *Nat. Rev. Mol. Cell Biol.* **18**, 361–374 (2017).
43. Abdulla, N., Vincent, C. T. & Kaur, M. Mechanistic insights delineating the role of cholesterol in epithelial mesenchymal transition and drug resistance in cancer. *Front. Cell Dev. Biol.* **9**, 728325 (2021).
44. Mitra, M. et al. Highly enantioselective epoxidation of olefins by H_2O_2 catalyzed by a non-heme Fe(II) catalyst of a chiral tetradentate ligand. *Dalton Trans.* **48**, 6123–6131 (2019).

45. Fürstner, A. Iron catalysis in organic synthesis: a critical assessment of what it takes to make this base metal a multitasking champion. *ACS Cent. Sci.* **2**, 778–789 (2016).
46. Badgley, M. A. et al. Cysteine depletion induces pancreatic tumor ferroptosis in mice. *Science* **368**, 85–89 (2020).
47. Ubellacker, J. M. et al. Lymph protects metastasizing melanoma cells from ferroptosis. *Nature* **585**, 113–118 (2020).
48. Rizzollo, F., More, S., Vangheluwe, P. & Agostinis, P. The lysosome as a master regulator of iron metabolism. *Trends Biochem. Sci.* **46**, 960–975 (2021).
49. Rodriguez, R. et al. Small-molecule-induced DNA damage identifies alternative DNA structures in human genes. *Nat. Chem. Biol.* **8**, 301–310 (2012).

Methods

Ethics

Fresh tumour samples were obtained by surgery from patients at Paul Brousse and Institut Curie care centres. All patients provided written informed consent for use of tumour samples. The study was approved by institutional regulatory boards (no. 587 and DATA190160). All cLip-1 in vivo experiments were performed in compliance with the German Animal Welfare Law and were approved by the Institutional Committee on Animal Experimentation and the Government of Upper Bavaria (no. ROB-55.2-2532.Vet_02-18-13). All intranodal injection mouse experiments complied with all relevant ethical regulations and were performed according to protocols approved by the Institutional Animal Care and Use Committee at Harvard T. H. Chan School of Public Health (protocol IS00003460). For mouse lymph and blood collection, animal experiments were performed in accordance with the European Community guidelines for the care and use of animals. Animal experiments were performed in agreement with the French guidelines for animal handling and approved by local ethics committees (agreement no. 16487-2018082108541206 v3).

Chemical synthesis

Starting materials were purchased at the highest commercial quality and used without further purification unless otherwise stated. Anhydrous solvents were obtained by passing the degassed solvents through molecular sieves and activated alumina columns. Reactions were monitored by thin layer chromatography (TLC) using aluminium plates coated with silica gel or neutral aluminium oxide from Merck (60 F_{254}). TLC plates were visualized by UV or by treatment with a ninhydrin, ceric ammonium molybdate or potassium permanganate solution and heating. Reaction products were purified by flash column chromatography on silica gel 60 (230–400 mesh, Macherey Nagel) or aluminium oxide (activated neutral, Sigma-Aldrich) using a CombiFlash NextGen System and a preparative HPLC Quaternary Gradient 2545 equipped with a photodiode array detector 2998 (Waters) fitted with a reverse-phase column (XBridge BEH C18 OBD prep column 5 µm, 30 × 150 mm). NMR spectroscopy was performed using Bruker 400 or 500 MHz instruments. Spectra were run in methanol-d_4, dimethylsulfoxide-d_6, methylene chloride-d_2 or chloroform-d at 298 K or 310 K as indicated. ^{1}H chemical shifts δ are expressed in ppm using the residual non-deuterated solvent as an internal standard, and the coupling constants J are specified in Hz. The following abbreviations are used: bs, broad singlet; s, singlet; d, doublet; dd, doublet of doublets; ddd, doublet of doublet of doublets; dt, doublet of triplets; dq, doublet of quadruplets; q, quadruplet; t, triplet; td, triplet of doublets, quint., quintet; and m, multiplet. ^{13}C chemical shifts δ are expressed in ppm using the residual non-deuterated solvent as an internal standard. The purity of the final compounds was determined to be >98% by UPLC–MS. Low-resolution mass spectra were recorded using a Waters Acquity H-class equipped with a photodiode array detector and a SQ Detector 2 (UPLC-MS) fitted with a reverse-phase column (Acquity UPLC BEH C18 1.7 µm, 2.1 × 50 mm). High-resolution MS spectra were recorded on a Thermo Scientific Q-Exactive Plus equipped with a Robotic TriVersa NanoMate Advion. Procedures for the synthesis of small molecules are detailed in the Supplementary Information.

NMR titration experiments

^{1}H NMR spectra were recorded on a Bruker 500 MHz spectrometer at 310 K using Bruker Topspin (v.4.1.4) software and analysed using MestRenova (v.5.0.1-35756) or Bruker Topspin (v.4.1.4) software, and chemical shifts δ are expressed in ppm using the residual non-deuterated solvent signals as an internal standard. All the solutions were prepared in methanol-d_4. For recordings of ^{1}H NMR spectra of Lip-1 titrated with $FeCl_3$ before the addition of TFA or sodium deuteroxide, 0.1–1 eq. of a solution of $FeCl_3$ (Alfa Aesar, 12357, 2 µl, 145 mM) was added to a solution of Lip-1 (Sigma-Aldrich, SML1414, 1 mg in 600 µl). Then, a solution of TFA (Sigma-Aldrich, T6508, lot STBG1988V, 20 µl, 3 eq. 438 mM) or a solution of sodium deuteroxide (Eurisotop, D076Y, lot R2621, 1 µl) was added. For recordings of ^{1}H NMR spectra of Lip-1 and naphthalene titrated with $FeCl_3$, 0–1 eq. of a solution of $FeCl_3$ (3 µl, 97 mM) was added over a solution of Lip-1 (1 mg in 500 µl) and naphthalene (Sigma-Aldrich, 147141, 1 eq., 100 µl, 28.9 mM). After each addition, the solution was stirred for few seconds and NMR spectra were recorded.

Cyclic voltammetry

Cyclic voltammetry[26] experiments were performed with a three-electrode cell. A saturated calomel electrode was used as reference, a steady glassy carbon electrode of diameter 3 mm was selected as the working electrode and a platinum wire as the counter-electrode. All cyclic voltammograms were recorded at room temperature with a µ-autolab III from Metrohm using Nova software (v.2.1) with a scan rate of 0.1 V s^{-1}. HPLC-grade acetonitrile and methanol were used for recordings. For all experiments, nBu$_4$NBF$_4$ in acetonitrile (0.1 M, 32.9 mg ml^{-1} stock solution) was used. A 10 ml of a stock solution of 1 mM $FeCl_3$ was prepared with 500 µl of 20 mM $FeCl_3$ solution in milliQ water and 9.5 ml acetonitrile. Then, 5 µl (0.2 eq.) of a 40 mM stock solution of DFO, Lip-1, metcLip-1 (in-house) or alcLip-1 (in-house, solubilized in acetonitrile or methanol) was added to 1 ml of 1 mM $FeCl_3$ solution until 1.0 eq. was reached. After each addition, the solution was stirred for few seconds and voltammograms were recorded.

Molecular modelling

All structures were optimized using the Gaussian 16 (ref. 50) set of programs at the BHLYP/SVP level for all atoms (sextet spin state for iron(III) complexes) (Gaussian 16, revision C.01). Thermal correction to the Gibbs free energy was computed at 310.15 K. Single points at the UMP2/SVP level were performed using the SMD solvation model (methanol). The results presented are ΔG_{310} in kcal mol^{-1}.

Fluorimetry of the iron(II) probe RPE

A solution of RPE (in-house, 10 mM) in DMSO was diluted with a solution of acetonitrile–acetate buffer (10 mM, pH 5, 2:1, v/v) to reach a concentration of 10 µM. In a 96-well plate, three solutions of RPE (100 µl, 10 mM) and 10, 20 or 50 eq. of Lip-1 (in-house 1, 2 or 5 µl of 10 mM stock solution in methanol, respectively) were prepared and the solutions were mixed several times. Then, 10 eq. $FeCl_3$ (1.0 µl of stock solution in acetonitrile–acetate buffer (10 mM, pH 5, 2:1, v/v)) was added to each solution and mixed again. Spectra were recorded with a fluorimeter (Tecan spark 10 M) (λ_{ex} = 510 nm, λ_{em} = 540–700 nm) using SoftMax Pro 7.1 GxP software. UPLC-grade acetonitrile and methanol as well as milliQ water were used.

Fluorescence-enabled inhibited autoxidation (FENIX) assay

A conical centrifuge tube (15 ml) was charged with unilamellar liposomes of egg phosphatidylcholine (0.4 ml of a 20 mM suspension in PBS, 100 nm average diameter), 134 ml of a 12 mM solution of (E)-1,2-*bis*((2-methyldecan-2-yl)oxy)diazene (Cayman, 32742) in ethanol and PBS (7.46 ml of 12 mM at pH 7.4) and vortexed. STY-Bodipy (3.8 µl of a 1.74 mM solution in DMSO) was then added and the suspension vortexed once. The liposome–initiator–dye mixture was transferred to a reservoir, and using a 300 µl multichannel pipette, a 96-well plate (black, Nunc) was charged with the mixture (295 µl per well). Test compounds (5 µl of a 0.24 mM solution in acetonitrile) were added to bring the final volume to 300 µl. The contents of the wells were manually mixed using a multichannel pipette and then mixed in a microplate reader for 1 min at 37 °C, after which the oxidation of STY-Bodipy was monitored by fluorescence ($\lambda_{ex}/\lambda_{em}$ = 488/518 nm) overnight. Data were collected using Agilent BioTek Gen5 software (v.3.08.01).

Antibodies

Antibodies are annotated as follows: WB, western blot; FCy, flow cytometry; FI, fluorescence imaging; Hu, used for human samples; Ms, used for mouse samples. Dilutions are indicated. Any antibody validation by the manufacturer is indicated and can be found on the manufacturers' websites. Our antibody validation knockdown (KD) and/or knockout (KO) strategies for relevant antibodies are indicated. The following primary antibodies were used: AIFM2/FSP1 (Merck, MABC1638, clone 6D8-11, lot Q3745998, WB, 1:500, Hu, KD validated in-house); catalase (Cell Signaling, 12980T, clone D4P7B, lot 3, FI, 1:200, Hu); CD3-BV510 (BioLegend, 317332, clone OKT3, lot B263750, FCy, 1:100, Hu); CD31-PE-Cy7 (BioLegend, 303118, clone WM59, lot B276836, FCy, 1:100, Hu); CD31-BV605 (BioLegend, 303122, clone WM59, lot 331683, FCy, 1:100, Hu); CD31-BV605 (BioLegend, 102427, clone 390, lot B375532, FCy, 1:100, Ms); CD44 (Abcam, ab189524, clone EPR18668, lot 1014086-32, WB, 1:30,000, Hu, KO and KD validated in-house); CD44-AF647 (Novus Biologicals, NB500-481AF488, clone MEM-263, lot P158343, FCy, 1:100, Hu); CD44-AF647 (Novus Biologicals, NB500-481AF647, clone MEM-263, lot D145771, FCy, 1:100, Hu); CD44-AF647 (BioLegend, 103018, clone IM7, lot B317762, FCy, 1:100, Ms); CD45-BV785 (BioLegend, 304048, clone HI30, lot B339809, FCy, 1:100, Hu); CD45-BV510 (BioLegend, 368526, clone 2D1, lot B373428, FCy, 1:100, Hu); CD45-BV510 (BioLegend, 103138, clone 30-F11, lot B386738, FCy, 1:100, Ms); CD163-PerCP/Cyanine5.5 (BioLegend, 326512, clone RM3/1, lot B291202, FCy, 1:100, Hu); COXIV (Abcam, ab16056, lot GR3206555-1, WB, 1:1,000, Hu); cytochrome *c* (Cell Signaling, 12963S, clone 6H2.B4, lot 2, FI, 1:200, Hu); EEA1 (Abcam, ab70521, clone 1G11, lot GR315680-1, FI, 1:200, Hu, validated by immunocytochemistry/immunofluorescence by manufacturer); FAP-AF700 (R&D Systems, FAB3715N, clone 427819, lot AEVI020011, FCy, 1:100, Hu); FAP-AF750 (Bio-Techne, FAB3715S-100UG, clone 427819, lot 1718688, FCy, 1:100, Hu); ferritin (Abcam, ab75973, clone EPR300AY, lot 10136442-29, WB, 1:1,000, Hu, validated by WB by manufacturer); fibronectin (Abcam, ab45688, clone F14, lot 1016266-35, WB, 1:1,000, Hu); FTH1 (Santa Cruz Biotechnology, sc-376594, clone B-12, lot G2622, WB, 1:200, Hu); GPX4 (Abcam, ab125066, clone EPNCIR144, lot GR3369574-4, WB, 1:2,000, Hu, KO validated by manufacturer, KD validated in-house); 4-HNE (Abcam, ab48506, clone HNEJ-2, lot 1062274-2, FI, 1:200, Hu); IRP2 (Novus Biologicals, NB100-1798, lot D-4, WB, 1:1,000, Hu); Lamin A/C (Cell Signaling, 2032S, lot 6, WB, 1:1,000, Hu); LAMP1 (Cell Signaling, 9091S, clone D2D11, lot 7, FI, 1:200, Hu); LAMP1 (Santa Cruz Biotechnology, sc-20011, clone H4A3, FI, 1:100, Ms); LAMP1 (Abcam, ab24170, lot GR3235630-1, WB, 1:1,000, Hu); LAMP2 (Abcam, ab25631, clone H4B4, lot 1011336-1, FI, 1:200, Hu); LAMP2 (Thermo Fisher Scientific, MA1-205, clone H4B4, lot YG377512, WB, 1:1,000, Hu); LIMPII (Proteintech, 27102-1-AP, WB, 1:1,000, Hu); NCOA4 (Abcam, ab86707, lot GR3244520-13, WB, 1:10,000, Hu, KD validated in-house); NDUFS1 (Abcam, ab157221, clone EPR11522(B), lot YJ110907DS, WB, 1:1,000, Hu); PDIA3 (Sigma-Aldrich, AMAB90988, clone CL2444, lot 02879, FI, 1:200, Hu; WB, 1:1,000, Hu); MHCII-APC/Cyanine7 (BioLegend, 107628, clone M5/114.12.2, lot B370049, FCy, 1:100, Ms); RCAS1 (Cell Signaling, 12290S, clone D2B6N, lot 1, FI, 1:200, Hu, WB, 1:1,000, Hu); SLC7A11/xCT (Cell Signaling, 12691S, clone D2M7A, lot 5, WB, 1:1,000, Hu, KD validated in-house); SOX4 (Santa Cruz Biotechnology, sc-518016, clone B-7, lot G2023, WB, 1:200, Hu); TFR1 (Life Technologies, 13-6800, clone H68.4, lot VJ313549, WB, 1:1,000, Hu, KO and KD validated in-house); TFR1-APC-AF750 (Beckman Coulter, A89313, clone YDJ1.2.2, lot 200060, FCy, 1:100, Hu); TFR1-PE (BioLegend, 334106, clone CY1G4, lot B364886, FCy, 1:100, Hu); γ-tubulin (Sigma-Aldrich, T5326, clone GTU-88, lot 0000140390, WB, 1:1,000, Hu, validated by manufacturer); and vimentin (Cell Signaling, 5741S, clone D21H3, lot 8, WB, 1:1,000, Hu). The following secondary antibodies were used: Alexa Fluor 647 anti-mouse (Abcam, ab150115, tissue labelling, 1:500, Ms); Alexa Fluor 647 anti-mouse (Invitrogen, A21237, lot 1485202, FI, 1:1,000, Hu); Alexa Fluor 647 anti-rabbit (Invitrogen, A21246, lot 2714437, FI, 1:1,000, Hu); donkey anti-rabbit IgG-H+L HRP-conjugated (Bethyl Laboratories, A120-108P, lot 13, WB, 1:10,000, Hu); goat anti-mouse IgG-H+L HRP-conjugated (Bethyl Laboratories, A90-116P, lot 39, WB, 1:10,000, Hu); and goat anti-rat IgG-H+L HRP-conjugated (Invitrogen, 31470, WB, 1:10,000, Hu).

Cell culture

HT-1080 cells, MDA-MB-231 and 4T1 cells were obtained from the ATCC. Dissociated human and mouse tumour cells and 4T1 cells were cultured in RPMI 1640 supplemented with GlutaMAX (Gibco, 61870010) and 10% FBS (Eurobio Scientific, CVFSVF00-01). HT-1080 cells were cultured in Dulbecco's Modified Eagle Medium (DMEM)–GlutaMAX (Gibco, 61965059) supplemented with 10% FBS (Gibco, 10270-106) and penicillin–streptomycin (BioWhittaker/Lonza, DE17-602E). MDA-MB-231 cells were cultured in DMEM–GlutaMAX supplemented with pyruvate (Thermo Fisher Scientific, 31966021) and supplemented with 10% FBS and penicillin–streptomycin (Gibco, 15140148). FC1242 and FC1245 mouse pancreatic cancer cells, 4a cells and human pancreatic hMIA-2D cells were a gift from the Tuveson laboratory (Cold Spring Harbor Laboratory) and were cultured in DMEM–GlutaMAX supplemented with 10% FBS and penicillin–streptomycin. Primary human pancreatic PDAC024T, PDAC030T, PDAC053T, PDAC054T, PDAC084T, PDAC090T and PDAC211T cells were grown in serum-free ductal medium DMEM/F12 (Gibco, 10565018) supplemented with 0.61 g in 500 ml nicotinamide (Sigma-Aldrich, 3376), 2.50 g in 500 ml glucose (Sigma-Aldrich, G6152), 1:200 ITS+ (Corning, 354352), 1:20 Nu-serum IV (Corning, 355104), 100 ng ml^{-1} cholera toxin, 1 μM dexamethasone (Sigma-Aldrich, D4902), 50 nM 3,3′,5-triiodo-L-thyronine (Sigma-Aldrich, T6397) and penicillin–streptomycin). Fresh bovine pituitary extract (Gibco, 13028-014, 22.7 ng ml^{-1}) and 50 ng ml^{-1} animal-free recombinant human EGF (Thermo Fisher Scientific, AF-100-15-1MG) were added to new medium when cells were split or plated. SUM159 cells were cultured in Ham F12, GlutaMAX (Gibco, 31765035), NEAA (Gibco, 11140050), antibiotic–antimycotic (Thermo Fisher Scientific, 15240062), insulin (Humalog, Cip: 3400934142680), hydrocortisone (Sigma-Aldrich, H0888-10G) and 5% FBS (Thermo Fisher Scientific, A5256701). Primary lung circulating tumour cells (Celprogen, 36107-34CTC, lot 219411, sex: female) and primary colon circulating tumour cells (Celprogen, 36112-39CTC, lot 20188, sex: female) were grown using stem cell complete medium (Celprogen, M36102-29PS) until the third passage. Circulating cancer cells were grown in stem cell ECM T75-flasks (Celprogen, E77002-07-T75). Pfa1 cells were cultured using DMEM high glucose and 10% FBS, 2 mM L-glutamine and 1% penicillin–streptomycin.

Dissociation of human and mouse tumour samples

Tumour samples were collected from patients after surgery. Tumour samples were from patients with PDAC, UPS, liposarcoma, angiosarcoma, epithelioid sarcoma or PDAC liver metastasis. Tumours were dissociated using a human tumour dissociation kit (Miltenyi, 130-095-929) according to the manufacturer's protocol. In brief, tumours were cut into small pieces (1–5 mm), put into the enzyme mix in RPMI and dissociated using gentleMACS Octo Dissociator with Heaters (Miltenyi) with the appropriate gentleMACS program (37C_h_TDK). Per tumour sample, 9.4 ml RPMI medium was used with the corresponding enzyme concentration according to the manufacturer's protocol. Mouse tumour samples were dissociated using a mouse tumour dissociation kit (Miltenyi, 130-096-730) according to the manufacturer's protocol. Tumours were cut into small pieces (1–5 mm), put into the enzyme mix in RPMI and dissociated using gentleMACS Octo Dissociator with Heaters (Miltenyi) with the appropriate gentleMACS program (37C_m_TDK). Subsequently, the dissociated tumour suspension was applied to a MACS SmartStrainer (30 μm) (Miltenyi). Samples were diluted with 1× PBS and centrifuged at 300*g*. The cell pellet was resuspended in RPMI

(with 10% FBS and penicillin–streptomycin), and cells were counted using an automated cell counter (Entek). The total population of dissociated cells is denoted as dissociated tumour cells, whereas the subpopulation corresponding to cancer cells from tumours by negative selection (see the section 'Flow cytometry') is denoted as dissociated tumour cancer cells.

Establishment of xenograft-derived primary cell cultures

These models were originally derived from patient-derived xenograft (PDX) models. The PDX fragments designated for cell culture were processed in a biosafety chamber. After mincing to small pieces, they were treated with collagenase type V (Sigma-Aldrich, C9263) and trypsin–EDTA (Gibco, 25200-056) and suspended in DMEM supplemented with 1% w/w penicillin–streptomycin and 10% FBS. After centrifugation, cells were resuspended in serum-free ductal medium adapted from previous protocols[51] at 37 °C in a 5% CO_2 incubator. Amplified cells were stored in liquid nitrogen. Cells were weaned from antibiotics for more than 48 h before testing. This protocol was used to establish the cells designated as PDAC024T, PDAC030T, PDAC053T, PDAC054T, PDAC084T, PDAC090T and PDAC211T.

Establishment of xenograft-derived pancreatic organoids

Xenograft-derived pancreatic organoid (XDPO) models were originally derived from PDX models. Xenografts were split into several small pieces and processed in a biosafety chamber. After mincing to small pieces, they were treated using a human tumour dissociation kit (Miltenyi, 130-095-929). Undigested pellets were digested with accutase (Thermo Fisher Scientific, A1110501) at 37 °C for 30 min. The pancreatic tissue slurry was transferred to a 100 µm tissue strainer and then placed into a 12-well plate coated with 150 µl GFR Matrigel (Corning, 354230). The samples were cultured in pancreatic organoid feeding medium, which consisted of advanced DMEM/F12 supplemented with 10 mM HEPES (Thermo Fisher Scientific, 15630056), 1× GlutaMAX (Thermo Fisher Scientific, 35050087), penicillin–streptomycin, 100 ng ml^{-1} animal-free recombinant human FGF10 (Thermo Fisher Scientific, 500-P151G-50UG), 50 ng ml^{-1} animal-free recombinant human EGF (Thermo Fisher Scientific, AF-100-15-1MG), 100 ng ml^{-1} recombinant human noggin (Bio-Techne, 6057-NG), WNT3A-conditioned medium (30% v/v), RSPO1-conditioned medium (10% v/v), 10 nM human gastrin 1 (Sigma-Aldrich, SCP0152), 10 mM nicotinamide (Sigma-Aldrich, N0636), 1.25 mM *N*-acetylcysteine (Sigma-Aldrich, A9165), 1× B27 (Thermo Fisher Scientific, 17504001), 500 nM A83-01 (Tocris, 2939/10) and 10.5 µM Y27632 (Tocris, 1254/1). The plates were incubated at 37 °C in a 5% CO_2 incubator, and the medium was changed every 3–4 days. This procedure was used to generate the XDPOs PDAC009T, PDAC003T, PDAC117T and PDAC372T.

Chemosensitivity profiling of XDPOs

For chemosensitivity profiling, XDPOs were plated into 96-well plates and then subjected to incrementally increasing concentrations of drugs. Cell viability was measured 72 h after treatment using CellTiter-Glo 3D (Promega, G9683). Doubling times of XDPO viability for vehicle-treated conditions were calculated on days 0 and 3. The ratio of day 3 over day 0 corresponded to the replication rate (RR) of the cells at 72 h. Doubling times were calculated using the formula $72 \times 2/RR$. Fluorescence and luminescence values were quantified using a Tristar LB941 plate reader (Berthold Technologies). Each experiment was performed at least three times with at least three replicates.

Cell death and viability assays

Cell death assay with Annexin-V and propidium iodide. PDAC053T cells were seeded in 6-well plates at a density of 2×10^5 cells per well. RSL3 (Sigma-Aldrich, SML2234, 0.1, 0.5, 2 and 10 µM) was added together with Lip-1 (1 µM), cLip-1 (1 µM), alcLip-1 (10 µM) or metcLip-1 (10 µM) on the following day. After 24 h, the medium was recovered and cells were trypsinized. Cells were collected, pelleted along with the recovered medium and washed with 1× PBS. Next, 100 µl of 1× Annexin-V binding buffer containing Annexin-V and propidium iodide was added according to the manufacturer's protocol (Annexin-V flow cytometry kit, Thermo Fisher Scientific, V13242). 1× PBS buffer containing 10% FBS and EDTA (0.1% v/v) was added for flow cytometry. Flow cytometry was performed using an AttuneTM NxT flow cytometer and data were analysed using FlowJo.

Cell death assay with Annexin-V and Sytox blue. PDAC053T cells were seeded in 6-well plates at a density of 2×10^5 cells per well. The following day, cells were transfected with siRNA as detailed in the section 'RNA interference'. Medium was replaced 6 h after transfection. Three days after transfection, cells were treated with the indicated concentrations of Fento-1 for 6 h. Cell death was analysed using Annexin-V AF488 (Thermo Fisher Scientific, A13201) and Sytox blue (Thermo Fisher Scientific, S34857). Flow cytometry was performed using an AttuneTM NxT flow cytometer and data were analysed using FlowJo.

LDH assay. LDH release was measured using a Cytotoxicity detection kit (Sigma-Aldrich, 11644793001) according to the manufacturer's protocol in a 96-well plate. Cell viability was assessed using a CellTiterGlo 2.0 (Promega, G9241) or CellTiter blue (Promega, G8081) kit according to the manufacturer's protocol in a 96-well plate. In brief, 4,000 cells (HT-1080, PDAC053T or 4T1) were seeded per well in clear-bottom and darkened 96-well plates (Greiner, 655090, lot E23063EG) 24 h before the experiment. Cells were then pretreated for 2 h with Lip-1 (10 µM), cLip-1 (10 µM), ferrostatin-1 (SML0583, 10 µM), DFO (Sigma-Aldrich, D9533, 100 µM), deferasirox (Cayman chemical, 16753, 10 µM), deferiprone (Sigma-Aldrich, Y0001976, 100 µM), α-tocopherol (100 µM), vitamin K3 (Sigma-Aldrich, M5625-25G, 10 µM), Z-VAD-FMK (Enzo Life Sciences, ALX-260-020-M005, 50 µM) or necrostatin-1 (Sigma-Aldrich, N9037, 20 µM). Subsequently, Fento-1 (10 µM, 6 h) was added. For dose–response measurements, cells were treated with varying amounts of the respective molecule for the time indicated. Samples were processed as detailed in the manufacturer's protocols and data were recorded on a SpectraMax ID3 plate reader (Molecular Devices). For standard-of-care cell-viability measurements, cells were plated at 2,000 cells per well 24 h before the experiment. Cells were incubated with serial dilutions of Fento-1, irinotecan (Sigma-Aldrich, I1406), 5-fluorouracil (5-FU; Alfa Aesar, A13456-06) or oxaliplatin (Bio-Techne, 2623) for 72 h.

MTT assay. Cells were plated in a 96-well plate, incubated for 24 h and then pretreated with Lip-1 (1 µM) for 10 min before treatment with vehicle control or Fento-1 for 24 h. After 24 h, the medium was carefully removed and 50 µl serum-free medium and 50 µl MTT solution (Cayman Chemical, 21795) were added per well. The plate was incubated at 37 °C for 3 h. After incubation, the solution was removed and 100 µl DMSO was added per well. The plate was covered and shaken on an orbital shaker for 15 min before reading the absorbance on a plate reader (OD = 590). For RSL3 treatment, Pfa1 cells were seeded in 96-well plates (2,000 cells per well) and cultured overnight. The following day, cells were treated with RSL3 (500 nM) and the indicated small molecules in serial dilution. For 4-OH-TAM treatment, Pfa1 cells were seeded in 96-well plates (500 cells per well) with 4-OH-TAM (1 µM) and a dilution series of the indicated compounds. After 24 h (for RSL3) or 72 h (for 4-OH TAM) incubation, cell viability was assessed using resazurin as a cell-viability indicator. Fluorescence intensity was measured at $\lambda_{ex}/\lambda_{em}$ = 540/590 nm using a SpectraMax iD5 microplate reader with SoftMax Pro v.7 software (Molecular Devices) after 4 h of incubation in standard cell culture medium containing 0.004% resazurin.

Alamar blue assay. The effect of sublethal doses of Fento-1 together with RSL3 or ML210 on cell viability was assessed using the Alamar blue assay. To determine cell viability, 3,000 HT-1080 or MDA-MB-231

cells were seeded in a 96-well plate with standard medium (10% FBS and 1% penicillin–streptomycin) around 20 h before treatment. Cells were pretreated with 0.5 µM Fento-1 and/or 0.5 µM Lip-1 for 1 h. After 48 h of RSL3 or ML210 (Sigma-Aldrich, SML0521-5MG) treatment, a cell-viability assay was performed. Alamar blue solution was made by dissolving 0.5 g resazurin sodium salt (Sigma-Aldrich, 263-718-5) in 100 ml sterile PBS and sterile filtrated through a 0.22 µm filter. After 2 h of incubation, viability was assessed by measuring the fluorescence using a 540 ± 20 nm excitation filter and a 590 ± 20 nm emission filter on a Spark microplate reader (Tecan).

IncuCyte measurements of the cytotoxicity of Fento-1. Kinetics of cell death were collected using an IncuCyte bioimaging platform (Essen). Cells were seeded in 96-well plates (3,000 cells per well) 1 day before treatment. Cells were treated with Fento-1 in combination with Lip-1 (0.5 µM) in FluoroBrite DMEM medium (Thermo Fisher Scientific A1896701). Four images per well were captured every hour, analysed and data were averaged. Cell death was measured on the basis of the incorporation of DRAQ7 (0.1 µM, Cell Signaling, 7406S). Data were collected as count of DRAQ7-positive cells per total number of cells in each condition.

Generation of HT-1080 DTP cancer cells

About 2×10^6 HT-1080 cells were plated in T75 flasks 24 h before adding doxorubicin (Clinisciences, HY-15142, 25 nM). Flasks were washed with 1× PBS buffer, and medium containing doxorubicin (25 nM) was replaced every 3–4 days. After 30 days of treatment with doxorubicin, 4,000 cells were plated in 96-well plates per well to assess cell viability after treatment with Fento-1.

Clonogenic survival analysis

About 1×10^6 SUM159 cells were plated in 10 cm dishes in complete growth medium. Seeded cells were treated with doxorubicin at the half maximal inhibitory concentration (IC_{50}) concentration (150 nM). After 72 h, cells were washed and treated with Fento-1 (5 µM, 72 h) or 0.2% DMSO without drug. After 72 h, cells were washed, and the treatment was replaced with complete growth medium. After 10–15 days, cells were washed, fixed and stained with acetic acid and methanol (1:7) and 1% Coomassie blue 1 h at room temperature. The number of colonies with >100 cells was counted using a SCAN1200 colony counter (Interscience).

Drug synergy analysis

Cells were plated in 96-well plates (5,000 cells per well). After 12 h, cells were treated with 5-FU (Selleckchem, S1209, 5 µM), gemcitabine (Selleckchem, S1714, 1 µM), oxaliplatin (Selleckchem, S1224, 20 µM), paclitaxel (Selleckchem, S1150, 0.1 µM) or SN-38 (Selleckchem, S4908, 0.1 µM) alone or in combination with Fento-1 (1.5 µM) for 72 h. Cell viability was estimated after the addition of PrestoBlue (Life Technologies, A13261) for 2 h following the manufacturer's instructions. To determine the existence of a synergistic effect on cell proliferation or cell viability between standard-of-care drugs and Fento-1, we used the software SynergyFinder. For the analysis of this effect, the ZIP score was used as a model for calculating synergy[52].

cLip-1 treatment in vivo

Mice were kept under standard conditions with water and food ad libitum and in a controlled environment (22 ± 2 °C, 55 ± 5% humidity, 12 h light–dark cycle). For animal studies, C57BL6/J mice were randomized into separate cages. Mice aged 12–24 weeks and sex-matched were used for all experiments. For the survival cohort study, *Rosa26-creERT2;Gpx4*$^{f/f}$ mice were intraperitoneally treated with tamoxifen (Sigma-Aldrich, T2859, 2 mg per day dissolved in Myglyol 812) on days 0 and 1 for deletion of *Gpx4* in the whole body except in the brain[2]. From day 2, cLip-1 (in-house, 10 mg per kg per day dissolved in 1× PBS containing 20% PEG400 and 5% Solutol HS15) or vehicle was intraperitoneally administered to the mice each day until the completion of the survival study. For histochemistry analyses, *Rosa26-creERT2;Gpx4*$^{f/f}$ mice treated with intraperitoneal tamoxifen injection (2 mg per day on days 0 and 1) were used. On day 7, cLip-1 (in-house, 10 and 100 mg kg^{-1}) or vehicle was intraperitoneally injected into the mice. At 1 h after the injection, mice were euthanized, and the kidney and liver samples were processed as described in the section 'Small-molecule labelling using click chemistry'.

Isolation of blood, serum and lymphatic fluid from mice

Balb/c mice (25-week-old females) were purchased from Charles River and housed at the CRCM animal core facility and randomized into separate cages. Mice aged 12–24 weeks and sex-matched were used for all experiments. Mice were housed under sterile conditions with sterilized food and water provided ad libitum and maintained on a 12 h light–dark cycle and 22 ± 2 °C, 55 ± 5% humidity. Mice were not subjected to any procedures before collection of lymph, blood and serum.

For lymph sample collection, 30 min before the beginning of the experiment, buprenorphine (Buprecare), an analgesic, was administered by intraperitoneal injection (0.5 mg kg^{-1}). Mice were euthanized by intraperitoneal injection of a ketamine–xylazine combination (ketamine 100 mg kg^{-1} (Imalgène) and xylazine 10 mg kg^{-1} (Rompum); 20 µl g^{-1}). After cutaneous and peritoneal incisions, the lymph in the intestinal lymph trunk[53] was collected using a glass capillary. Lymph samples were placed in cryotubes, frozen at −20 °C and stored at −80 °C.

For blood and serum sample collection, after lymph collection, we performed a terminal cardiac puncture (23 G needle with a 1–2 ml syringe) by thoracotomy to collect a large volume of blood without anticoagulants. Next, 100–200 µl of the blood sample was placed in a vial, frozen at −20 °C and stored at −80 °C. The rest of the blood sample was left to stand at room temperature for 30 min, then centrifuged at 2,000*g* for 15 min. The supernatant (serum) was collected in a vial, frozen at −20 °C and stored at −80 °C.

Quantitative proteomics

Sample preparation. HT-1080 cells were grown in 148 cm^2 round dishes at 70% confluence and treated with Fento-1 (1 µM, 48 h). Whole-cell extracts were collected and then centrifuged at 500*g* for 5 min at 4 °C, washed 3× with ice-cold 1× PBS and lysed using lysis buffer (8 M urea, 200 mM sodium bicarbonate and complete protease inhibitor cocktail (Roche, 000000011697498001)). Lysis was achieved by incubating on a rotating wheel at 25 r.p.m. for 45 min at 4 °C. Lysates were centrifuged at 20,000*g* for 20 min at 4 °C, and the supernatant that contained total protein was used for quantitative global proteomic analysis. In brief, 30 µg total protein cell lysate was reduced by incubating with 5 mM dithiothreitol at 57 °C for 30 min and then alkylated with iodoacetamide (10 mM, 30 min) at room temperature in the dark. Trypsin/LysC (Promega) was added at 1:100 (w/w) enzyme to substrate. Digestion was performed overnight at 37 °C. Samples were then loaded onto custom-made C18 StageTips (AttractSPE Disk Bio C18-100.47.20, Affinisep) for desalting. Peptides were eluted using a ratio of 40:60 acetonitrile and H_2O + 0.1% formic acid and vacuum concentrated to dryness with a SpeedVac. Peptides were reconstituted in 0.3% TFA before liquid chromatography–tandem mass spectrometry (LC–MS/MS).

LC–MS/MS analyses. LC was performed with a Vanquish Neo LC system (Thermo Scientific) coupled to an Orbitrap Astral mass spectrometer, interfaced by a Nanospray Flex ion source (Thermo Scientific). Peptides were injected onto a C18 column (75 µm inner diameter × 50 cm double nanoViper PepMap Neo, 2 µm, 100 Å, Thermo Scientific) regulated at 50 °C and separated with a linear gradient from 100% buffer A (100% H_2O and 0.1% formic acid) to 28% buffer B (100% acetonitrile and 0.1% formic acid) at a flow rate of 300 nl min^{-1} over 104 min. The instrument was operated in data-independent acquisition (DIA) mode. MS full

scans were recorded on the Orbitrap mass analyser in centroid mode for ranges 380–980 *m/z* with a resolution of 240,000, a normalized automatic gain control (AGC) target set at 500% and a maximum injection time of 5 ms. The DIAs in the Astral analyser were performed in centroid mode for a mass range of 380–980 *m/z* with a window width of 2 Da (without overlap), a maximum injection time of 3 ms and a normalized AGC target of 500% after fragmentation using higher-energy collisional dissociation (25% normalized collision energy).

Data processing. For identification, the data were searched against the *Homo sapiens* (UP000005640) UniProt database using Spectronaut (v.18.7 or v.19; Biognosys) by directDIA + analysis using default search settings. Enzyme specificity was set to trypsin, and a maximum of two missed cleavages were allowed. Carbamidomethyl was set as a fixed modification, and amino-terminal acetylation and oxidation of methionine were set as variable modifications. The resulting files were further processed using myProMS (v.3.10; https://github.com/bioinfo-pf-curie/myproms)[54]. For protein quantification, XICs from proteotypic peptides shared between compared conditions (TopN matching) with missed cleavages and carbamidomethylation were allowed. Median and scale normalization at the peptide level was applied on the total signal to correct the XICs for each biologically independent replicate ($n = 5$). To evaluate the significance of the change in protein abundance, a linear model (adjusted on peptides and biological replicates) was performed, and a two-sided *t*-test was applied on the fold change estimated by the model. The *P* values were then adjusted using the Benjamini–Hochberg false-discovery rate procedure. The MS proteomics raw data have been deposited to the ProteomeXchange Consortium through the PRIDE partner repository[55].

Intranodal mouse metastasis models and in vivo administration of Fento-1

Mouse breast cancer cells (4T1) were transplanted into 6–8-week-old female Balb/c mice (syngeneic with the 4T1 model). Mice were housed at the Harvard Medical School animal core facility and randomized into separate cages. Mice were housed under sterile conditions with sterilized food and water provided ad libitum and maintained on a 12 h light–dark cycle and 22 ± 2 °C, 55 ± 5% humidity. To perform injections into lymph nodes, the lymphatics were first traced by injecting 2% Evans Blue dye (Sigma-Aldrich, E2129) into the foot pedal 5 min before performing intranodal injections. After injecting Evans Blue dye, the mice were anaesthetized using isoflurane and a small (5–10 mm) incision was made in the region of the right popliteal lymph node. The lymph node was located on the basis of Evans Blue staining, immobilized with forceps, and 1–2 × 10^4 cells suspended in 1× PBS were injected in a volume of 10 µl into the popliteal lymph node using a 27 G Hamilton syringe. Injection into the lymph node was confirmed by visible swelling of the lymph node. The incision was closed using surgical glue (3M VetBond Tissue Adhesive, 1469SB) and the mice were closely monitored for signs of pain or distress. Once tumours were palpable in at least 75% of the mice (approximately 1 week after injection), 10 µl Fento-1 (0.003 mg per animal) or vehicle was delivered intralymphatically into the tumour-bearing lymph node every other day until the experimental end point. Intranodal tumour diameters were measured 3 times per week with calipers until any tumour in the mouse cohort reached 2.0 cm in its largest diameter, which was the predetermined experimental end point for these experiments. For all experiments, this maximum permitted tumour diameter was not exceeded. At that point, all mice in the cohort were euthanized, per approved protocols, for analyses of intranodal tumour diameter, tumour mass and other parameters. At the experimental endpoint, data on tumour formation were collected in a manner blinded to sample identity or treatment. For survival-curve determinations, tumour-sized-based survival rate methods were applied, with 1.5 cm as the recommended predetermined survival rate per ethically acceptable cut-off values for determining therapeutic efficacy in mouse studies[56]. Tumour sizes were measured in two dimensions, length (*x* axis) and width (*y* axis), with the *x* axis conventionally defined as the longest axis of the tumour. Tumour sizes are represented as tumour diameter (cm) or tumour volume (cm^3), as extrapolated by 0.5 × length × $width^2$, as indicated for each in vivo experiment. Tumour samples were frozen in 10% DMSO in FBS (1 °C min^{-1} until −80 °C) for subsequent cellular analyses. No formal randomization techniques were used. However, animals were allocated randomly to treatment groups and specimens were processed in an arbitrary order. For all experiments, mice were kept on a normal chow diet and fed ad libitum.

Fluorescence imaging

Cells were plated on coverslips and treated as indicated. Bodipy 665/676 (Thermo Fisher Scientific, B3932, 10 µM, 45 min), LysoTracker Deep Red (Thermo Fisher Scientific, L12492, 100 nM, 45 min), DND-189 LysoSensor (Thermo Fisher Scientific, L7535, 100 nM, 1 h), Liperfluo (Dojindo, L248, 1 µM, 1 h) and SQSS (in-house, 50 nM, 1 h) were added to live cells before fixation. For colocalization studies, cells were treated with Fento-1 (1 µM, 1 h) or marmycin (in-house, 1 µM, 1 h) at the indicated temperature 16 h after transduction. At 16 h after transduction the BacMam-transduced cells were treated with RSL3 (1 µM) for 15 min or for 3 h 15 min and then treated with Bodipy 665/676 for 45 min to give the final time points of 1 h and 4 h. For colocalization of lipid peroxides with lysosomes, cells were treated with RSL3 (1 µM) and either Bodipy 665/676 and DND-189 LysoSensor or Liperfluo and LysoTracker Deep Red for 1 h. To assess the fluorescence intensity of Fento-1 in the presence of α-tocopherol, cells were pretreated with α-tocopherol (Sigma-Aldrich, PHR1031, 100 µM, 2 h) and then with Fento-1 (1 µM). Cells were then washed 3 times with 1× PBS, fixed with 2% paraformaldehyde in 1× PBS for 12 min and then washed 3 times with 1× PBS. For antibody staining, cells were permeabilized with 0.1% Triton X-100 in 1× PBS for 5 min and washed 3 times with 1× PBS. Subsequently, cells were blocked in 2% BSA (Euromedex, 04-100-812-E), 0.2% Tween-20 and 1× PBS (blocking buffer) for 20 min at room temperature. Cells were incubated with the relevant antibody in blocking buffer for 1 h at room temperature, washed 3 times with 1× PBS and were incubated with secondary antibodies for 1 h. Finally, coverslips were washed 3 times with 1× PBS and mounted using Vectashield containing DAPI (Vector Laboratories, H-1200-10). Bodipy 665/676 and Liperfluo-treated cells were fixed using ice-cold reagents and placed at 4 °C immediately after mounting on coverslips and imaged. Fluorescence images were acquired using a Deltavision real-time microscope (Applied Precision), a thunder microscope (Leica) or an Apotome Weiss microscope with Deltavision imaging software, Thunder Leica image acquisition software or Apotome Zeiss Imaging software, respectively. A ×40/1.4NA, ×60/1.4NA or ×100/1.4NA objective was used for acquisitions, and all images were acquired as *z* stacks. Images were deconvoluted using SoftWorx (ratio conservative, 15 iterations, Applied Precision) and processed with Fiji 2.0.0-rc-69/1.52n. Images were taken in black and white and colouring was applied with Fiji. Fluorescence intensity is displayed as arbitrary units and is not comparable between different panels. Colocalization quantification was calculated using Fiji 2.0.0-rc-69/1.52n. Nuclei were detected using DAPI or Hoechst fluorescence as indicated.

Bright-field microscopy and digital photographs

Bright-field images were acquired using a CKX41 microscope (Olympus) and cellSens Entry imaging software (Olympus).

Small-molecule labelling using click chemistry

In-cell click labelling. Cells on coverslips were treated as indicated with cDFO (in-house, 100 µM, 15 min), cLip-1 (in-house, 1 µM, 1 h or 2 h), metcLip-1 (in-house, 10 µM, 1 h), alcLip-1 (in-house, 10 µM, 1 h) or cCW (1 µM, 1 h), then fixed and permeabilized as indicated in the section 'Fluorescence imaging'. LysoTracker Deep Red was added to live cells for

45 min before fixation. The click reaction cocktail was prepared using a Click-iT EdU Imaging kit (Invitrogen, C10337) according to the manufacturer's protocol. In a typical experiment, we mixed 50 µl of 10× Click-iT reaction buffer with 20 µl $CuSO_4$ solution, 1 µl Alexa-Fluor-azide, 50 µl reaction buffer additive (sodium ascorbate) and 379 µl ultrapure water to reach a final volume of 500 µl. Coverslips were incubated with the click reaction cocktail in the dark at room temperature for 30 min, then washed 3 times with 1× PBS. Immunofluorescence imaging was then performed as described in the section 'Fluorescence imaging'.

Click labelling in tissues. Kidney and liver tissue samples collected from cLip-1-treated mice were fixed in 4% paraformaldehyde in 1× PBS overnight at 4 °C. Fixed tissues were incubated in 10% sucrose in 1× PBS for 30 min and then incubated in 20% sucrose in 1× PBS at 4 °C for 4 h, followed by embedding in OCT mounting compound (TissueTek, Sakura) on dry ice and stored at −80 °C. Frozen tissues were cut into 5-µm-thick sections using a Cryostat Microm HM 560 (Thermo Fisher Scientific) at −30 °C. Tissue sections were post-fixed with 1% paraformaldehyde in 1× PBS for 10 min and subsequently incubated with 100% acetone for 10 min at −20 °C. Sections were incubated in blocking solution (1× PBS containing 3% BSA and 0.2% Triton X-100) for 30 min. The specimens were labelled using a click reaction as described above. For costaining with a lysosomal marker, the click-labelled specimens were incubated with anti-LAMP1 or antibody diluted in 1× PBS containing 10% normal goat serum overnight at 4 °C. The next day, sections were incubated with secondary antibody in 1× PBS containing 1% BSA and 0.3% Triton X-100 for 2 h at room temperature. Nuclei were visualized with Hoechst 33342 staining, and slides were mounted in Aqua/PolyMount (Polysciences). Images were acquired using a fluorescence microscope (DS-Qi2, Nikon) or a confocal microscope (LSM880, Carl Zeiss) and the corresponding appropriate filter sets for fluorophores.

Western blotting

Cells were treated as indicated and then washed with 1× PBS. Proteins were solubilized in 2× Laemmli buffer containing benzonase (VWR, 70664-3, 1:100). Extracts were incubated at 37 °C for 1 h, heated at 94 °C for 10 min and quantified using a NanoDrop 2000 spectrophotometer (Thermo Fisher Scientific). Protein lysates were resolved by SDS–PAGE electrophoresis (Invitrogen sure-lock system and Nu-PAGE 4-12% Bis-Tris precast gels). In a typical experiment, 10–20 µg of total protein extract were loaded per lane in 2× Laemmli buffer containing bromophenol blue. On each gel, a size marker was run: 3 µl PageRuler (Thermo Fisher Scientific, 26616) or 3 µl PageRuler plus (Thermo Fisher Scientific, 26620) and 17 µl 2× Laemmli buffer. Proteins were then transferred onto nitrocellulose membranes (Amersham Protran 0.45 µm) using a Trans-Blot SD semi-dry electrophoretic transfer cell (Bio-Rad) using 1× NuPage transfer buffer (Invitrogen, NP00061) with 10% methanol. Membranes were blocked with 5% non-fat skimmed milk powder (Régilait) in 0.1% Tween-20 and 1× PBS for 20 min. Membranes were cut at the appropriate marker size to enable the probing of several antibodies on the same membrane. Blots were then probed with the relevant primary antibodies in 5% BSA, 0.1% Tween-20 and 1× PBS or in 5% non-fat skimmed milk powder in 0.1% Tween-20 and 1× PBS at 4 °C overnight with gentle motion in a hand-sealed transparent plastic bag. Membranes were washed with 0.1% Tween-20 and 1× PBS 3 times and incubated with horseradish-peroxidase-conjugated secondary antibodies (Jackson Laboratories) in 5% non-fat skimmed milk powder (Régilait) in 0.1% Tween-20 and 1× PBS for 1 h at room temperature and washed 3 times with 0.1% Tween-20 and 1× PBS. Antigens were detected using SuperSignal West Pico PLUS (Thermo Fisher Scientific, 34580) and SuperSignal West Femto (Thermo Fisher Scientific, 34096) chemiluminescent detection kits. Signals were recorded using a Fusion Solo S Imaging System (Vilber) with FusionCapt Advance software. Images were processed using Fiji 2.0.0-rc-69/1.52n software. Full scans of blots are provided in the Supplementary Information.

Transduction

PDAC053T cells were seeded in 4-well plates at a density of 2×10^5 cells per well 24 h before the experiment in 1 ml cell culture medium. Cells were then transduced with CellLight Lysosomes-GFP, BacMam 2.0 (Thermo Fisher Scientific, C10596), CellLight ER-GFP, BacMam 2.0 (Thermo Fisher Scientific, C10590) or CellLight Mitochondria-GFP, BacMam 2.0 (Thermo Fisher Scientific, C10600) according to the manufacturer's instructions. In brief, 70 µl BacMam reagent was added to the medium and mixed. Cells were incubated for 16 h.

RNA interference

Cells were plated 24 h before the experiments. Cells were transfected with the specified siRNA using jetPRIME (Polyplus, 114-15) according to the manufacturer's protocol with 100 nM siRNA. In brief, PDAC053T cells were seeded in 6-well plates at a density of 2×10^5 cells per well and transfected 24 h later. The medium was replaced after 6 h. Analysis was performed 72 h after transfection. Suitable siRNAs were designed by Dharmacon for specific downregulation of target genes. siRNA sequences are provided in the Supplementary Information.

Flow cytometry

Cells were washed with ice-cold 1× PBS. For antibody staining, cells were incubated with Fc block (Human TruStain FcX, BioLegend, 422302, 1:20) for 15 min, then incubated with antibodies in ice-cold 10% FBS, 1× PBS, 2 mM EDTA for 20 min at 4 °C and then washed with 1× PBS and resuspended in 10% FBS, 1× PBS and 2 mM EDTA before analysis using a BD LSR Fortessa X-20 flow cytometer with FACS DIVA software (v.9.0.1).

Flow cytometry with iron probes. PDAC053T and HT-1080 cells were seeded in 6-well plates at a density of 2×10^5 cells per well. On the next day, Lip-1 (10 µM), hydroxychloroquine (Sigma-Aldrich, H0915, 100 µM) or bafilomycin A1 (Sigma-Aldrich, B1793, 75 nM) was added to PDAC053T cells for 1 h and to HT-1080 cells for 30 min. For PDAC053T cells, after 30 min of treatment with compounds, RPE[27] (in-house, 40 µM) or HMRhoNox-M[28] (in-house, 1 µM) probes were added for 30 min. For HT-1080 cells, after 15 min of treatment with compounds, RPE[27] (in-house, 40 µM) or HMRhoNox-M[28] (in-house, 1 µM) probes were added and left for 15 min. After incubation with the iron probes, the medium was removed and cells were washed with 1× PBS once before trypsinization. Cells were collected, pelleted, washed with 1× PBS and finally 200 µl of 1× PBS buffer containing 10% FBS and EDTA (0.1% v/v) was added. Data were recorded on a BD LSR Fortessa X-20.

Flow cytometry with Bodipy-C11 581/591. PDAC053T cells were seeded in 6-well plates at the density of 1×10^5 cells per well. On the next day, cells were treated with Lip-1 (1 µM), cLip-1 (in-house, 1 µM), metclip-1 (in-house, 10 µM), alcLip-1 (in-house, 10 µM) and Bodipy-C11 581/591 (200 nM) before adding RSL3 (100 nM). After 1 h, the medium was removed and cells were washed with 1× PBS twice before trypsinization. Cells were collected, pelleted, washed with 1× PBS and finally 250 µl of 1× PBS buffer containing 10% FBS and EDTA (0.1% v/v) was added for flow cytometry. PDAC053T, HT-1080 and 4T1 cells were seeded in 6-well plates at a density of 2×10^5 cells per well. On the next day, cells were treated with bafilomycin A1 (75 nM) and hydroxychloroquine (10 µM) for 2 h before adding RSL3 (200 nM for PDAC053T and HT-1080, 500 nM for 4T1). After 1 h, cells were treated with Bodipy-C11 581/591 (4 µM) for an additional 1 h. The medium was removed and cells were washed with 1× PBS twice before trypsinization. Cells were collected, pelleted, washed with 1× PBS and finally 250 µl of 1× PBS buffer containing 10% FBS and EDTA (0.1% v/v), was added for flow cytometry. Data were recorded on an AttuneTM NxT flow cytometer (Thermo Fisher Scientific) using Attune NxT (v.4.2.0).

Analyses of lysosomal glutathione and lysosomal hydroxy radicals. Cells were incubated with SQSS (in-house, 100 nM, 1 h) or 1-Red (in-house, 100 nM, 24 h). HT-1080 cells were incubated with RSL3 (1 μM), ML210 (10 μM, Sigma-Aldrich, SML0521), FIN56 (5 μM, Sigma-Aldrich, SML1740), buthionine sulfoximine (10 μM, Sigma-Aldrich, B2515) or erastin (10 μM, Sigma-Aldrich, 329600) for the indicated time points. Data were recorded on an AttuneTM NxT flow cytometer (Thermo Fisher Scientific).

Analyses of lysosomal iron content. Typically, 2×10^5 dissociated human tissue cells were incubated in medium (RPMI 1610, 10% FBS and penicillin–streptomycin) with HMRhoNox-M[28] (in-house, 1 μM, 1 h). Lysosomal iron content of human tumour samples and healthy adjacent tissues was analysed with the following antibody and stain panel: DAPI (0.1 μg ml^{-1}), CD3-BV510 (BioLegend, 317332), CD31-PE-Cy7 (BioLegend, 303118), CD44-AF647 (Novus Biologicals, NB500-481AF647), CD45-BV785 (BioLegend, 304048), CD163-PerCP/Cyanine5.5 (BioLegend, 326512), FAP-AF700 (R&D Systems, FAB3715N) and TFR1-APC-AF750 (Beckman Coulter, A89313). The live tumour cancer cells corresponded to $DAPI^-CD45^-CD31^-FAP^-$ cells. Data were recorded on a BD LSRFortessa X-20 or AttuneTM NxT flow cytometer (Thermo Fisher Scientific).

Analyses of CD44 in Fento-1-treated tumour samples. Typically, 2×10^5 dissociated tumour cells were incubated in medium (RPMI 1610, 10% FBS and penicillin–streptomycin) with Fento-1 (in-house, 1 μM, 24 h). Cells were pretreated with Lip-1 (1 μM), cLip-1 (in-house, 1 μM), α-tocopherol (100 μM) or deferiprone (100 μM) for 2 h. α-Tocopherol was kept pure under inert atmosphere, and a fresh stock solution was prepared throughout the study before each experiment. The following antibody and stain panel was used for subsequent flow cytometry analysis: Sytox blue (Thermo Fisher Scientific, S34857, 1 μM), CD31-BV605 (BioLegend, 303122), CD45-BV510 (BioLegend, 368526, lot B373428), CD44-AF647 (Novus Biologicals, NB500-481AF647), TFR1-PE (BioLegend, 334106) and FAP-AF750 (Novus Biologicals, FAB3715S-100UG). The live tumour cells corresponded to Sytox $blue^-CD45^-CD31^-FAP^-$ cells. Data were recorded on an AttuneTM NxT flow cytometer (Thermo Fisher Scientific). For flow cytometry analyses of CD44 levels in mouse 4T1 tumours, typically, 2×10^5 dissociated tumour cells were used per condition. Freshly dissociated cells were stained using the following antibody and stain panel: Sytox blue (Thermo Fisher Scientific, S34857, 1 μM), CD31-BV605 (BioLegend, 102427), CD44-AF647 (BioLegend, 103018), CD45-BV510 (BioLegend, 103138) and MHCII-APC/Cyanine7 (BioLegend, 107628). The live tumour cancer cells corresponded to Sytox $blue^-CD45^-CD31^-MCHII^+$ cells. Data were recorded on an AttuneTM NxT flow cytometer (Thermo Fisher Scientific). All data were analysed using FlowJo (v.10.10.0).

FACS

Sorting of human cells was performed using the following antibodies: CD31-PE-Cy7 (BioLegend, 303118), CD44-AF647 (Novus Biologicals, NB500-481AF647) and CD45-BV785 (BioLegend, 304048). The sorted cells corresponded to $CD45^-CD31^-CD44^+$ cells and $CD45^-CD31^-CD44^-$ cells, which were isolated on a FACSAria Fusion (BD) using FACS DIVA (v.9.0.1). ICP-MS experiments were conducted using $CD44^{high}$ and $CD44^{low}$ tumour cells as described in the section 'ICP-MS'. Sorting of mouse cells was performed using the following antibodies: CD44-AF647 (BioLegend, 103018) and MHCII-APC/Cyanine7 (BioLegend, 107628). The sorted cells corresponded to $MHCII^+CD44^{high}$ cells and $MHCII^+CD44^{low}$ cells. Sorted cells were centrifuged at 300*g* and cell pellets were processed for subsequent applications.

ICP-MS

Glass vials equipped with Teflon septa were cleaned with nitric acid 65% (VWR, Suprapur, 1.00441.0250), washed with ultrapure water (Sigma-Aldrich, 1012620500) and dried. Cells were collected and washed twice with 1× PBS. Cells were then counted using an automated cell counter (Entek) and transferred in 200 μl 1× PBS or ultrapure water to the cleaned glass vials. The same volume of 1× PBS or ultrapure water was transferred into separate vials for background subtraction, at least in duplicate per experiment. For tissue samples, a small piece of about 1 mm^3 was transferred into a clean preweighed vial. Samples were lyophilized using a freeze dryer (Christ, 2-4 LDplus). Vials with tissue samples were subsequently weighed to determine the tissue dry weight. Samples were then mixed with nitric acid 65% and heated at 80 °C overnight in the same glass vials closed with a lid carrying a Teflon septum. Samples were then cooled to room temperature and diluted with ultrapure water to a final concentration of 0.475 N nitric acid and transferred to metal-free centrifuge vials (VWR, 89049-172) for subsequent MS analyses. Amounts of metal were measured using an Agilent 7900 ICP-QMS in low-resolution mode, taking natural isotope distribution into account. Sample introduction was achieved with a micronebulizer (MicroMist, 0.2 ml min^{-1}) through a Scott spray chamber. Isotopes were measured using a collision–reaction interface with helium gas (5 ml min^{-1}) to remove polyatomic interferences. Scandium and indium internal standards were injected after inline mixing with the samples to control the absence of signal drift and matrix effects. A mix of certified standards was measured at concentrations spanning those of the samples to convert count measurements to concentrations in the solution. Values were normalized against cell number or tissue dry weight.

Liposome preparation and lipid oxidation studies

Liposomal structures were prepared using the traditional lipid film hydration method. In brief, 100 μl of a stock solution (1 mg ml^{-1} chloroform) of 18:1 (Δ9-*cis*) PC (DOPC, Avanti Polar Lipids) was dissolved in 400 μl chloroform and transferred into a round-bottom flask. The organic solvent was removed under reduced pressure in a rotary evaporator for 15 min at 200 r.p.m. in a water bath at 37 °C. Afterwards, the lipid film was dried with a vacuum pump overnight. The sample was hydrated with 1 ml of 0.1 mM sodium acetate buffer (pH 4.5) and vortexed every 5 min for 20 min. Liposomes were extruded by passing the suspension through 2 polycarbonate membranes (pore size 0.2 mm) 20 times. For the control experiment, 200 μl of the liposome solution was added into an Eppendorf tube and heated at 37 °C with agitation at 800 r.p.m. Then, 5 μl of an aqueous solution of iron(II) triflate (1.4 mg in 1.5 ml) and 13 μl of 0.1 mM acetate buffer (pH 4.5) were added. At $t = 0$ min 13 μl of an aqueous solution of H_2O_2 (10 μl H_2O_2 (30%) in 1 ml) was added. For the Fento-1 experiment, 200 μl of the liposome solution was added to an Eppendorf tube and heated at 37 °C at 800 r.p.m. Then, 13 μl of a 1 mM solution of Fento-1 in DMSO and 5 μl of an aqueous solution of iron(II) triflate (1.4 mg in 1.5 ml) were added. At $t = 0$ min, 13 μl of an aqueous solution of H_2O_2 (10 μl H_2O_2 (30%) in 1 ml) was added. DOPC oxidation was recorded with a QExactive mass spectrometer (Thermo Fisher Scientific) equipped with a TriVersa NanoMate ion source (Advion Biosciences) as detailed in the section 'MS-based lipidomics'. Samples were injected at 0.5 h, 1 h, 2 h, 3 h, 4 h, 7 h and 24 h reaction times.

Isolation of lysosome-enriched fractions

HT-1080 cells were treated with Fento-1 (10 μM) for 1 h, and lysosome-enriched fractions were isolated using a Lysosome Isolation kit (Abcam, ab234047) according to the manufacturer's protocol. In brief, 2×10^7 cells were washed and centrifuged at 600*g* for 10 min and the supernatant was removed. Cells were resuspended in lysosome isolation buffer, vortexed and incubated on ice for 2 min. Complete cell disruption was obtained using a dounce homogenizer. After adding lysosome enrichment buffer, the homogenate was centrifuged at 500*g* for 10 min at 4 °C. The supernatant was added to the top of a discontinuous gradient density and an ultracentrifugation at 145,000*g* for 2 h at 4 °C was performed.

The lysosome-enriched fraction was present in the top 10% of the gradient volume. For MS-based lipidomics, the lysosomal fraction was mixed with 2 volumes of 1× PBS, vortexed and centrifuged at 18,000*g* for 30 min at 4 °C. Next, 200 µl of 150 mM sodium bicarbonate was added to the pellet and the sample was flash-frozen in liquid nitrogen. Lipidomic analyses were performed on these flash-frozen samples. For western blot analyses, the protein content of the lysosomal-enriched gradient supernatant was quantified using a Qbit 1 fluorometer (Thermo Fisher Scientific) and a protein quantification kit (Thermo Fisher Scientific, Q33212). Equal total protein amounts of total cell extracts and lysosome-enriched extracts were loaded for comparison for western blot analyses.

MS-based lipidomics

For comparison of ferroptosis inducers, HT-1080 cells were treated with Fento-1 (in house, 1 µM), erastin (10 µM), RSL3 (100 nM) or iFSP1 (10 µM, Sigma-Aldrich, SML2749) for 24 h. For cotreatment with ferroptosis inhibitors, HT-1080 cells were pretreated with α-tocopherol (100 µM), deferiprone (100 µM) or Lip-1 (10 µM) for 2 h, and then with Fento-1 (1 µM) for 24 h. Dissociated human tumour samples were pretreated with 100 µM α-tocopherol and then with 1 µM Fento-1 for 24 h. PDAC053T cells were treated with 1 µM Fento-1 for 6 h or 24 h. Dissociated mouse tumour samples were counted and processed directly after dissociation and pretreated with α-tocopherol (100 µM) for 2 h and then with Fento-1 (1 µM, 24 h). Cells were subsequently washed with 1× PBS and then with 150 mM ammonium bicarbonate. Cells were then resuspended in 150 mM ammonium bicarbonate and centrifuged at 300*g* for 5 min. The supernatant was removed and cells were resuspended in 1 ml of 150 mM ammonium bicarbonate. The solutions were centrifuged at 12,000 r.p.m. for 10 min and the supernatant was removed. Next, 200 µl of 150 mM sodium bicarbonate was added to the pellet and samples were flash-frozen in liquid nitrogen. Lipidomic analyses were performed on the same day for all technical and biological replicates for a given dataset. For lipidomic analyses, 200 µl cell lysate was spiked with 1.64 µl internal standard lipid mixture containing 300 pmol phosphatidylcholine (PC) 17:0-17:0, 50 pmol phosphatidylethanolamine (PE) 17:0-17:0, 50 pmol phosphatidylinositol (PI) 16:0-16:0, 50 pmol phosphatidylserine (PS) 17:0-17:0, 30 pmol phosphatidic acid (PA) 17:0-17:0, 30 pmol phosphatidylglycerol (PG), 30 pmol lysophosphatidylcholine (LPC) 12:0, 30 pmol lysophosphatidylethanolamine (LPE) 17:1, 30 pmol lysophosphatidylserine (LPS) 17:1 and 30 pmol lysophosphatidic acid (LPA) 17:0 and subjected to lipid extraction at 4 °C as previously described[57]. In brief, the sample was extracted with 1 ml chloroform and methanol (10:1) for 2 h at 4 °C with vigorous shaking in a thermomixer (1,000 r.p.m.). The lower organic phase was collected and dried in a SpeedVac vacuum concentrator. The remaining aqueous phase was re-extracted with 1 ml chloroform and methanol (2:1) for 1 h at the same temperature and shaking conditions. The lower organic phase was collected and evaporated in a SpeedVac vacuum concentrator. Lipid extracts were dissolved in 100 µl infusion mixture consisting of 7.5 mM ammonium acetate dissolved in propanol, chloroform and methanol (4:1:2 (v/v/v)). For the in vitro liposome experiments, 1 µl of each reaction mixture taken at different time points was added to 100 µl infusion mixture consisting of 7.5 mM ammonium acetate dissolved in propanol, chloroform and methanol (4:1:2 (v/v/v)) containing 300 pmol PC 17:0-17:0. Samples were analysed by direct infusion in a QExactive mass spectrometer (Thermo Fisher Scientific) equipped with a TriVersa NanoMate ion source (Advion Biosciences). In brief, 5 µl of sample was infused with the gas pressure and voltage set to 1.25 psi and 0.95 kV, respectively. PC and oxidized PC (PC_{Ox}) were detected in the 10:1 extract by positive-ion mode FTMS as protonated adducts by scanning m/z = 580–1,000 Da, at $R_{m/z=200}$ = 280,000 with lock mass activated at a common background (m/z = 680.48022) for 30 s. Every scan is the average of 2 microscans, and the AGC was set to 10^6 and the maximum ion injection time (IT) was set to 50 ms. PE, oxidized PE (PE_{Ox}) and LPE were detected as deprotonated adducts and LPC were detected as acetate adducts in the 10:1 extract by negative-ion mode FTMS by scanning m/z = 420–1,050 Da, at $R_{m/z=200}$ = 280,000 with lock mass activated at a common background (m/z = 529.46262) for 30 s. Every scan is the average of 2 microscans, AGC was set to 10^6 and the maximum ion IT was set to 50 ms. PI, oxidized PI (PI_{Ox}), PS, oxidized PS (PS_{Ox}), lysophosphatidylinositol (LPI) and lysophosphatidylserine (LPS) were detected in the 2:1 extract, by negative-ion mode FTMS as deprotonated ions by scanning m/z = 400–1,100 Da, at $R_{m/z=200}$ = 280,000 with lock mass activated at a common background (m/z = 529.46262) for 30 s. Every scan is the average of 2 microscans, the AGC was set to 10^6 and the maximum ion IT was set to 50 ms. Annotation of the oxidized phospholipids only details the number of additional oxygen atoms and double bonds present in a given mass and it can potentially refer to several different structures with the same monoisotopic mass. All data were acquired in centroid mode. All lipidomic data were analysed with the lipid identification software LipidXplorer (v.1.2.8; http://genomebiology.com/2011/12/1/R8). Tolerance for MS and identification was set to 2 ppm. Data were normalized against internal standards and total input to the respective lipid species. Lipidomic data were clustered using a correlation distance and Ward linkage, and represented as heat maps of normalized values.

Glycerol quantification

HT-1080 cells were treated with Fento-1 (in-house, 1 or 2 µM, 24 h). Glycerol was quantified using a Glycerol-glo assay (Promega, J3150) according to the manufacturer's protocol. In brief, the assay was performed in a 96-well plate and 4,000 cells were plated per well 24 h before the experiment. A standard curve was prepared for each biological experiment and three technical replicates were performed for each condition and each biological replicate. Luminescence signals were recorded using a SpectraMax ID3 plate reader (Molecular Devices). Data were exported and analysed using Excel (Microsoft) and Prism software.

Software for illustrations

Illustrations were created using Fiji 2.0.0-rc-69/1.52n, Prism 10.0.3 and Adobe Illustrator 26.0.2. Illustrations in Figs. 2b and 4 were created using BioRender (https://biorender.com).

Statistical and reproducibility

Results are presented as the mean ± s.e.m. or s.d. as indicated. For box plots, boxes represent the interquartile range and median, and whiskers indicate the minimum and maximum values. Prism (v.10.0.3) software was used to calculate *P* values using a two-sided Mann–Whitney test, two-sided unpaired *t*-test, Kruskal–Wallis test with Dunn's post-test, one-way ANOVA, two-way ANOVA or Mantel–Cox log-rank test as indicated. Prism (v.10.0.3) software was used to generate graphical representations of quantifications unless stated otherwise. Sample sizes (n) are indicated in the figure legends and were not predetermined. A minimum of n = 3 independent experiments were performed as a standard, and sample sizes were increased in more complex experiments to ensure reproducibility. Exact *P* values are indicated in the figures.

Reporting summary

Further information on research design is available in the Nature Portfolio Reporting Summary linked to this article.

Data availability

Lipidomics data are presented in the Supplementary Tables 1–4 and 7–12. Quantitative proteomic raw data have been deposited to the ProteomeXchange Consortium through the PRIDE[55] partner repository with the dataset identifier PXD054449. Source data are provided with this paper.

50. Frisch, M. J. et al. *Gaussian 09, Revision B.01* (Gaussian, 2010).
51. Schreiber, F. S. et al. Successful growth and characterization of mouse pancreatic ductal cells: functional properties of the *Ki-RAS*^{G12V} oncogene. *Gastroenterology* **127**, 250–260 (2004).
52. Yadav, B., Wennerberg, K., Aittokallio, T. & Tang, J. Searching for drug synergy in complex dose–response landscapes using an interaction potency model. *Comput. Struct. Biotechnol. J.* **13**, 504–513 (2015).
53. Ionac, M. One technique, two approaches, and results: thoracic duct cannulation in small laboratory animals. *Microsurgery* **23**, 239–245 (2003).
54. Poullet, P., Carpentier, S. & Barillot, E. myProMS, a web server for management and validation of mass spectrometry-based proteomic data. *Proteomics* **7**, 2553–2556 (2007).
55. Perez-Riverol, Y. et al. The PRIDE database resources in 2022: a hub for mass spectrometry-based proteomics evidences. *Nucleic Acids Res.* **50**, D543–D552 (2022).
56. Workman, P. et al. Guidelines for the welfare and use of animals in cancer research. *Br. J. Cancer* **102**, 1555–1577 (2010).
57. Sampaio, J. L. et al. Membrane lipidome of an epithelial cell line. *Proc. Natl Acad. Sci. USA* **108**, 1903–1907 (2011).

Acknowledgements R.R. is supported by the European Research Council under the European Union's Horizon 2020 research and innovation programme (grant agreement no. 647973), Ligue Contre le Cancer (Equipe Labellisée), Fondation pour la Recherche Médicale, Fondation Charles Defforey–Institut de France, Klaus Grohe Foundation, Fondation Bettencourt Schueller, Région Ile-de-France, Institut National du Cancer (PLBIO-2022-099) and Agence Nationale de la Recherche (ANR-23-CE44-0030 and ANR-23-IAHU-0006). V.G. thanks the UPSaclay and CNRS for financial support. This work was granted access to the HPC resources of CINES under the allocation 2020-A0070810977 made by GENCI. M.C. received funding from the Deutsche Forschungsgemeinschaft (DFG) (CO 291/7-1, 428858739 and the Priority Program SPP 2306 (CO 291/9-1, 461385412; CO 291/10-1, 461507177; CO 291/9-2, CO 291/10-2, CO 291/14-1) and CRC 353 (CO 291/11-1; 471011418), the German Federal Ministry of Education and Research (BMBF) VIP+ programme NEUROPROTEKT (03VP04260), the BMBF programme FERROPATH (01EJ2205B) and the European Research Council under the European Union's Horizon 2020 research and innovation programme (grant agreement no. 884754). J.P.F.A. acknowledges institutional support of the University of Würzburg and additional support from the Deutsche Forschungsgemeinschaft (DFG), FR 3746/3-1, FR 3746/5-1, FR 3746/6-1 and CRC205 (INST 269/886-1), the European Union (ERC-Consolidator, DeciFERR, Horizon Europe ERC grant no. 101126134) and the Deutsche Jose Carreras Leukämie Stiftung (DJCLS 01R/2022). J.M.U. is supported by the Breast Cancer Alliance Young Investigator Grant and The Ludwig Center at Harvard. A.C. is supported by the Landry Cancer Biology Research Fellowship. A.C. and C.S.F. were funded by NIH NIDDK (T32DK128781). E.C.-J. and C. Ginestier are supported by Ligue Contre le Cancer (Equipe Labellisée). D.A.P. is supported by the Natural Sciences and Engineering Research Council of Canada (RGPIN-2022-05058). The ICP-MS platform at Institut de Physique du Globe de Paris is supported by IPGP multidisciplinary program PARI and Région Ile-de-France (SESAME grant agreement no. 12015908). The cell and tissue imaging facilities (PICT-IBiSA) of Institut Curie are part of the France Bioimaging National Infrastructure (ANR-10-INBS-04 and ANR-24-INBS-0005 FBI BIOGEN), the MS platform is supported by Région Ile-de-France (N°EX061034) and ITMO Cancer of Aviesan and INCa supported by funds administered by INSERM (no. 21CQ016-00), and the cytometry platform is part of the Institut Curie. We thank S. Hidalgo for assistance with ICP-MS experiments; and R.R. thanks S. Balasubramanian, S. L. Schreiber, J.-M. Lehn and E. M. Carreira for support.

Author contributions R.R. conceptualized the study and directed the research. R.R., T.C., L.B., S.M. and J.M.U. designed the experiments. T.C., L.B., L.C., A.V. and C. Gaillet performed chemical synthesis, NMR spectroscopy and MS. L.B. and L.G. performed cyclic voltammetry. A.U. measured RTA activity in vitro. V.G. performed molecular modelling. S.M., L.B., S.S., F.S., A.P.-B. and L.K.T. performed transductions, transfections, fluorescence imaging, flow cytometry, western blotting, lysosome isolation, cell death and cell viability assays. S.M. prepared samples for ICP-MS. J.L.S. performed lipidomics. F.S., B.L. and D.L. performed quantitative proteomics. L.S. and N.S. performed bioinformatics. E.D.K., C.B., P.S.-C., M.E., N.D., J.L.I., F.P.F. and J.Z. performed colony-formation, synthetic lethality and combination therapy assays. A.S.C., G.P., D.T. and S.B. selected intraoperative healthy and tumour tissue samples. S.M. and S.S. performed analyses of human tumour tissues. E.M. and B.P. performed evaluation of cLip-1 in vivo. A.C., M.S., C.S.F. and K.J.S. performed intralymphatic treatments of 4T1 tumour-bearing mice. All the authors contributed to data analyses. R.R., T.C. and S.M. wrote the article. E.C-.J., C. Ginestier, P.H., S.W., D.A.P., J.P.F.A., B.R.S., M.C. and J.M.U. commented on the manuscript.

Competing interests Institut Curie filed a patent application (PCT/EP2025/051999) related to lipid degraders to induce ferroptosis in cancer. M.C. and B.P. hold patents for some of the compounds described herein and are co-founders of ROSCUE Therapeutics. B.R.S. is an inventor on patents and patent applications involving ferroptosis; co-founded and serves as a consultant to ProJenX and Exarta Therapeutics; holds equity in Sonata Therapeutics; and serves as a consultant to Weatherwax Biotechnologies and Akin Gump Strauss Hauer & Feld. All the other authors declare no competing interests.

Additional information

Supplementary information The online version contains supplementary material available at https://doi.org/10.1038/s41586-025-08974-4.

Correspondence and requests for materials should be addressed to Raphaël Rodriguez.

Peer review information *Nature* thanks the anonymous reviewers for their contribution to the peer review of this work. Peer reviewer reports are available.

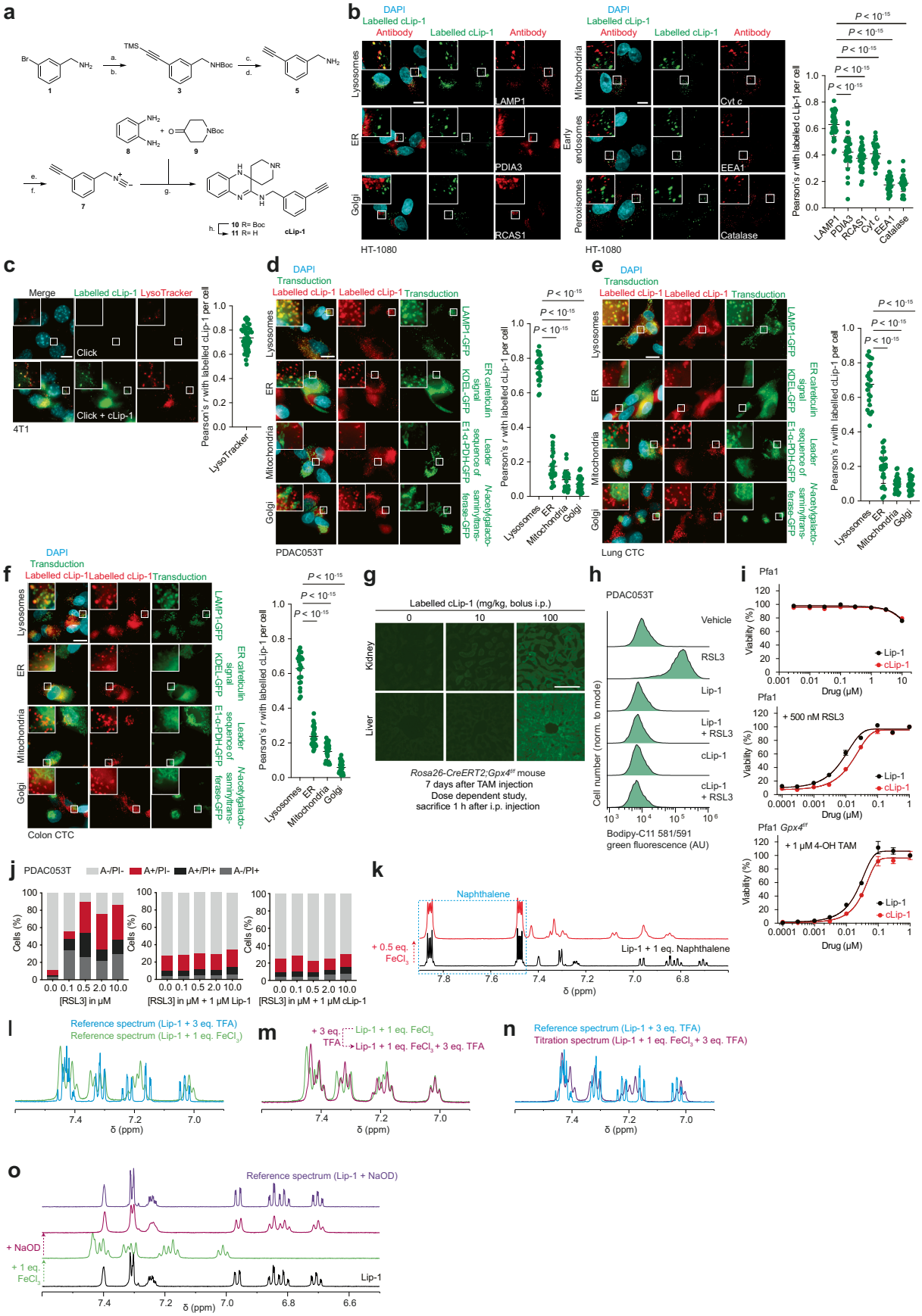

Extended Data Fig. 1 | See next page for caption.

Extended Data Fig. 1 | Inactivation of lysosomal iron inhibits ferroptosis (Part 1). a, Chemical synthesis of cLip-1. **b**, Fluorescence imaging of labelled cLip-1 (1 μM, 2 h) and specific markers of cellular organelles. Scale bars, 10 μm. $n = 3$ independent experiments. Data are mean ± s.d. **c**, Fluorescence imaging of labelled cLip-1 (1 μM, 1 h) and LysoTracker. Scale bar, 10 μm. $n = 3$ independent experiments. Data are mean ± s.d. **d-f**, Fluorescence imaging of labelled cLip-1 (1 μM, 1 h) and BacMam transduced cells of GFP-labelled cell organelle markers. Scale bar, 10 μm. $n = 3$ independent experiments. Data are mean ± s.d. **g**, Fluorescence imaging of labelled cLip-1 in proximal kidney and liver tissues of a *Rosa26-CreERT2;Gpx4*$^{f/f}$ mouse treated with cLip-1 (0, 10 and 100 mg/ kg/ day; sacrificed 1 h after i.p. injection). Scale bar, 100 μm. **h**, Bodipy-C11 581/591 flow cytometry of cells treated with Lip-1 (1 μM), cLip-1 (1 μM) and RSL3 (100 nM) for 1 h. **i**, Viability of cells (top, after 72 h of incubation; middle, incubation for 24 h and cotreatment with RSL3 (500 nM); bottom, incubation for 72 h and cotreatment with 4-OH TAM to knock out *Gpx4*. Data are mean ± s.d. **j**, Annexin-V/ Propidium Iodide (A/ PI) staining in cells treated for 24 h. RSL3: $n = 2$ independent experiments; RSL3 + Lip-1: $n = 3$ independent experiments; RSL3 + cLip-1: $n = 3$ independent experiments. **k**, ^{1}H NMR spectra of Lip-1 and naphthalene titrated with $FeCl_3$. **l-n**, ^{1}H NMR spectra of Lip-1 titrated with $FeCl_3$ then TFA. **o**, ^{1}H NMR spectra of Lip-1 titrated with $FeCl_3$ and then sodium deuteroxide (NaOD). **k-o**, NMR spectra recorded at 310 K in methanol-d_4. **b, d-f**, 1-way ANOVA. AU, arbitrary unit.

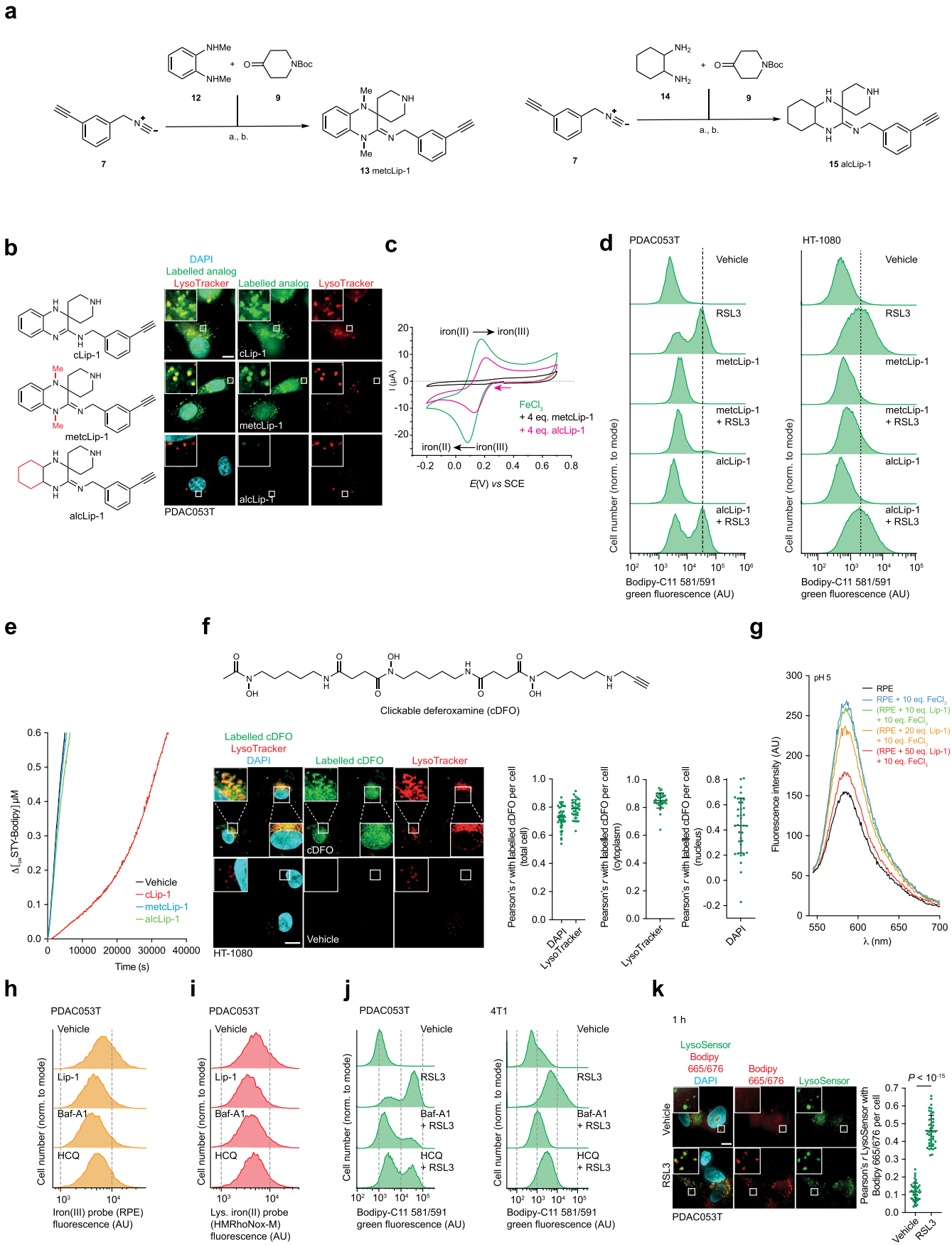

Extended Data Fig. 2 | See next page for caption.

Extended Data Fig. 2 | Inactivation of lysosomal iron inhibits ferroptosis (Part 2). a, Chemical syntheses of metcLip-1 and alcLip-1. **b**, Fluorescence imaging of labelled cLip-1 (10 μM, 2 h), metcLip-1 (10 μM, 2 h) and alcLip-1 (10 μM, 2 h). Scale bar, 10 μm. **c**, Cyclic voltammetry of a $FeCl_3$ solution (reduction potentials = pink arrow). Data recorded in the presence of metcLip-1 or alcLip-1. **d**, Bodipy-C11 581/591 flow cytometry of cells treated with metcLip-1 (10 μM), alcLip-1 (10 μM) and RSL3 (100 nM) for 1 h. Representative of $n = 3$ independent experiments for PDAC053T and $n = 1$ for HT-1080. **e**, FENIX assay of cLip-1, metcLip-1 and alcLip-1. **f**, Molecular structure of cDFO and fluorescence imaging of labelled cDFO (100 μM, 15 min). Scale bar, 10 μm. $n = 3$ independent experiments. Data are mean ± s.d. **g**, Fluorescence emission spectra of RPE at pH 5 in the presence of $FeCl_3$ and Lip-1. **h**, RPE flow cytometry of cells treated for 30 min and then cotreated with the probe for 30 min. HCQ (100 μM). Representative of $n = 3$ independent experiments. **i**, HMRhoNox-M flow cytometry of cells treated for 30 min and then cotreated with the probe for 30 min. HCQ (100 μM). Representative of $n = 3$ independent experiments. **j**, Bodipy-C11 581/591 flow cytometry of cells treated with RSL3 (200 nM for PDAC053T, 500 nM for 4T1, 1 h) and Baf-A1 or HCQ (10 μM) used 2 h prior. Representative of $n = 3$ independent experiments. **k**, Fluorescence imaging of Bodipy 665/676 in cells treated with RSL3 (1 μM, 1 h). Scale bar, 10 μm. $n = 3$ independent experiments. Two-sided unpaired *t*-test. Data are mean ± s.d. Concentrations used unless stated otherwise: Lip-1 (10 μM), Baf-A1 (75 nM).

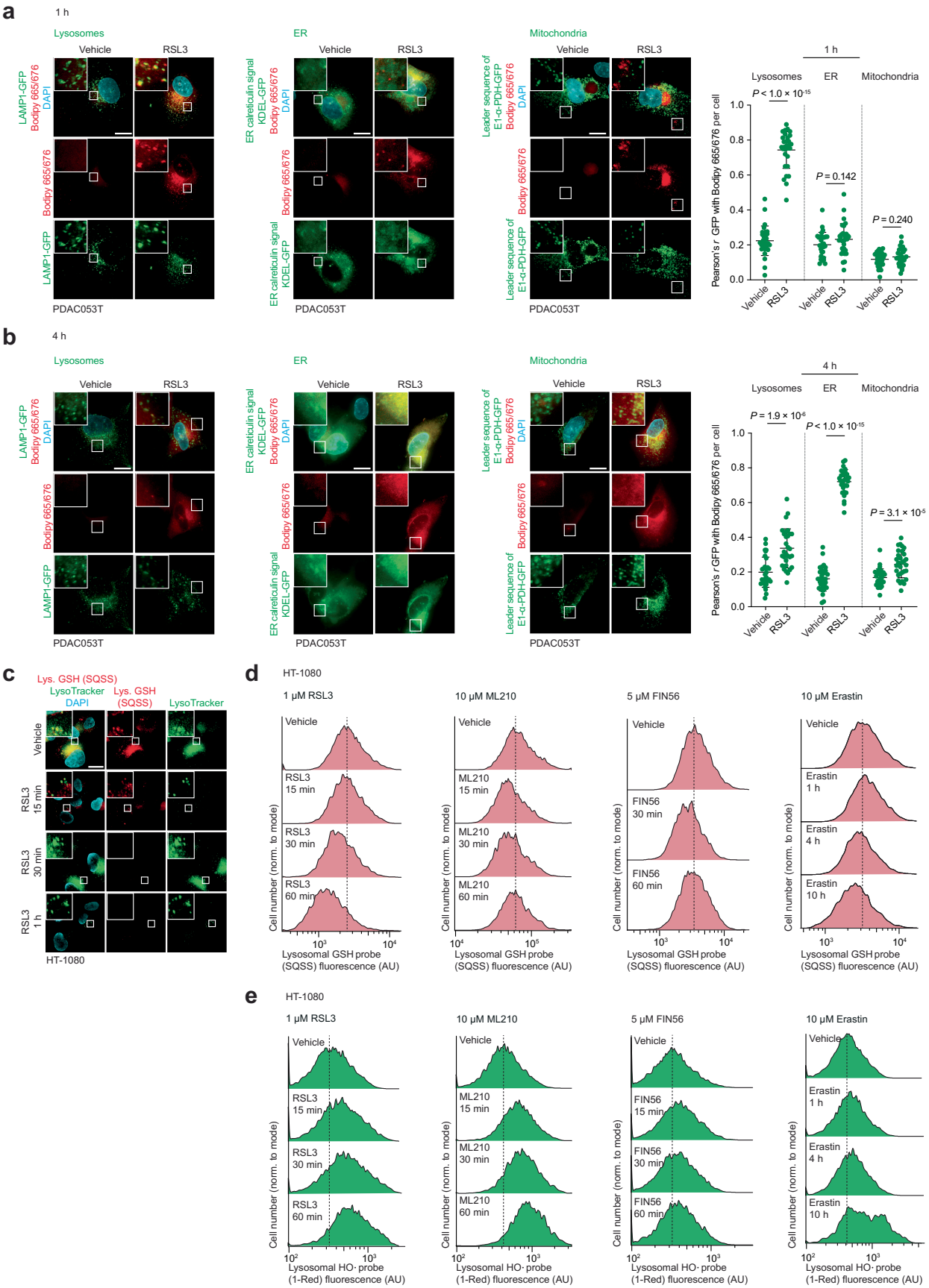

Extended Data Fig. 3 | See next page for caption.

Extended Data Fig. 3 | Ferroptosis inducers initiate lipid peroxidation in lysosomes. a, Fluorescence imaging of Bodipy 665/676 and BacMam transduced cells of GFP-labelled cell organelle markers treated with RSL3 (1 μM, 1 h). Scale bars, 10 μm. $n = 3$ independent experiments. Data are mean ± s.d. **b**, Fluorescence imaging of Bodipy 665/676 and BacMam transduced cells of GFP-labelled cell organelle markers treated with RSL3 (1 μM, 4 h). Scale bars, 10 μm. $n = 3$ independent experiments. Data are mean ± s.d. **c**, Fluorescence imaging of the lysosomal GSH probe (SQSS) and a lysosomal marker in cells treated with RSL3 (1 μM). Scale bar, 10 μm. Representative of $n = 3$ independent experiments. **d**, SQSS flow cytometry of cells treated with ferroptosis inducers. **e**, 1-Red flow cytometry of cells treated with ferroptosis inducers. **a**, **b**, Two-sided unpaired *t*-test.

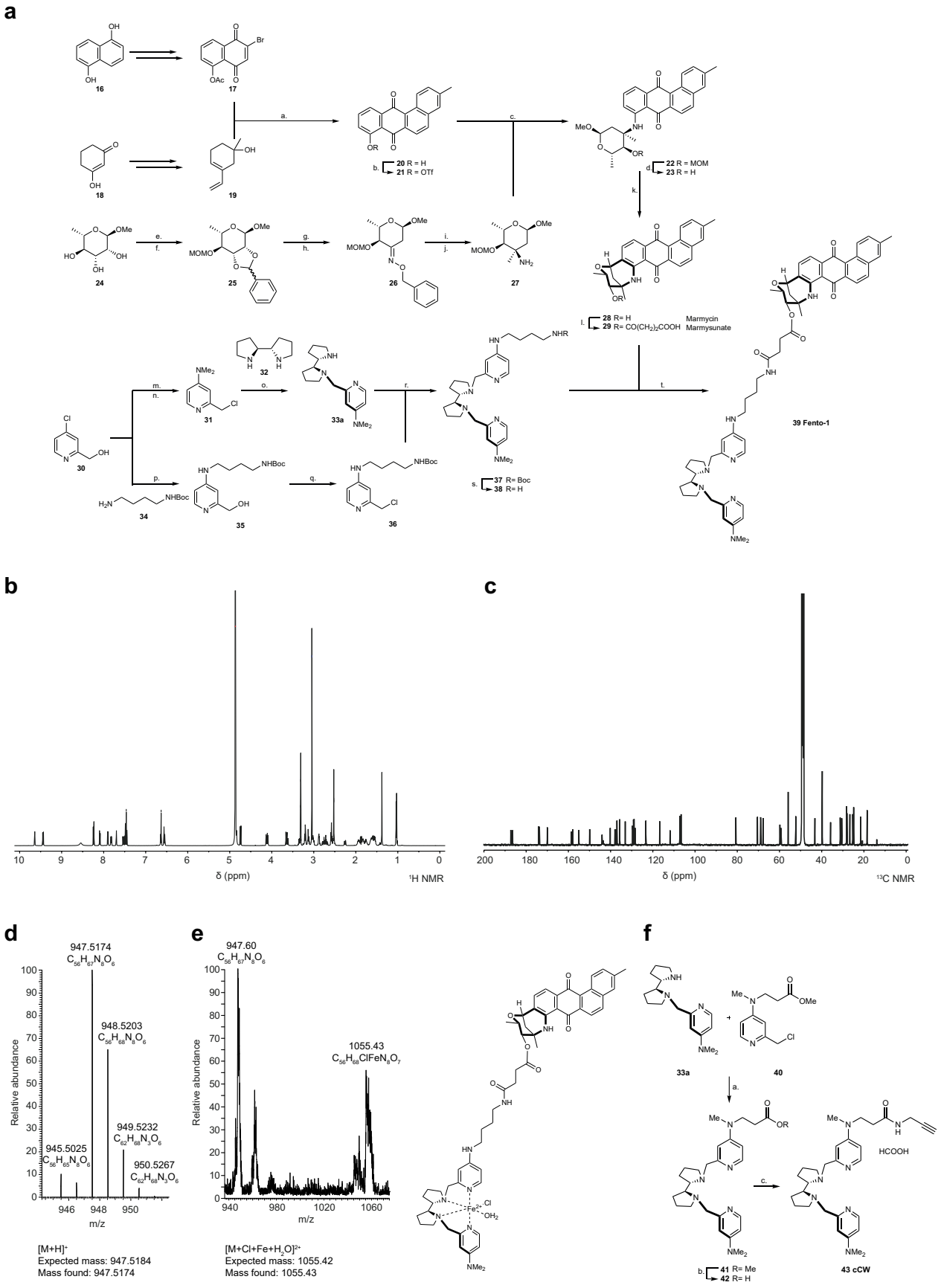

Extended Data Fig. 4 | Chemical synthesis and spectral data of Fento-1. **a**, Chemical synthesis of Fento-1. **b**, ^{1}H NMR spectrum of Fento-1. **c**, ^{13}C NMR spectrum of Fento-1. **d**. High-resolution mass spectrum (HRMS) of Fento-1. **e**, Low-resolution mass spectrum (LRMS) of a Fento-1-iron complex. **f**, Chemical synthesis of cCW. **b**, **c**, NMR spectra recorded at 298 K in methanol-d_4. Full description, Supplementary Information.

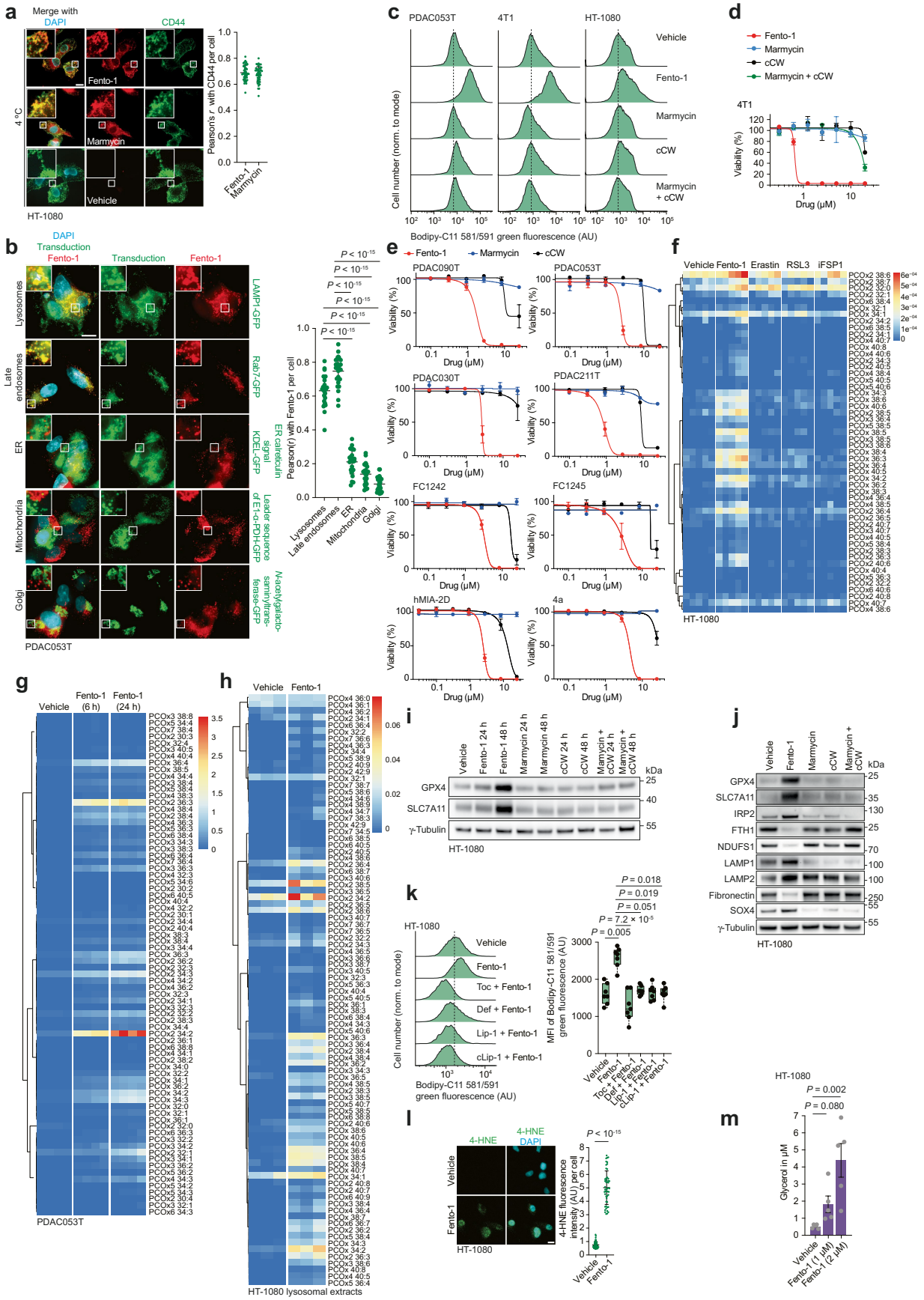

Extended Data Fig. 5 | See next page for caption.

Extended Data Fig. 5 | Fento-1 induces the oxidation of phospholipids and cell death by activating lysosomal iron (Part 1). a, Fluorescence imaging of Fento-1, marmycin and the cell surface marker CD44 in cells treated at 4 °C for 1 h. Scale bar, 10 μm. *n* = 3 independent experiments. Data are mean ± s.d. **b**, Fluorescence imaging of Fento-1 in BacMam transduced cells of GFP-labelled cell organelle markers. Scale bar, 10 μm. *n* = 3 independent experiments. Data are mean ± s.d. **c**, Bodipy-C11 581/591 flow cytometry of cells treated with Fento-1, marmycin and cCW alone or in combination for 6 h. Representative of *n* = 3 independent experiments. **d**, Viability of cells treated for 6 h. Data are mean ± s.e.m. *n* = 3 independent experiments. **e**, Viability of cells treated for 72 h. Data are mean ± s.e.m. *n* = 3 independent experiments. **f**, Lipidomics of oxidised phospholipids in cells treated with Fento-1 or ferroptosis inducers for 24 h. *n* = 5 independent experiments. **g**, Lipidomics of oxidised phospholipids in cells treated with Fento-1. *n* = 4 independent experiments. Full heatmap, Supplementary Information. **h**, Lipidomics of oxidised phospholipids of lysosomal extracts in cells treated with Fento-1 (10 μM, 1 h). *n* = 3 independent experiments. **i**, Western blot of proteins from cells treated with Fento-1, marmycin, cCW or marmycin + cCW. γ-tubulin is a sample loading control. Representative of *n* = 3 independent experiments. **j**, Western blot of proteins from cells treated with Fento-1, marmycin, cCW or marmycin + cCW (48 h). γ-tubulin is a sample processing control. Representative of *n* = 2 independent experiments with similar results. **k**, Bodipy-C11 581/591 flow cytometry of cells treated with Fento-1 (24 h) and inhibitors used 2 h prior. *n* = 7 independent experiments. Box plots: interquartile range, centre lines = medians and whiskers = the minimum and maximum values. **l**, Fluorescence imaging of 4-HNE treated with Fento-1 (1 h). Two-sided unpaired *t*-test. *n* = 3 independent experiments. Data are mean ± s.d. Scale bar, 10 μm. **m**, Quantification of glycerol in cells treated with Fento-1 (24 h). Data are mean ± s.e.m. *n* = 5 independent experiments. Concentrations used unless stated otherwise: Fento-1 (1 μM), marmycin (1 μM), cCW (1 μM), erastin (10 μM), RSL3 (100 nM), iFSP1 (10 μM), Toc (100 μM), Def (100 μM), Lip-1 (1 μM) and cLip-1 (1 μM). **k, m**, Kruskal–Wallis test with Dunn's post-test. Phosphatidylcholine (PC) lipids displayed in the main figures. Phosphatidylethanolamine (PE), phosphatidylinositol (PI), phosphatidylserine (PS), Supplementary Information.

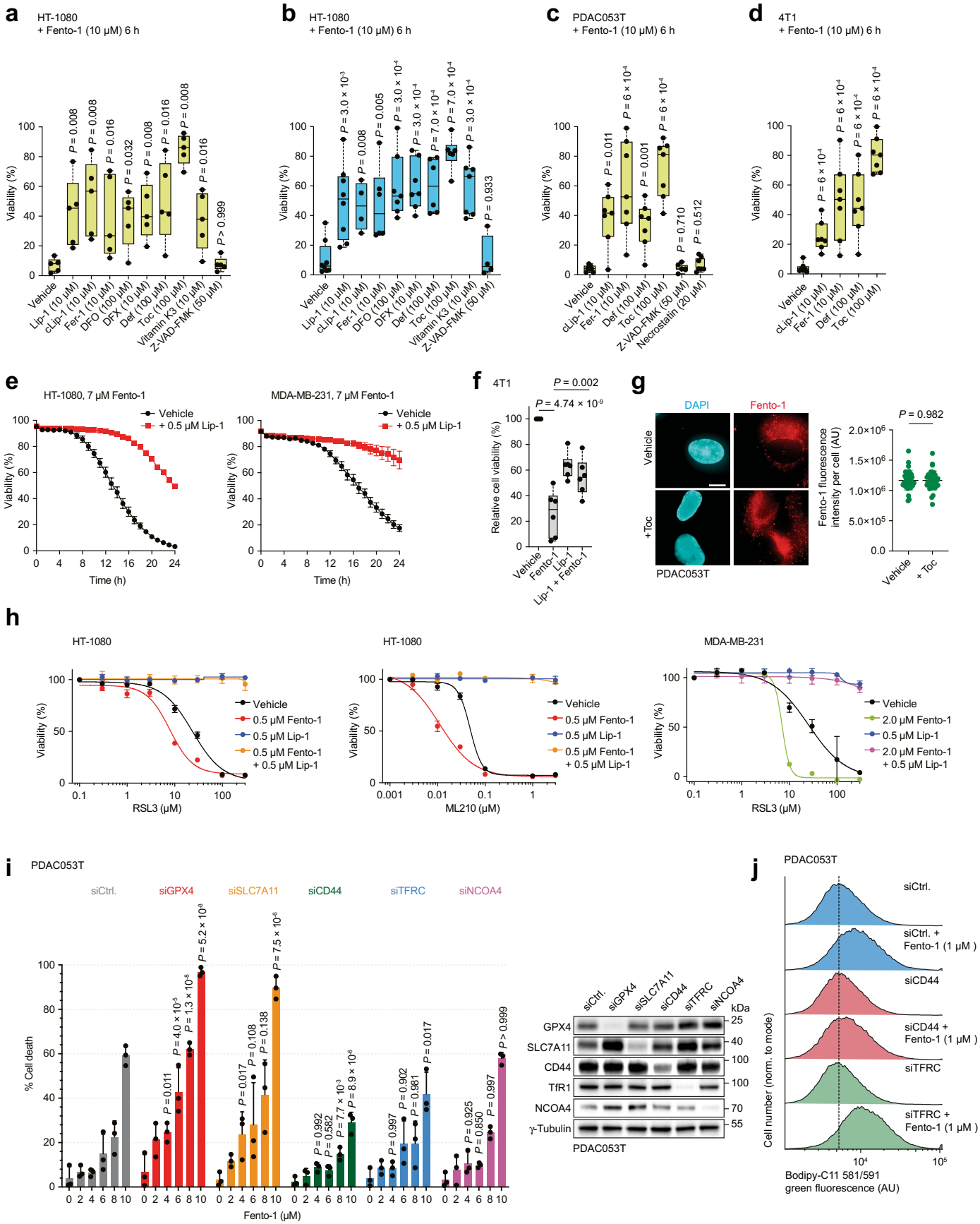

Extended Data Fig. 6 | See next page for caption.

Extended Data Fig. 6 | Fento-1 induces the oxidation of phospholipids and cell death by activating lysosomal iron (Part 2). a, CellTiterGlo luminescence of cells treated with Fento-1 (10 μM, 6 h) and inhibitors used 2 h prior. $n = 5$ independent experiments. **b**, Resorufin fluorescence of cells treated with Fento-1 (10 μM, 6 h) and inhibitors used 2 h prior. Vehicle, Lip-1: $n = 8$ independent experiments, clip-1 and Z-VAD-FMK: $n = 4$ independent experiments, Fer-1, Def and Toc: $n = 6$ independent experiments, DFO, DFX and Vitamin K3: $n = 7$ independent experiments. **c, d**, CellTiterGlo luminescence of cells treated with Fento-1 (10 μM, 6 h) and inhibitors used 2 h prior. $n = 7$ independent experiments. **e**, Incucyte cell viability measurement. Representative of $n = 3$ independent experiments. Data are mean ± s.e.m. **f**, Viability of cells treated with Fento-1 (10 μM, 24 h) or Lip-1 (1 μM, 24 h) or Fento-1 (10 μM, 24 h) and Lip-1 (1 μM, 30 min prior). 1-way ANOVA. $n = 6$ technical replicates. **g**, Fluorescence imaging of Fento-1. Fento-1 (1 μM, 1 h) and Toc (100 μM, 2 h prior). Scale bar, 10 μm. $n = 3$ independent experiments. Two-sided unpaired *t*-test. Data are mean ± s.d. **h**, Viability of cells treated for 48 h. $n = 3$ independent experiments. Data are mean ± s.d. **i**, Left: Cell death in knock-down cells measured by Annexin-V/ Sytox blue in cells treated with Fento-1 for 6 h. $n = 3$ independent experiments. 2-way ANOVA. Data are mean ± s.d. Right: Western blot of proteins in knock-down cells. γ-tubulin is a sample processing control. **j**, Bodipy-C11 581/591 flow cytometry of knock-down cells treated for 6 h. Box plots: interquartile range, centre lines = medians and whiskers = the minimum and maximum values. **a-d**, Two-sided Mann–Whitney test compared to vehicle.

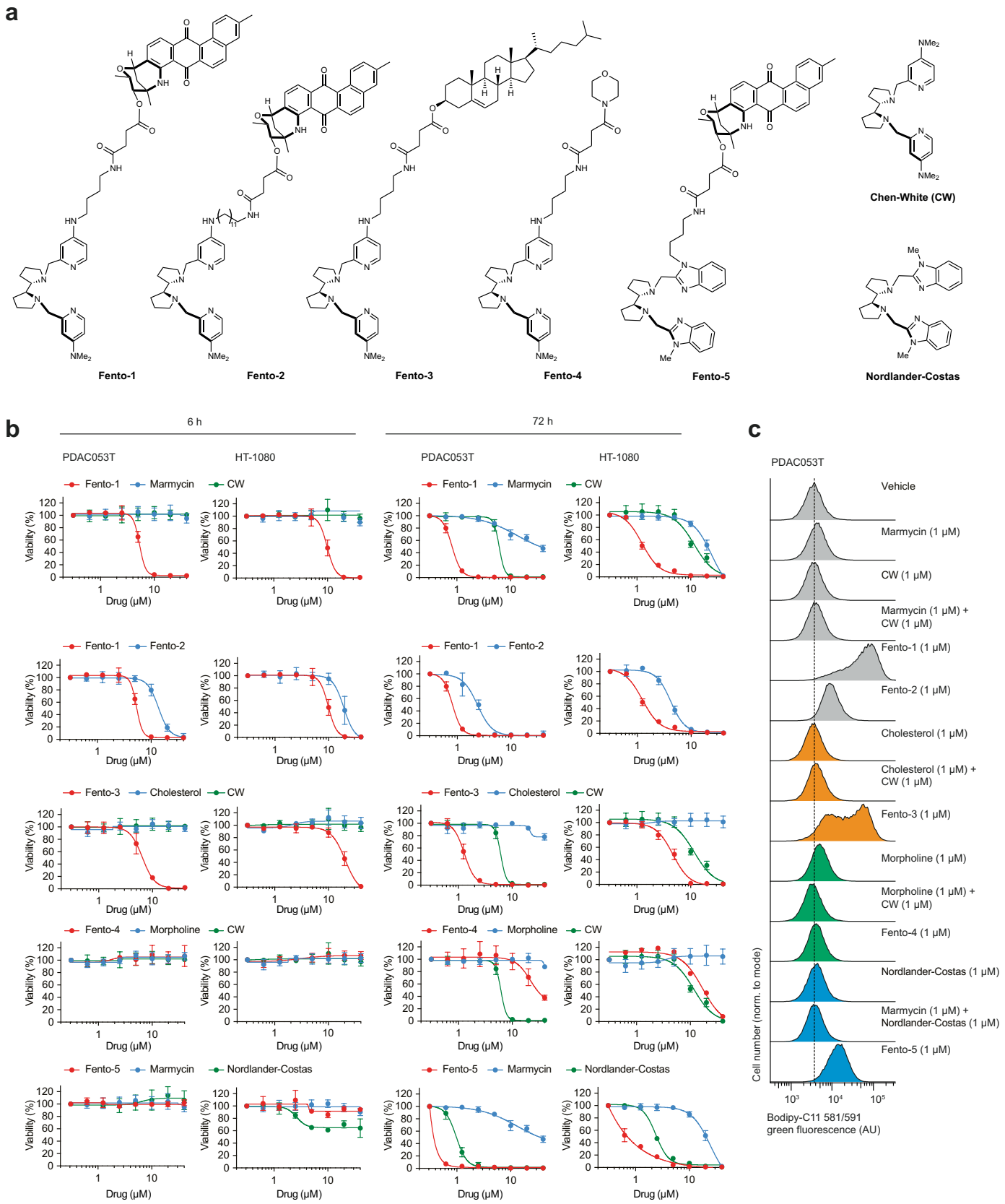

Extended Data Fig. 7 | Fentomycin analogues. a, Molecular structures. **b**, Viability of cells treated for 6 h or 72 h. Data are mean ± s.d. $n = 3$ independent experiments. **c**, Bodipy-C11 581/591 flow cytometry of cells treated for 6 h. Representative of $n = 3$ independent experiments.

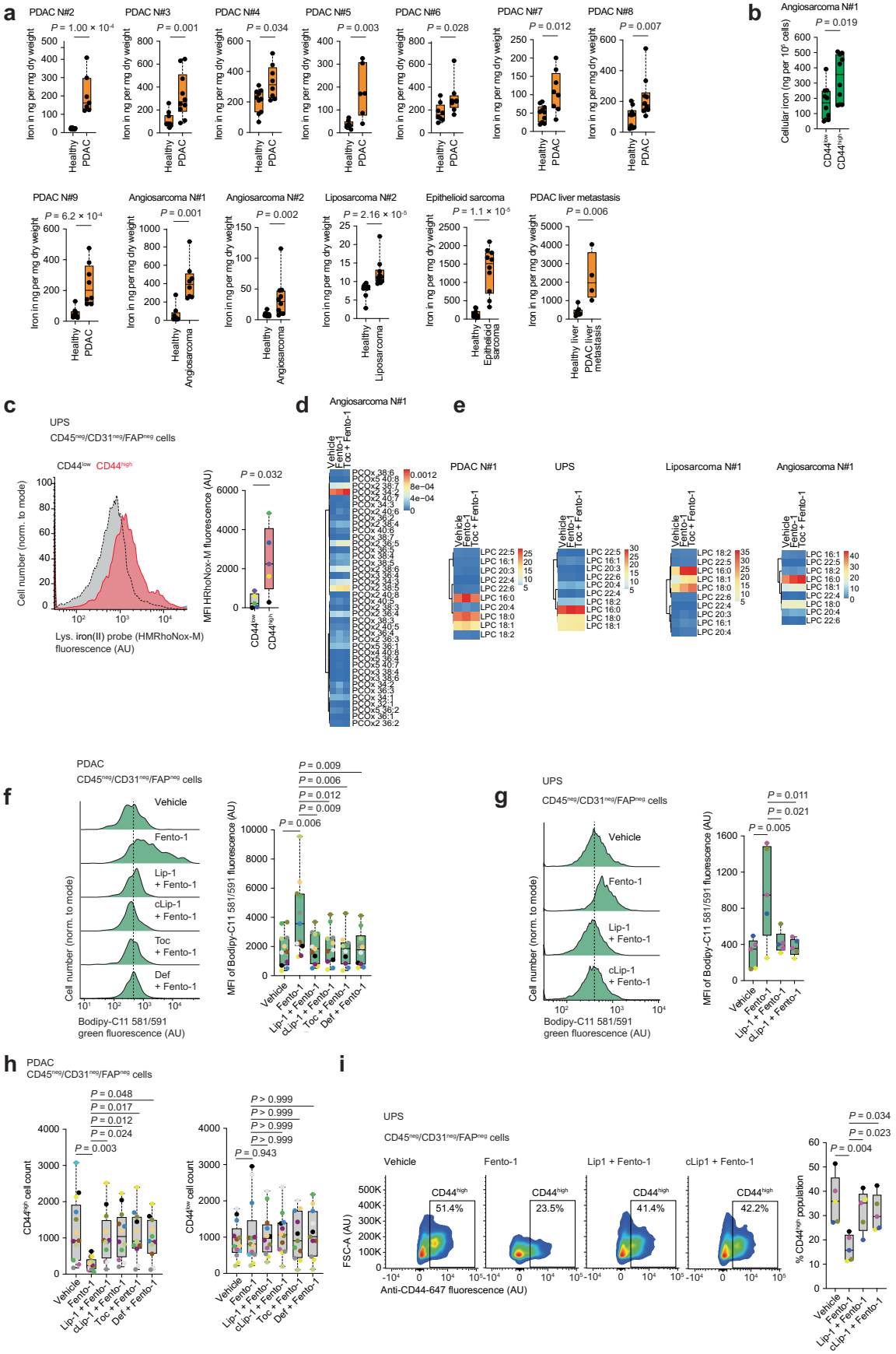

Extended Data Fig. 8 | See next page for caption.

Extended Data Fig. 8 | Fento-1 induces ferroptosis in CD44^{high} iron-rich cancer cells (Part 1). a, ICP-MS of healthy and cancer tissues from patients. PDAC #2: healthy $n = 10$ tissue pieces, PDAC $n = 7$ tissue pieces; PDAC #3: healthy $n = 10$ tissue pieces, PDAC $n = 10$ tissue pieces; PDAC #4: healthy $n = 10$ tissue pieces, PDAC $n = 8$ tissue pieces; PDAC #5: healthy $n = 8$ tissue pieces, PDAC $n = 6$ tissue pieces; PDAC #6: healthy $n = 8$ tissue pieces, PDAC $n = 8$ tissue pieces; PDAC #7: healthy $n = 10$ tissue pieces, PDAC $n = 8$ tissue pieces; PDAC #8: healthy $n = 10$ tissue pieces, PDAC $n = 10$ tissue pieces; PDAC #9: healthy $n = 8$ tissue pieces, PDAC $n = 8$ tissue pieces; angiosarcoma #1: healthy $n = 8$ tissue pieces, angiosarcoma $n = 8$ tissue pieces; angiosarcoma #2: healthy $n = 10$ tissue pieces, angiosarcoma $n = 10$ tissue pieces; liposarcoma #2: healthy $n = 10$ tissue pieces, liposarcoma $n = 10$ tissue pieces; epithelioid sarcoma: healthy $n = 10$ tissue pieces, epithelioid sarcoma $n = 10$ tissue pieces; PDAC liver metastasis: healthy $n = 7$ tissue pieces, PDAC liver metastasis $n = 4$ tissue pieces. **b**, ICP-MS of dissociated human tumour cancer cells. $n = 10$ replicates. **c**, HMRhoNox-M flow cytometry of cancer cells from human UPS. $n = 5$ patients. **d**, Lipidomics of oxidised phospholipids in dissociated human tumour cells treated with Fento-1 (24 h) and Toc used 2 h prior. **e**, Lipidomics of lysophospholipids in dissociated human tumour cells treated with Fento-1 (24 h) and Toc used 2 h prior. **f**, Bodipy-C11 581/591 flow cytometry of dissociated human PDAC cancer cells treated with Fento-1 (24 h) and inhibitors used 2 h prior. $n = 11$ patients. **g**, Bodipy-C11 581/591 flow cytometry of dissociated UPS cancer cells treated with Fento-1 (24 h) and inhibitors used 2 h prior. $n = 5$ patients. **h**, Flow cytometry cell counting of dissociated human PDAC CD44$^{high/low}$ cancer cells treated with Fento-1 (24 h) and inhibitors used 2 h prior. $n = 13$ patients. **i**, CD44 flow cytometry of dissociated UPS cancer cells treated with Fento-1 (24 h) and inhibitors used 2 h prior. $n = 5$ patients. Concentrations used unless stated otherwise: Fento-1 (1 μM), Toc (100 μM), Def (100 μM), Lip-1 (1 μM) and cLip-1 (1 μM). **a, b, c**, Two-sided Mann–Whitney test. **f-i**, 1-way ANOVA. **c, f-i**, each coloured dot represents a tumour of a distinct patient for a given panel. Box plots: interquartile range, centre lines = medians and whiskers = the minimum and maximum values.

Extended Data Fig. 9 | See next page for caption.

Extended Data Fig. 9 | Fento-1 induces ferroptosis in CD44^{high} iron-rich cancer cells (Part 2). a, Viability of cells treated with Fento-1 or standard-of-care chemotherapy for 72 h. Data are mean ± s.e.m. $n = 3$ independent experiments. **b**, Viability of PDAC-derived organoids treated with Fento-1 or standard-of-care chemotherapy for 72 h. Data are mean ± s.e.m. IC_{50}-values are indicated. PDAC009T: Oxaliplatin, 5-FU and SN-38 $n = 4$ independent experiments, Fento-1 $n = 2$ independent experiments. PDAC003T: Oxaliplatin $n = 6$ independent experiments, 5-FU and SN38 $n = 4$ independent experiments, Fento-1 $n = 3$ independent experiments. PDAC117T: Oxaliplatin, 5-FU and SN-38 $n = 7$ independent experiments, Fento-1 $n = 3$ independent experiments. PDAC372T: Oxaliplatin, 5-FU and SN-38 $n = 4$ independent experiments, Fento-1 $n = 3$ independent experiments. **c**, Viability of cells treated with standard-of-care chemotherapy and sublethal doses of Fento-1 (1.5 µM, 72 h). 1-way ANOVA. Data are mean ± s.e.m. $n = 3$ independent experiments. **d**, Synergy score of standard-of-care chemotherapy and Fento-1 in human primary PDAC cells. **e**, Viability of cells treated with Fento-1 (72 h) in naive cells or cells pretreated with Doxo (25 nM) for 30 days, then treated with Fento-1 for 72 h. Data are mean ± s.e.m. $n = 5$ independent experiments. **f**, Bright field images of cells treated with Doxo (25 nM, 30 days). Scale bar, 100 µm. Representative of $n = 3$ independent experiments with similar results. **g**, CD44 flow cytometry of cells treated with Doxo (25 nM) or Fento-1 (1 µM) for 10 days. Representative of $n = 3$ independent experiments. **h**, Western blot of mesenchymal and iron homeostasis markers in cells treated with Doxo (25 nM) for 10 days. Lamin A/C is a sample loading control. Representative of $n = 3$ independent experiments with similar results. **i**, Western blot of mesenchymal and iron homeostasis markers in cells treated with Fento-1 (1 µM) for 10 days. γ-tubulin is a sample loading control. Representative of $n = 3$ independent experiments with similar results. Doxo, doxorubicin.

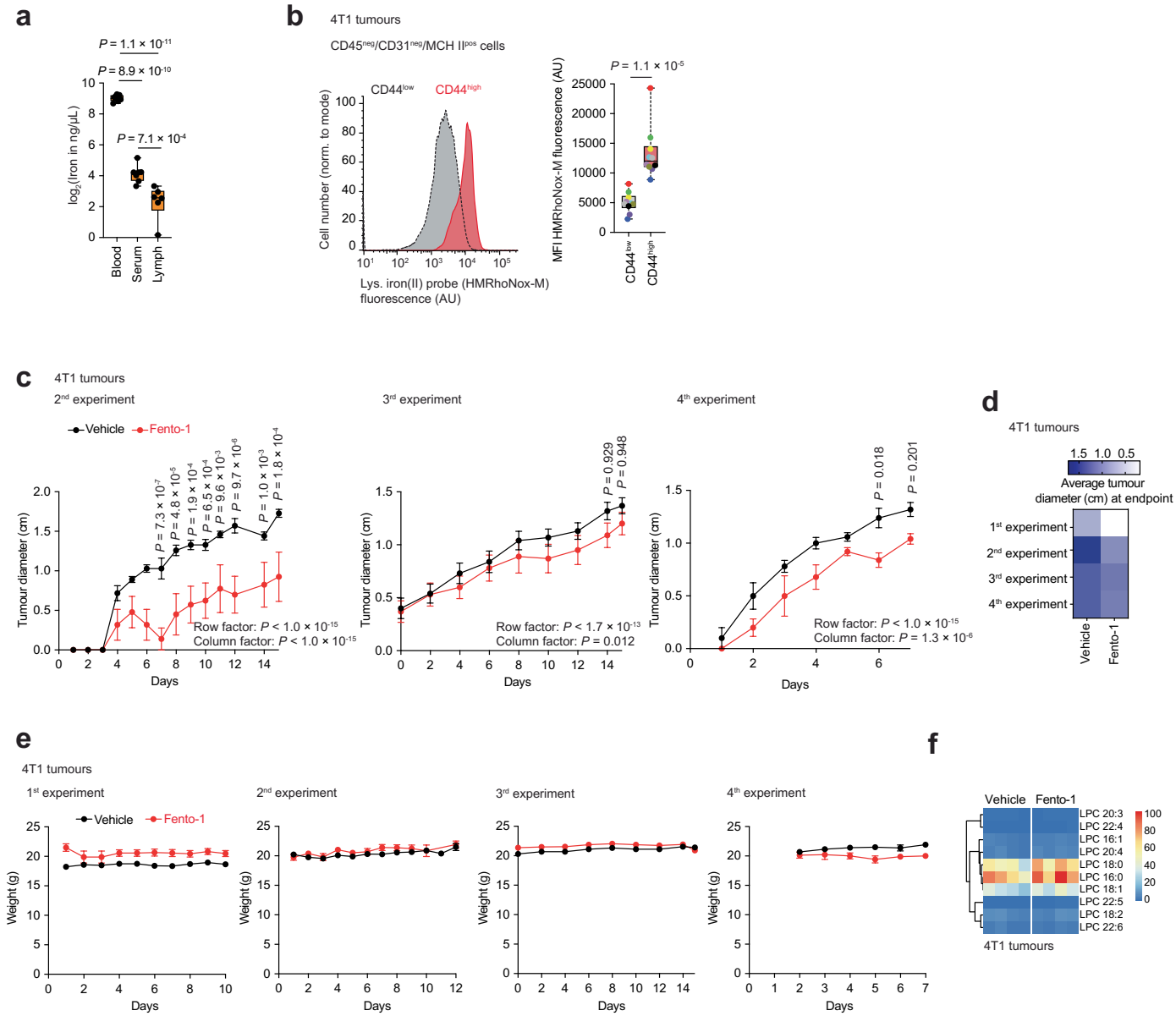

Extended Data Fig. 10 | Fento-1 induces ferroptosis in CD44^{high} iron-rich cancer cells (Part 3). a, ICP-MS of blood, serum and lymphatic fluid from mice. Blood and serum: $n = 7$ mice; Lymph: $n = 6$ mice. 1-way ANOVA. **b**, HMRhoNox-M flow cytometry of dissociated mouse tumour cancer cells. $n = 10$ mice. Each coloured dot represents a tumour of a distinct mouse. Two-sided Mann–Whitney test. **c**, Tumour diameter in mice treated with Fento-1 (0.003 mg per animal every-other-day). 2-way ANOVA. Data are mean ± s.e.m. 2nd experiment: vehicle $n = 10$ mice, Fento-1 $n = 5$ mice; 3rd experiment: $n = 10$ mice for each group; 4th experiment: $n = 5$ mice for each group. **d**, Tumour diameter in tumour-bearing mice treated with Fento-1 (0.003 mg compound per animal every-other-day). $n = 4$ independent experiments. 1st experiment: $n = 5$ mice for each group; 2nd experiment vehicle: $n = 10$ mice, Fento-1: $n = 5$ mice; 3rd experiment: $n = 10$ mice for each group; 4th experiment: $n = 5$ mice for each group. **e**, Mice body weight of mice treated as in Fig. 3h and Extended Data Fig. 10c. 1st experiment: $n = 5$ mice for each group; 2nd experiment: vehicle $n = 10$ mice, Fento-1 $n = 5$ mice; 3rd experiment: $n = 10$ mice for each group; 4th experiment: $n = 5$ mice for each group. Data are mean ± s.e.m. **f**, Lipidomics of lysophospholipids in tumours of tumour-bearing mice treated with Fento-1 as in Fig. 3j. $n = 4$ 4T1 tumours. LPC lipids displayed. LPE, LPS, Supplementary Information. Box plots: interquartile range, centre lines = medians and whiskers = the minimum and maximum values.

nature portfolio

Corresponding author(s): Raphaël RODRIGUEZ

Last updated by author(s): Mar 7, 2025

Reporting Summary

Nature Portfolio wishes to improve the reproducibility of the work that we publish. This form provides structure for consistency and transparency in reporting. For further information on Nature Portfolio policies, see our Editorial Policies and the Editorial Policy Checklist.

Statistics

For all statistical analyses, confirm that the following items are present in the figure legend, table legend, main text, or Methods section.

n/a	Confirmed	
☐	☒	The exact sample size (*n*) for each experimental group/condition, given as a discrete number and unit of measurement
☐	☒	A statement on whether measurements were taken from distinct samples or whether the same sample was measured repeatedly
☐	☒	The statistical test(s) used AND whether they are one- or two-sided *Only common tests should be described solely by name; describe more complex techniques in the Methods section.*
☐	☒	A description of all covariates tested
☐	☒	A description of any assumptions or corrections, such as tests of normality and adjustment for multiple comparisons
☐	☒	A full description of the statistical parameters including central tendency (e.g. means) or other basic estimates (e.g. regression coefficient) AND variation (e.g. standard deviation) or associated estimates of uncertainty (e.g. confidence intervals)
☐	☒	For null hypothesis testing, the test statistic (e.g. *F*, *t*, *r*) with confidence intervals, effect sizes, degrees of freedom and *P* value noted *Give P values as exact values whenever suitable.*
☒	☐	For Bayesian analysis, information on the choice of priors and Markov chain Monte Carlo settings
☒	☐	For hierarchical and complex designs, identification of the appropriate level for tests and full reporting of outcomes
☐	☒	Estimates of effect sizes (e.g. Cohen's *d*, Pearson's *r*), indicating how they were calculated

Our web collection on statistics for biologists contains articles on many of the points above.

Software and code

Policy information about availability of computer code

Data collection

Flow cytometry:
Attune NxT using Attune NxT Sovtware v4.2.0
FACSAria Fusion (BD) using FACS DIVA software v9.0.1
BD LSR Fortessa X-20 flow cytometer using FACS DIVA software v9.0.1

Western blot:
FusionCapt Advance Software

Fluorescent imaging:
Deltavision imaging software, Thunder Leica image acquisition software or Apotome Zeiss Imaging Software

Brightfield Imaging:
cellSens Entry imaging software (Olympus)

Plate reader:
SpectraMax ID3 plate reader (Molecular Devices), exported as Excel files
SpectraMax iD5 microplate reader with SoftMax Pro v7 software (Molecular Devices)

NMR:
Bruker Topspin 4.1.4 software

Cyclic Voltammetry:
Nova software

Fluorimetry:
SoftMax Pro 7.1 GxP

Molecular modeling:
Gaussian 16, Revision C.01

Lipidomics:
LipidXplorer v 1.2.8 (http://genomebiology.com/2011/12/1/R8)

FENIX assay:
Agilent BioTek Gen5 v. 3.08.01

Data analysis

Softwares:

Microsoft Excel and PRISM 10.0.3 unless stated otherwise

Flow cytometry:
FlowJo software v 10.10.0

Image processing:
FIJI 2.0.0-rc-69/1.52n

Lipidomics:
LipidXplorer v 1.2.8 (http://genomebiology.com/2011/12/1/R8)

Quantitative proteomics:
myProMS (v3.10) (https://github.com/bioinfo-pf-curie/myproms), Poullet P et al., 2007

Illustrations:
FIJI 2.0.0-rc-69/1.52n
Prism 10.0.3
Adobe Illustrator 26.0.2
biorender.com

Statistics:
Prism 10.0.3

NMR:
MestRenova v.5.0.1-35756
Bruker Topspin 4.1.4 software

Drug synergy:
SynergyFinder software

For manuscripts utilizing custom algorithms or software that are central to the research but not yet described in published literature, software must be made available to editors and reviewers. We strongly encourage code deposition in a community repository (e.g. GitHub). See the Nature Portfolio guidelines for submitting code & software for further information.

Data

Policy information about availability of data

All manuscripts must include a data availability statement. This statement should provide the following information, where applicable:

- Accession codes, unique identifiers, or web links for publicly available datasets
- A description of any restrictions on data availability
- For clinical datasets or third party data, please ensure that the statement adheres to our policy

Lipidomics data are presented in Supplementary Tables. Quantitative proteomics raw data have been deposited to the ProteomeXchange Consortium via the PRIDE partner repository with the dataset identifier PXD054449 (reviewer_pxd054449@ebi.ac.uk; password: o1gh7kRYdTEP). For identification, the data were searched against the Homo sapiens (UP000005640) Uniprot database using Spectronaut v18.7 or 19 (Biognosys).

Research involving human participants, their data, or biological material

Policy information about studies with human participants or human data. See also policy information about sex, gender (identity/presentation), and sexual orientation and race, ethnicity and racism.

Reporting on sex and gender	No gender or sex reporting was performed for biopsies of human tumours. Tumour samples collected were anonimised for patient and data protection purposes in accordance with hospital guidelines and the French law and not analysed by sex.
Reporting on race, ethnicity, or	Tumour samples were anonymous and no reporting of race, ethnicity or other socially relevant groupings were performed in accordance with French law.

other socially relevant groupings	
Population characteristics	Pancreatic ductal adenocarcinoma (PDAC), undifferentiated pleomorphic sarcoma (UPS), liposarcoma, angiosarcoma, epitheloid sarcoma, PDAC liver metastasis were obtained as anonymous samples.
Recruitment	No selection of the participants
Ethics oversight	Fresh tumour samples were obtained by surgery from patients at Paul Brousse and Institut Curie care centres. All patients provided written informed consent for use of tumour samples. The study was approved by institutional regulatory boards (no. 587 and DATA190160).

Note that full information on the approval of the study protocol must also be provided in the manuscript.

Field-specific reporting

Please select the one below that is the best fit for your research. If you are not sure, read the appropriate sections before making your selection.

☒ Life sciences ☐ Behavioural & social sciences ☐ Ecological, evolutionary & environmental sciences

For a reference copy of the document with all sections, see nature.com/documents/nr-reporting-summary-flat.pdf

Life sciences study design

All studies must disclose on these points even when the disclosure is negative.

Sample size	No sample size calculation was performed, but a minimum of n = 3 chosen for cell biology experiments. For in vivo experiments, mouse cohort groups were either 5 or 10. No sample size calculation was performed for human tumour samples, and analyses were performed on availability of these rare samples post-surgery, depending on availability from the patients.
Data exclusions	No data were excluded from the analyses.
Replication	Experiments were performed at least three times unless stated otherwise. Replication was successful and all data are displayed in the manuscript. All replicates of all experiments noted in the captions and/ or the statistical analysis, with data available as source files.
Randomization	For in vivo experiments, mice were allocated randomly into experimental groups. For tumour samples, these were grouped by tumour type (PDAC, UPS etc.) and not randomized. Material was available from the hospital and collected in an anonymous fashion for the analysis, other than the indication of the type of tumour.
Blinding	Investigators were blinded to group allocation during data collection for ICP-MS, lipidomics and proteomics experiments. Data analyses were not blinded.

Reporting for specific materials, systems and methods

We require information from authors about some types of materials, experimental systems and methods used in many studies. Here, indicate whether each material, system or method listed is relevant to your study. If you are not sure if a list item applies to your research, read the appropriate section before selecting a response.

Materials & experimental systems

n/a	Involved in the study
☐	☒ Antibodies
☐	☒ Eukaryotic cell lines
☒	☐ Palaeontology and archaeology
☐	☒ Animals and other organisms
☒	☐ Clinical data
☒	☐ Dual use research of concern
☒	☐ Plants

Methods

n/a	Involved in the study
☒	☐ ChIP-seq
☐	☒ Flow cytometry
☒	☐ MRI-based neuroimaging

Antibodies

Antibodies used	Antibodies are annotated below as follows. WB, Western blot; FCy, flow cytometry; FI, fluorescence imaging. Hu, used for human samples. Ms, used for mouse samples. Dilutions are indicated. Any antibody validation by manufacturer is indicated and can be found on the manufacturers' websites. Our antibody validation knockdown (KD) and/or knockout (KO) strategies for relevant antibodies are indicated. Primary antibodies: AIFM2/FSP1 (Merck, MABC1638, clone 6D8-11, lot Q3745998, WB, 1:500, Hu, KD validated in-house), Catalase

(Cell Signaling, 12980T, clone D4P7B, lot 3, FI, 1:200, Hu), CD3-BV510 (BioLegend, 317332, clone OKT3, lot B263750, FCy, 1:100, Hu), CD31-PE-Cy7 (BioLegend, 303118, clone WM59, lot B276836, FCy, 1:100, Hu), CD31-BV605 (BioLegend, 303122, clone WM59, lot 331683, FCy, 1:100, Hu), CD31-BV605 (BioLegend, 102427, clone 390, lot B375532, FCy, 1:100, Ms), CD44 (Abcam, ab189524, clone EPR18668, lot 1014086-32, WB, 1:30000, Hu, KO and KD validated in-house), CD44-AF647 (Novus Biologicals, NB500-481AF488, clone MEM-263, lot P158343, FCy, 1:100, Hu), CD44-AF647 (Novus Biologicals, NB500-481AF647, clone MEM-263, lot D145771, FCy, 1:100, Hu), CD44-AF647 (BioLegend, 103018, clone IM7, lot B317762, FCy, 1:100, Ms), CD45-BV785 (BioLegend, 304048, clone HI30, lot B339809, FCy, 1:100, Hu), CD45-BV510 (BioLegend, 368526, clone 2D1, lot B373428, FCy, 1:100, Hu), CD45-BV510 (BioLegend, 103138, clone 30-F11, lot B386738, FCy, 1:100, Ms), CD163-PerCP/Cyanine5.5 (BioLegend, 326512, clone RM3/1, lot B291202, FCy, 1:100, Hu), COXIV (Abcam, ab16056, lot GR3206555-1, WB, 1:1000, Hu), Cytochrome c (Cell Signaling, 12963S, clone 6H2.B4, lot 2, FI, 1:200, Hu), EEA1 (Abcam, ab70521, clone 1G11, lot GR315680-1, FI, 1:200, Hu, validated by ICC/IF by manufacturer), FAP-AF700 (R&D Systems, FAB3715N, clone 427819, lot AEVI020011, FCy, 1:100, Hu), FAP-AF750 (Bio-Techne, FAB3715S-100UG, clone 427819, lot 1718688, FCy, 1:100, Hu), Ferritin (Abcam, ab75973, clone EPR300AY, lot 10136442-29, WB, 1:1000, Hu, validated by WB by manufacturer), Fibronectin (Abcam, ab45688, clone F14, lot 1016266-35, WB, 1:1000, Hu), FTH1 (Santa Cruz Biotechnology, sc-376594, clone B-12, lot G2622, WB, 1:200, Hu), GPX4 (Abcam, ab125066, clone EPNCIR144, lot GR3369574-4, WB, 1:2000, Hu, KO validated by manufacturer, KD validated in-house), 4-Hydroxynonenal (4-HNE) (Abcam, ab48506, clone HNEJ-2, lot 1062274-2, FI, 1:200, Hu), IRP2 (Novus Biologicals, NB100-1798, lot D-4, WB, 1:1000, Hu), Lamin A/C (Cell Signaling, 2032S, lot 6, WB, 1:1000, Hu), LAMP1 (Cell Signaling, 9091S, clone D2D11, lot 7, FI, 1:200, Hu), LAMP1 (Santa Cruz Biotechnology, sc-20011, clone H4A3, FI, 1:100, Ms), LAMP1 (Abcam, ab24170, lot GR3235630-1, WB, 1:1000, Hu), LAMP2 (Abcam, ab25631, clone H4B4, lot 1011336-1, FI, 1:200, Hu), LAMP2 (Thermo Fisher Scientific, MA1-205, clone H4B4, lot YG377512, WB, 1:1000, Hu), LIMPII (Proteintech, 27102-1-AP, WB, 1:1000, Hu), NCOA4 (Abcam, ab86707, lot GR3244520-13, WB, 1:10000, Hu, KD validated in-house), NDUFS1 (Abcam, ab157221, clone EPR11522(B), lot YJ110907DS, WB, 1:1000, Hu), PDIA3 (Sigma-Aldrich, AMAB90988, clone CL2444, lot 02879, FI, 1:200, Hu; WB, 1:1000, Hu), MHCII-APC/Cyanine7 (BioLegend, 107628, clone M5/114.12.2, lot B370049, FCy, 1:100, Ms), RCAS1 (Cell Signaling, 12290S, clone D2B6N, lot 1, FI, 1:200, Hu, WB, 1:1000, Hu), SLC7A11/xCT (Cell Signaling, 12691S, clone D2M7A, lot 5, WB, 1:1000, Hu, KD validated in-house), SOX4 (Santa Cruz Biotechnology, sc-518016, clone B-7, lot G2023, WB, 1:200, Hu), Transferrin receptor 1 (TfR1, Life Technologies, 13-6800, clone H68.4, lot VJ313549, WB, 1:1000, Hu, KO and KD validated in-house), TfR1-APC-AF750 (Beckman Coulter, A89313, clone YDJ1.2.2, lot 200060, FCy, 1:100, Hu), TfR1-PE (BioLegend, 334106, clone CY1G4, lot B364886, FCy, 1:100, Hu), gamma-tubulin (Sigma-Aldrich, T5326, clone GTU-88, lot 0000140390, WB, 1:1000, Hu, validation by manufacturer), Vimentin (Cell Signaling, 5741S, clone D21H3, lot 8, WB, 1:1000, Hu).

Secondary antibodies: Alexa Fluor 647 anti-mouse (Abcam, ab150115, tissue labelling, 1:500, Ms), Alexa Fluor 647 anti-mouse (Invitrogen, A21237, lot 1485202, FI, 1:1000, Hu), Alexa Fluor 647 anti-rabbit (Invitrogen, A21246, lot 2714437, FI, 1:1000, Hu), donkey anti-rabbit IgG-h+l HRP-conjugated (Bethyl Laboratories, A120-108P, lot 13, WB, 1:10000, Hu), goat anti-mouse IgG-h+l HRP-conjugated (Bethyl Laboratories, A90-116P, lot 39, WB, 1:10000, Hu), goat anti-rat IgG-h+l HRP-conjugated (Invitrogen, 31470, WB, 1:10000, Hu).

Validation

Any antibody validation by the manufacturer is indicated and can be found on the manufacturers' websites. Our antibody validation knockdown (KD) and/or knockout (KO) strategies performed in our laboratory for relevant antibodies are indicated above an were performed and verified in the laboratory with relevant CRISPR or siRNA approaches (denoted as in-house in the list above). Information of antibody validation by manufacturers are indicated in thee list above. All this information is also detailed in the methods section.

Eukaryotic cell lines

Policy information about cell lines and Sex and Gender in Research

Cell line source(s)

HT-1080 cells, MDA-MB-231 and 4T1 cells were obtained from the ATCC. FC1242 and FC1245 murine pancreatic cancer cells, 4a cells and human pancreatic hMIA-2D cells were a gift from the Tuveson laboratory (CSHL).
Primary human pancreatic PDAC024T, PDAC030T, PDAC053T, PDAC054T, PDAC084T, PDAC090T and PDAC211T cells were obtained as described in the "Establishment of xenograft derived pancreatic cell cultures" paragraph.
Xenograft derived pancreatic organoids (XDPO) PDAC009T, PDAC003T, PDAC117T and PDAC372T were obtained as described in the "Establishment of xenograft derived pancreatic organoids" paragraph.
Primary lung circulating tumour cells were from Celprogen.
Primary colon circulating tumour cells were from Celprogen.
Pfa1 cells were generated in the Conrad laboratory (Seiler A et al., 2008).
SUM159 cells were a genrous gift from Dr. S.Ethier (Karmanos Cancer Center, Detroit, MI, USA).

Authentication

Authentication was relied on by the commercial source where applicable (ATCC, Celprogen).
No authentication of human derived pancreatic cancer cells/ organoids was performed. These cells were generated from primary sources directly in the Iovanna lab. Pfa1 cells and derivatives were generated in the Conrad lab (Seiler A et al., 2008) and SUM159 cells were a generous gift from Dr. S.Ethier (Karmanos Cancer Center, Detroit, MI, USA). These cells, and the generously gifted cells from the Tuveson laboratory (see above) were not further authenticated.

Mycoplasma contamination

Cells were regularly tested negative for mycoplasma contamination.

Commonly misidentified lines
(See ICLAC register)

No commonly misidentified cell lines were used in this study.

Animals and other research organisms

Policy information about studies involving animals; ARRIVE guidelines recommended for reporting animal research, and Sex and Gender in Research

Laboratory animals	cLip-1 treatment in vivo: Mice were kept under standard conditions with water and food ad libitum and in a controlled environment (22 ± 2 °C, 55 ± 5% humidity, 12 h light/dark cycle). For animal studies, Rosa26-CreERT2;Gpx4f/f (C57BL6/J) mice were randomised into separate cages. 12 to 24-week-old sex-matched mice were used for all experiments. Isolation of blood, serum and lymphatic fluid from mice: Balb/C mice (25-week-old adult female mice) were purchased from Charles River and grown at the CRCM animal core facility and randomised into separate cages. Mice were housed under sterile conditions with sterilised food and water provided ad libitum and maintained on a 12 h light/dark cycle and 22 ± 2 °C, 55 ± 5% humidity. Intranodal murine metastasis models and Fento-1/Marmycin/CW treatment: Murine breast cancer cells (4T1) were transplanted into 6 to 8-week-old female Balb/c mice (syngeneic with the 4T1 model). Mice were grown at the Harvard medical school animal core facility and randomised into separate cages. Mice were housed under sterile conditions with sterilised food and water provided ad libitum and maintained on a 12 h light/dark cycle and 22 ± 2 °C, 55 ± 5% humidity.
Wild animals	The study did not involve wild animals.
Reporting on sex	As detailed in the Methods.
Field-collected samples	The study did not involve samples collected from the field.
Ethics oversight	All cLip-1 in vivo experiments were performed in compliance with the German Animal Welfare Law and have been approved by the Institutional Committee on Animal Experimentation and the Government of Upper Bavaria (approved no. ROB-55.2-2532.Vet_02-18-13). All intranodal injection mouse experiments complied with all relevant ethical regulations and were performed according to protocols approved by the Institutional Animal Care and Use Committee at Harvard T.H. Chan School of Public Health (protocol IS00003460). For mouse lymph and blood collection, animal experiments were performed in accordance with the European Community guiding in the care and use of animals. Animal experiments were performed in agreement with the French Guidelines for animal handling and approved by local ethics committee (Agreement no. 16487-2018082108541206 v3).

Note that full information on the approval of the study protocol must also be provided in the manuscript.

Plants

Seed stocks	*Report on the source of all seed stocks or other plant material used. If applicable, state the seed stock centre and catalogue number. If plant specimens were collected from the field, describe the collection location, date and sampling procedures.*
Novel plant genotypes	*Describe the methods by which all novel plant genotypes were produced. This includes those generated by transgenic approaches, gene editing, chemical/radiation-based mutagenesis and hybridization. For transgenic lines, describe the transformation method, the number of independent lines analyzed and the generation upon which experiments were performed. For gene-edited lines, describe the editor used, the endogenous sequence targeted for editing, the targeting guide RNA sequence (if applicable) and how the editor was applied.*
Authentication	

Flow Cytometry

Plots

Confirm that:

☒ The axis labels state the marker and fluorochrome used (e.g. CD4-FITC).

☒ The axis scales are clearly visible. Include numbers along axes only for bottom left plot of group (a 'group' is an analysis of identical markers).

☒ All plots are contour plots with outliers or pseudocolor plots.

☒ A numerical value for number of cells or percentage (with statistics) is provided.

Methodology

Sample preparation	Flow cytometry: Cells were washed with ice-cold 1× PBS. For antibody staining, cells were incubated with Fc block (Human TruStain FcX, Biolegend, 422302, 1:20) for 15 min, then incubated with antibodies in ice cold 10% FBS, 1× PBS, 2 mM EDTA for 20 min at 4 °C and then washed with 1× PBS and resuspended in 10% FBS, 1× PBS, 2 mM EDTA before analysis using a BD LSR Fortessa

X-20 flow cytometer. Flow cytometry with iron probes: PDAC053T and HT-1080 cells were seeded in 6-well plates at the density of 2× 10e5 cells/well. On the following day, Lip-1 (10 µM), hydroxychloroquine (HCQ, Sigma-Aldrich, H0915, 100 µM), Bafilomycin A1 (Baf-A1, Sigma-Aldrich, B1793, 75 nM) were added to PDAC053T for 1 h and in HT-1080 for 30 min. In PDAC053T, after 30 min of treatment with compounds, RPE (in-house, 40 µM) or HMRhoNox-M (in-house, 1 µM) probes were added for 30 min. In HT-1080, after 15 min of treatment with compounds, RPE (in-house, 40 µM) or HMRhoNox-M (in-house, 1 µM) probes were added and left for 15 min. After incubation with iron probes, the media was removed and cells were washed with 1× PBS once before trypsinization. Cells were harvested, pelleted, washed with 1× PBS and finally 200 µL of 1× PBS buffer containing 10% FBS and EDTA (0.1% v/v) was added. Data were recorded on a BD LSR Fortessa X-20. Flow cytometry with Bodipy-C11 581/591: PDAC053T cells were seeded in 6-well plates at the density of 1x 10e5 cells/well. On the next day, cells were treated with Lip-1 (1 µM), cLip-1 (in house, 1 µM), metclip-1 (in house, 10 µM), alcLip-1 (in house, 10 µM) and Bodipy-C11 581/591 (200 nM) before adding RSL3 (100 nM). After 1 h, the media was removed and cells were washed with 1× PBS twice before trypsinization. Cells were harvested, pelleted, washed with 1× PBS and finally 250 µL of 1× PBS buffer containing 10% FBS and EDTA (0.1% v/v), was added for flow cytometry. PDAC053T, HT-1080 and 4T1 cells were seeded in 6-well plates at the density of 2× 10e5 cells/well. On the next day, cells were treated with Baf-A1 (75 nM) and HCQ (10 µM) for 2 h before adding RSL3 (200 nM for PDAC053T and HT-1080, 500 nM for 4T1). Then after 1 h, cells were treated with Bodipy-C11 581/591 (4 µM) for an additional hour. The media was removed and cells were washed with 1× PBS twice before trypsinization. Cells were harvested, pelleted, washed with 1× PBS and finally 250 µL of 1× PBS buffer containing 10% FBS and EDTA (0.1% v/v), was added for flow cytometry. Data were recorded on an AttuneTM NxT Flow Cytometer (Thermo Fisher Scientific). Flow cytometry analyses of lysosomal GSH and lysosomal hydroxyl radicals: Cells were incubated with SQSS (in house, 100 nM, 1 h) or 1-Red (in house, 100 nM, 24 h). HT-1080 cells were incubated with RSL3 (1 µM), ML210 (10 µM, Sigma-Aldrich, SML0521), FIN56 (5 µM, Sigma-Adrich, SML1740), Buthionine sulfoximine (BSO, 10 µM, Sigma-Aldrich, B2515) or erastin (10 µM, Sigma-Aldrich, 329600) for the indicated time points. Data were recorded on an AttuneTM NxT Flow Cytometer (Thermo Fisher Scientific). Flow cytometry analyses of lysosomal iron content: Typically 2× 10e5 dissociated human tissue cells were incubated in media (RPMI 1610, 10% FBS, penicillin/streptomycin) with HMRhoNox-M (in-house, 1 µM, 1 h). Lysosomal iron content of human tumour samples and healthy adjacent tissues was analysed with the following antibody and stain panel: DAPI (0.1 µg/mL), CD3-BV510 (BioLegend, 317332), CD31-PE-Cy7 (BioLegend, 303118), CD44-AF647 (Novus Biologicals, NB500-481AF647), CD45-BV785 (BioLegend, 304048), CD163-PerCP/Cyanine5.5 (BioLegend, 326512), FAP-AF700 (R&D Systems, FAB3715N), TfR1-APC-AF750 (Beckman Coulter, A89313). The live tumour cells corresponded to DAPIneg/CD45neg/CD31neg/FAPneg cells. Data were recorded on a BD LSRFortessa X-20. Flow cytometry analyses of CD44 in Fento-1 treated tumour samples: Typically 2× 10e5 dissociated tumour cells were incubated in media (RPMI 1610, 10% FBS, penicillin/streptomycin) with Fento-1 (in house, 1 µM, 24 h). Cells were pre-treated with Lip-1 (1 µM), cLip-1 (in house, 1 µM), Toc (100 µM) or Def (100 µM) for 2 h. Toc was kept pure under inert atmosphere and a fresh stock solution was prepared throughout the study before each experiment. The following antibody and stain panel was used for subsequent flow analysis: SYTOX blue (Thermo Fisher Scientific, S34857, 1 µM), CD31-BV605 (BioLegend, 303122), CD45-BV510 (BioLegend, 368526, lot B373428), CD44-AF647 (Novus Biologicals, NB500-481AF647), TfR1-PE (BioLegend, 334106), FAP-AF750 (Novus Biologicals, FAB3715S-100UG). The live tumour cells corresponded to SYTOX blueneg/CD45neg/CD31neg/FAPneg cells. Data were recorded on an AttuneTM NxT Flow Cytometer (Thermo Fisher Scientific). For flow cytometry analyses of CD44 levels in mouse 4T1 tumours, typically 2× 10e5 dissociated tumour cells were used per condition. Freshly dissociated cells were stained using the following antibody and stain panel: SYTOX blue (Thermo Fisher Scientific, S34857, 1 µM), CD31-BV605 (BioLegend, 102427), CD44-AF647 (BioLegend, 103018), CD45-BV510 (BioLegend, 103138), MHCII-APC/Cyanine7 (BioLegend, 107628). The live tumour cells corresponded to SYTOX blueneg/CD45neg/CD31neg/MCH IIpos cells. Data were recorded on an AttuneTM NxT Flow Cytometer (Thermo Fisher Scientific). All data were analysed with FlowJo software v. 10.10.0.

Fluorescence-activated cell sorting:
Sorting of human cells was performed using the following antibodies: CD31-PE-Cy7 (BioLegend, 303118), CD44-AF647 (Novus Biologicals, NB500-481AF647), CD45-BV785 (BioLegend, 304048). The sorted cells corresponded to CD45neg/CD31neg/CD44pos cells and CD45neg/CD31neg/CD44neg cells and were isolated on a FACSAria Fusion (BD). ICP-MS experiments were conducted in CD44high and CD44low tumour cells as described in the ICP-MS section. Sorting of mouse cells was performed using the following antibodies: CD44-AF647 (Biolegend, 103018), MHCII-APC/Cyanine7 (BioLegend, 107628). The sorted cells corresponded to MHCIIpos/CD44high cells and MHCIIpos/CD44low cells. Sorted cells were centrifuged at 300× g and cell pellets were processed for subsequent applications.

Instrument

Flow cytometers: BD LSRFortessa X-20, Thermo Fisher Attune NxT and BD FACSAria Fusion sorter.

Software

FlowJo software v. 10.10.0

Cell population abundance

Cell sorting allows to obtain a satisfactory purity

Gating strategy

The live human tumour cells corresponded to DAPIneg/CD45neg/CD31neg/FAPneg cells
The live murine tumour cells corresponded to SYTOX blueneg/CD45neg/CD31neg/MCH IIpos cells.
The sorted human cells corresponded to CD45neg/CD31neg/CD44pos cells and CD45neg/CD31neg/CD44neg cells.
The sorted murine cells corresponded to MHCIIpos/CD44pos cells and MHCIIpos/CD44neg cells.

☒ Tick this box to confirm that a figure exemplifying the gating strategy is provided in the Supplementary Information.